

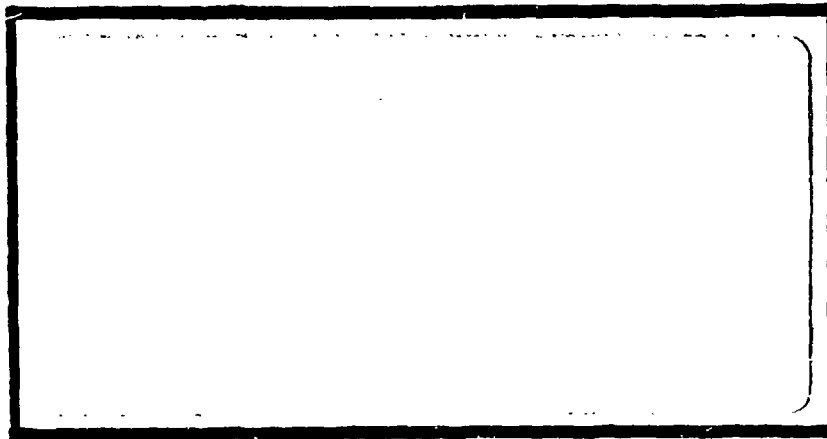
DTIC FILE COPY

1

AD-A202 570



DTIC  
 E  
 JAN 23 1980  
 S H D



DEPARTMENT OF THE AIR FORCE  
 AIR UNIVERSITY  
**AIR FORCE INSTITUTE OF TECHNOLOGY**

Wright-Patterson Air Force Base, Ohio

DISTRIBUTION STATEMENT A

Approved for public release;  
Distribution Unlimited

89 1 17 014

1

AFIT/GAE/AA/88D-36

INVESTIGATION OF CRACK GROWTH IN  
TITANIUM-ALUMINIDE  
AT ELEVATED TEMPERATURES

THESIS

Ernest A. Staubs  
Captain, USAF

AFIT/GAE/AA/88D-36

DTIC  
E1  
S JAN 23 1989 D  
H

Approved for public release; distribution unlimited

AFIT/GAE/AA/88D-36

INVESTIGATION OF CRACK GROWTH IN  
TITANIUM-ALUMINIDE AT ELEVATED TEMPERATURES

THESIS

Presented to the Faculty of the School of Engineering  
of the Air Force Institute of Technology

Air University

In Partial Fulfillment of the  
Requirements for the Degree of  
Master of Science in Aeronautical Engineering

Ernest A. Staubs

Captain, USAF

December 1988

Approved for public release; distribution unlimited

## Preface

The purpose of this study was to investigate crack growth behavior in Titanium-Aluminide (Ti<sub>3</sub>Al) at elevated temperatures in support of the Retirement for Cause (RFC) maintenance program. RFC was initiated by the USAF to conserve valuable jet engine resources and reduce life cycle costs. With a better understanding of crack propagation in potential jet engine materials, we can reduce ~~waste~~ while maintaining a safe flying force. This study has greatly increased my understanding of fracture mechanics and, I hope, has helped with the RFC program.

I would like to thank Dr. Theodore Nicholas and Capt. Steve Balsone of the Materials Laboratory Metals Behavior Branch for the use of their facilities and their help bringing this effort to a successful conclusion. I would also like to thank my thesis advisor, Dr. Shankar Mall, for his overall guidance during this study. Special thanks go to Mr. George Ahrens, UDRI, for demonstrating the test equipment, maintaining instrument calibrations, and making necessary repairs; my experiments wouldn't have been as successful without his help.



<b>Accession For</b>	
NTIS GRA&I	<input checked="" type="checkbox"/>
DTIC TAB	<input type="checkbox"/>
Unannounced	<input type="checkbox"/>
Justification	
By _____	
Distribution/	
Availability Codes	
Dist	Avail and/or Special
A-1	

## Table Of Contents

	Page
Preface . . . . .	ii
List of Figures . . . . .	iv
List of Tables . . . . .	vii
Abstract . . . . .	viii
I. Introduction . . . . .	1
Background . . . . .	1
Objective . . . . .	3
Scope . . . . .	4
Approach . . . . .	5
II. Elevated Temperature Crack Growth . . . . .	6
Time-Dependent Crack Growth . . . . .	7
Cycle-Dependent Crack Growth . . . . .	9
Mixed-Mode Crack Growth . . . . .	10
III. Description of Test Equipment . . . . .	13
IV. Test Procedures . . . . .	21
General . . . . .	21
Sustained Load Tests . . . . .	26
Fatigue Baseline Test . . . . .	30
Hold Time Tests . . . . .	31
Data Analysis . . . . .	34
V. Experimental Results and Discussion . . . . .	41
VI. Model Development . . . . .	58
VII. Conclusions and Recommendations . . . . .	78
Appendix A: History of Test Specimens . . . . .	80
Appendix B: Fatigue Precracking of Test Specimens . . . . .	85
Appendix C: Crack Growth Curves for Specimens . . . . .	87
Appendix D: Crack Growth Program . . . . .	112
Bibliography . . . . .	116
Vita . . . . .	118

## List of Figures

Figure	Page
1. Frequency Dependence of Crack Growth Rate . . . . .	7
2. Typical Crack Growth Rate Curve . . . . .	11
3. Test System Diagram . . . . .	14
4. Swedish Creep Frame . . . . .	16
5. Compact Tension Specimen . . . . .	18
6. Instrumentation Placement . . . . .	19
7. Types of Tests . . . . .	22
8. Typical Compliance Curve . . . . .	25
9. Crack Tip Tunneling . . . . .	28
10. Comparison of Crack Length Calculated from Compliance with Visual Measurements . . . . .	36
11. Reduction of Data Scattering with Polynomial Curve Fit . . . . .	39
12. Sustained Load Crack Growth at 750° C . . . . .	42
13. Sustained Load Crack Growth Rate Curves . . . . .	44
14. Crack Growth Rate Curves for 750° C . . . . .	47
15. Crack Growth per Cycle Curves for 750° C . . . . .	49
16. Fracture Surfaces for Specimens 88-102 and 88-104 . . . . .	53
17. Fracture Surfaces for Specimens 88-105 and 88-112 . . . . .	54
18. Fracture Surfaces for Specimens 88-113 and 88-114 . . . . .	55
19. Fracture Surfaces for Specimens 88-115 and 88-116 . . . . .	56
20. Fracture Surface for Specimen 88-117 . . . . .	57
21. Baseline Sustained Load Crack Growth Rate . . . . .	59
22. Baseline Fatigue Crack Growth Rate . . . . .	60
23. MSE Model Parameters . . . . .	63

Figure	Page
24. Sample MathCAD Template for MSE Model . . . . .	64
25. MSE Model for Creep Crack Growth . . . . .	66
26. MSE Model for Fatigue Crack Growth . . . . .	67
27. Model Versus Actual Crack Growth Rate for 2 Minute Hold Test .	69
28. Model Versus Actual Crack Growth Rate for 5 Minute Hold Test .	70
29. Model Versus Actual Crack Growth Rate for 10 Minute Hold Test	71
30. Comparison of Test Data with Linear Model at Constant Stress Stress Intensity . . . . .	73
31. Schematic Representation of Crack Growth Rates at Constant Intensity . . . . .	74
32. Modified Model for 2 Minute Hold Test . . . . .	75
33. Modified Model for 5 Minute Hold Test . . . . .	76
34. Modulus Versus Temperature for $Ti_3Al$ . . . . .	82
35. Strength Versus Temperature for $Ti_3Al$ . . . . .	83
36. Ductility Versus Temperature for $Ti_3Al$ . . . . .	84
37. Crack Growth Versus Time for Specimen 88-102 . . . . .	88
38. Crack Growth Rate Versus Stress Intensity Factor for Specimen 88-102 . . . . .	89
39. Crack Growth Versus Time for Specimen 88-104 . . . . .	90
40. Crack Growth Rate Versus Stress Intensity Factor for Specimen 88-104 . . . . .	91
41. Crack Growth Versus Time for Specimen 88-105 . . . . .	92
42. Crack Growth Rate Versus Stress Intensity Factor for Specimen 88-105 . . . . .	93
43. Crack Growth Versus Time for Specimen 88-112 . . . . .	94
44. Crack Growth Rate Versus Stress Intensity Factor for Specimen 88-112 . . . . .	95
45. Crack Growth Versus Time for Specimen 88-113 . . . . .	96

Figure	Page
46. Crack Growth Rate Versus Maximum Stress Intensity for Specimen 88-113 . . . . .	97
47. Crack Growth per Cycle Versus Maximum Stress Intensity for Specimen 88-113 . . . . .	98
48. Crack Growth per Cycle Versus Delta Stress Intensity for Specimen 88-113 . . . . .	99
49. Crack Growth Versus Time for Specimen 88-114 . . . . .	100
50. Crack Growth Rate Versus Maximum Stress Intensity for Specimen 88-114 . . . . .	101
51. Crack Growth per Cycle Versus Maximum Stress Intensity for Specimen 88-114 . . . . .	102
52. Crack Growth per Cycle Versus Delta Stress Intensity for Specimen 88-114 . . . . .	103
53. Crack Growth Versus Time for Specimen 88-115 . . . . .	104
54. Crack Growth Rate Versus Maximum Stress Intensity for Specimen 88-115 . . . . .	105
55. Crack Growth per Cycle Versus Maximum Stress Intensity for Specimen 88-115 . . . . .	106
56. Crack Growth per Cycle Versus Delta Stress Intensity for Specimen 88-115 . . . . .	107
57. Crack Growth Versus Time for Specimen 88-116 . . . . .	108
58. Crack Growth Rate Versus Stress Intensity Factor for Specimen 88-116 . . . . .	109
59. Crack Growth per Cycle Versus Maximum Stress Intensity for Specimen 88-116 . . . . .	110
60. Crack Growth per Cycle Versus Delta Stress Intensity for Specimen 88-116 . . . . .	111



## List of Tables

Table	Page
I. Compact Tension Specimen Dimensions . . . . .	18
II. Test Matrix . . . . .	23
III. MSE Model Constants . . . . .	65
IV. Compact Tension Specimen Composition . . . . .	81
V. Heat Treatment of the $Ti_3Al$ Alloy . . . . .	81
VI. Specimen Precrack Parameters . . . . .	86

Abstract

This study investigates crack growth under sustained loads and sustained loads with periodic fatigue cycles at elevated temperatures in a titanium-aluminide alloy ( $Ti_3Al$ ). The objectives are to determine the creep crack growth characteristics and to determine the applicability of linear cumulative damage modeling to the  $Ti_3Al$  alloy. All tests were conducted on standard compact tension specimens of  $Ti_3Al$  under isothermal conditions. Sustained load tests were used to characterize time dependent crack growth behavior at elevated temperatures. A fatigue test and several sustained load tests with periodic fatigue cycles (hold-time tests) were used to test the applicability of linear cumulative damage modeling. The fatigue cycles were conducted at 0.1 Hz with a load ratio of 0.3. Hold times for the combined tests varied from 2 to 10 minutes. The linear elastic stress intensity factor,  $K$ , was used a correlating parameter for all the tests. A model was generated using baseline data from the sustained load and fatigue tests and compared with the hold-time tests to measure its accuracy.

The test results showed that sustained load crack growth is insensitive to temperature. Crack growth rates for all tested temperatures were only a factor of five apart between the slowest and fastest growth rates. The threshold stress intensity level,  $K_{th}$ , was estimated to be  $20 \text{ MPa}\sqrt{m}$ ; the stress intensity at failure,  $K_{IC}$ , was calculated to be about  $46 \text{ MPa}\sqrt{m}$ . Both were insensitive to temperature.

The results from the fatigue and hold-time tests showed crack growth rates increased with decreasing hold time, indicating that linear cumulative damage modeling could be used to predict crack growth in  $Ti_3Al$ . Results from the hold-time tests showed that the crack growth per cycle for hold times under ten minutes was faster than a simple summation of the fatigue and creep crack growth contributions. The crack growth per cycle was consistently two to three times faster than the fatigue baseline data, even below the estimated creep crack growth threshold stress intensity, indicating that some creep-fatigue interaction did occur.

A linear cumulative damage model was developed using data from the sustained load and fatigue tests. Crack growth rates calculated using the model were accurate or conservative for the ten minute hold time test, but were 2 to 3 times less than the growth rates for the other hold time tests based on summation of the sustained load and fatigue growth rates only. A mixed-mode correction factor added to the model produced more accurate results.

# INVESTIGATION OF CRACK GROWTH IN TITANIUM-ALUMINIDE AT ELEVATED TEMPERATURES

## I. Introduction

### Background

In the past, the Air Force removed a component from service when it reached its low cycle fatigue design life. This was based on very conservative statistical models which resulted in the early retirement of many useful components. Engine disks, for example, reached their design life when 1 in 1000 developed a 0.03 inch crack. Once the design life was met, all parts were removed even though 80 percent of the parts could have at least 10 more useful lifetimes (8). This proved to be a necessary, but wasteful way to avert potential disasters. The Engine Structural Integrity Program (ENSIP) now requires a damage tolerant design approach for all new engines. Accurate crack growth predictions are part of this design approach (22:1). In addition, the Air force has adopted the "Retirement for Cause" (RFC) program. The purpose of the RFC program is to periodically inspect components for cracks and replace them only if the part is unsafe.

For a successful RFC program, an accurate method to predict crack growth propagation under a variety of loading conditions is essential. There is, therefore, a need to develop a crack growth model. A successful model should predict crack growth accurately, or at the very least,

conservatively. Since materials react differently to different loading and temperature conditions, the model must be able to account for those differences. Otherwise, different models would be required for every possible environment. Linear cumulative damage modeling does just that. The model uses results from different types of tests and combines them to predict growth rates under a variety of possible test conditions. While not always successful, this type of modeling has been quite accurate for predicting crack growth in some alloys (22:12). Accurate crack growth predictions can lead to a longer useful life for expensive components.

Linear elastic fracture mechanics (LEFM) has been widely used to predict useful life at lower temperatures. As operating environments in the jet engine turbines become increasingly hostile due to higher temperatures, the increased size of the plastic zone in front of the crack tip can make the application of LEFM to crack growth prediction questionable (5:1). Crack growth in a number of nickel-based superalloys tested at elevated temperatures has been successfully characterized with LEFM parameters, but since different materials can react differently to high temperature environments, each must be tested to determine what, if any LEFM parameters can be used to describe crack growth.

Crack growth at elevated temperatures has been shown to be cycle dependent, time dependent, or a combination of the two called mixed mode (17:86). The dominant factor contributing to crack growth depends on the alloy and the test conditions. Factors like temperature, environment, frequency, hold time, and applied load can significantly affect crack growth. These factors are discussed in more detail in section II.

## Objective

Titanium-aluminide alloys are currently being considered for high temperature jet engine structures.  $Ti_3Al$  is a high strength, high temperature, low density material. These properties are essential to produce rotating turbine structures (10:1). Before it can be used in these structures, however, its fatigue and fracture characteristics must be understood.

This study investigates crack growth in  $Ti_3Al$  at elevated temperatures under sustained load and sustained load with periodic fatigue cycles under isothermal conditions in a laboratory air environment. Crack growth under sustained loads with periodic fatigue cycles represents a condition of constant speed and constant temperature in a jet aircraft turbine (22:1). The sustained load tests will be used to characterize the creep crack growth behavior of  $Ti_3Al$  at elevated temperatures. A fatigue test at elevated temperature will be conducted to determine baseline fatigue crack growth rates. Data from sustained load tests with periodic fatigue cycles will be compared with the baseline data from the sustained load and fatigue tests to determine the applicability of linear cumulative damage modeling to crack growth rates in  $Ti_3Al$  at elevated temperatures. The resulting model, if successful, could then be used as a tool to help determine time-to-failure for a component with an existing flaw.

## Scope

The American Society for Testing and Materials currently has no standard for evaluating creep crack growth behavior at elevated temperatures (20:4). Studies have identified a number of parameters to correlate crack growth in materials at elevated temperatures. Sadananda and Shahinian (18:327,16:439) have identified the linear elastic stress intensity factor,  $K$ , the non-linear elastic parameter,  $J^*$  integral, the  $C^*$  energy integral, and reference stress,  $\sigma_{ref}$  to name but a few. Studies on crack growth behavior in Inconel 718 by Miller, Harms, and Heil (12:49, 8:119, 9:105) have successfully used the stress intensity factor,  $K$ , as a correlating parameter for sustained load, thermal fatigue, and mechanical fatigue in that alloy. Those studies have also proven the applicability of linear cumulative damage modeling to predict crack growth rates under a variety of loading and temperature conditions in Inconel 718, but no effort has been made to determine the applicability of linear cumulative damage modeling to  $Ti_3Al$ .

A study by Pernot and current research by Burgess on crack growth in  $Ti_3Al$  has concentrated on fatigue crack growth at elevated temperatures and thermal-mechanical fatigue crack growth at temperatures below 650° C (14:59). No studies were found relating to creep crack growth in this alloy or to crack growth under sustained load with periodic fatigue cycles, especially at elevated temperatures. This study will, therefore, investigate crack growth in  $Ti_3Al$  under sustained load at elevated temperatures. Since differing specimen geometry can affect crack growth rate, all testing will be limited to specimens with the same geometry, in this case, the compact tension geometry.

## Approach

Nine standard compact tension (CT) specimens were tested. Since different mechanical behavior has been found in tests from different batches of the same alloy (15:685-703), all specimens tested were cut from the same plate to eliminate possible material differences as a source of error. Isothermal sustained load and fatigue tests were conducted on the specimens to generate baseline crack growth rates under these conditions. The specimens were tested at 700° C, 750° C, and 800° C under sustained load conditions to characterize creep crack growth behavior and to generate a baseline creep crack growth rate model for the Ti<sub>3</sub>Al alloy at elevated temperatures. The experimental equipment and procedures used for these tests are described in sections 3 and 4 respectively; test results are presented in section 5.

A fatigue test and several sustained load tests with periodic fatigue cycles (hold time tests) were conducted at 750° C with a frequency of 0.1 Hz and a load ratio of 0.3. The tests with periodic fatigue cycles used hold times of 2, 5, and 10 minutes. The baseline data from the fatigue test and the 750° C sustained load test was modeled using the stress intensity factor,  $K$ , as a correlating parameter. These models were then combined using linear cumulative damage modeling techniques to predict crack growth rates for sustained load tests with periodic fatigue cycles. Damage model development is explained in more detail in section 6. These results were compared with hold time tests conducted on the alloy to verify the accuracy of the model.



## II. Elevated Temperature Crack Growth

This study investigates crack growth in  $Ti_3Al$  at elevated temperatures. A better understanding of fracture mechanics is required as design practices lead more and more to a damage tolerant approach instead of a damage resistant approach. At higher temperatures, components can fail from the propagation of single cracks subjected to cyclic, static, or combined loading (18:327). A single crack can grow due to stress concentrations caused by bending moments, thermal stresses, or existing flaws (17:87). In their review of crack growth at elevated temperatures, Sadananda and Shahinian concluded that crack growth at elevated temperatures can be due to time-dependent processes, cycle-dependent processes, or a combination of the two (17:103).

The time-dependent process is due to creep effects or environmental effects. Cycle-dependent crack growth is primarily due to fatigue damage which provides a driving force for crack growth (17:88). The third process, mixed-mode, is dominated by neither of the two previous processes. The mixed-mode process is the most difficult to analyze since the interactions between the time and cycle-dependent processes can cause crack growth rates to increase or decrease depending on the test conditions (17:104).

Saxena and Bassani reviewed a number of variables which determine crack growth behavior at elevated temperatures. In their review, they found that loading frequency (and hold time) had a significant affect on elevated temperature crack growth. The relationship between loading frequency and crack growth rate is shown in Figure 1 (19:363).

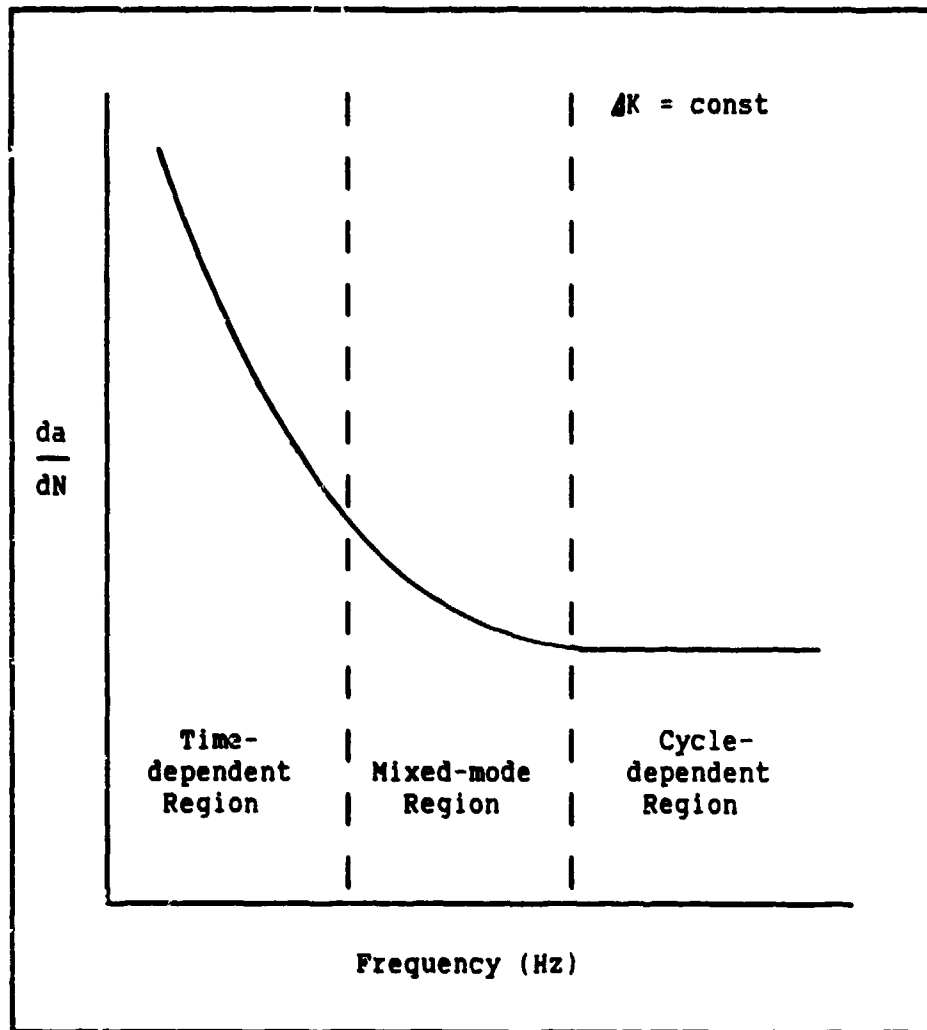


Figure 1. Frequency Dependence of Crack Growth Rate

#### Time-Dependent Crack Growth

Time-dependent crack growth at elevated temperatures is usually due to creep effects, environmental effects, or combinations of the two (17:87). Creep crack growth results from a balance between high stress intensities at the crack tip resulting in crack growth and plastic deformation which blunts the crack tip retarding growth (16:449).

Environmental factors include temperature and thermally activated processes like oxidation. Environmental factors can tend to increase or decrease crack growth depending on the material.

There are essentially two types of creep crack growth: creep-ductile and creep-brittle. Crack growth occurs when the processes contributing to crack growth are greater than those retarding crack growth (17:103). The creep-ductile material is characterized by a large plastic zone around the tip, causing high crack tip stresses to relax quickly (6:39, 18:331); crack growth can only occur if the crack tip can move forward before the plastic flow around the crack blunts the crack tip (17:103). Crack growth in creep-ductile materials can only be analyzed with nonlinear methods (17:105). In the case of a creep-brittle material, crack growth occurs under small scale viscoplasticity. Local rupture usually occurs before the stresses at the crack tip can be relaxed, indicating that linear elastic fracture mechanics can be used to characterize crack growth (4:141, 6:47, 17:105, 18:330,338). Sustained load crack growth rates at elevated temperatures in several nickel based superalloys have been successfully analyzed using stress intensity as a correlating parameter (16:439).

Increased temperature usually increases the crack growth rate for a given alloy, since it lowers the elastic modulus of the material. The decrease in yield stress caused by increased temperatures, however, can cause increased plasticity, decreasing crack growth rates. Tests on Inconel 718 have shown increased crack growth rates from 425° to 650° C and then a decrease in the crack growth rate at 760° C due to plastic deformation at the crack tip retarding the crack growth (16:443,

17:87,96, 18:341). Other tests have shown that crack growth rates in oxygen environments are much faster than in a vacuum. The increased crack growth rates are caused by oxidation of the area around the crack tip, creating additional stresses or weakening the material at the crack tip (19:367).

#### Cycle-Dependent Crack Growth

Cycle-dependent crack growth at elevated temperatures is due to fatigue damage which provides a driving force for crack growth. Cycle-dependent crack growth is usually insensitive to variations in temperature (17:87); it is more sensitive to the frequency and shape of the loading and unloading cycles.

As shown previously in Figure 1 crack growth rate is significantly affected by frequency. Saxena and Bassani reviewed a number of studies, and in all cases found that crack growth increases with decrease in frequency or increase in hold time (19:358). In their review of fatigue crack growth behavior they determined that the increase in fatigue crack growth rates was caused by environmental attack or by creep cavitation (19:362-363).

Crack growth rates are significantly affected by the shape of the loading and unloading waveform. In cases where the time for a total cycle is constant, crack growth rates are faster with a slow loading and fast unloading cycle than they are with a fast loading and slow unloading cycle; growth rates for waveforms with equal loading and unloading cycles fall between the two (19:364). Saxena and Bassani attributed the

increased crack growth in the slow loading cycle to time-dependent damage at the crack tip (19:365).

As was the case with time-dependent crack growth, the ability to use linear elastic fracture mechanics to predict crack growth rates depends on the size of the plastic zone around the crack tip. When crack growth rates can be described using LEFM, the crack growth rate,  $da/dN$ , is usually plotted versus the change in stress intensity,  $\Delta K$ , on a log-log plot (Figure 2).

#### Mixed-Mode Crack Growth

Mixed-mode crack growth is not dominated by time-dependent or cycle-dependent processes. Crack growth in this region can not usually be predicted with a linear summation of the individual crack growth processes since interactions between the processes can cause increased or decreased crack growth rates compared to the linear summation of the processes (17:88). The interactive effects are not limited to stress intensities above the threshold value for both time and cycle-dependent crack growth. Studies have shown that these interactive effects can even occur below the threshold stress intensity for one of the processes (17:104). Mixed-mode crack growth usually depends on hold time effects and the amplitude and frequency of the fatigue cycles.

Hold time effects depend on the environment and the applied stress intensity during the hold time. If the applied stress intensity is below the time-dependent threshold stress intensity, environmental degradation can still occur, increasing the crack growth rate; if it is above the threshold stress intensity, crack tip blunting caused by creep

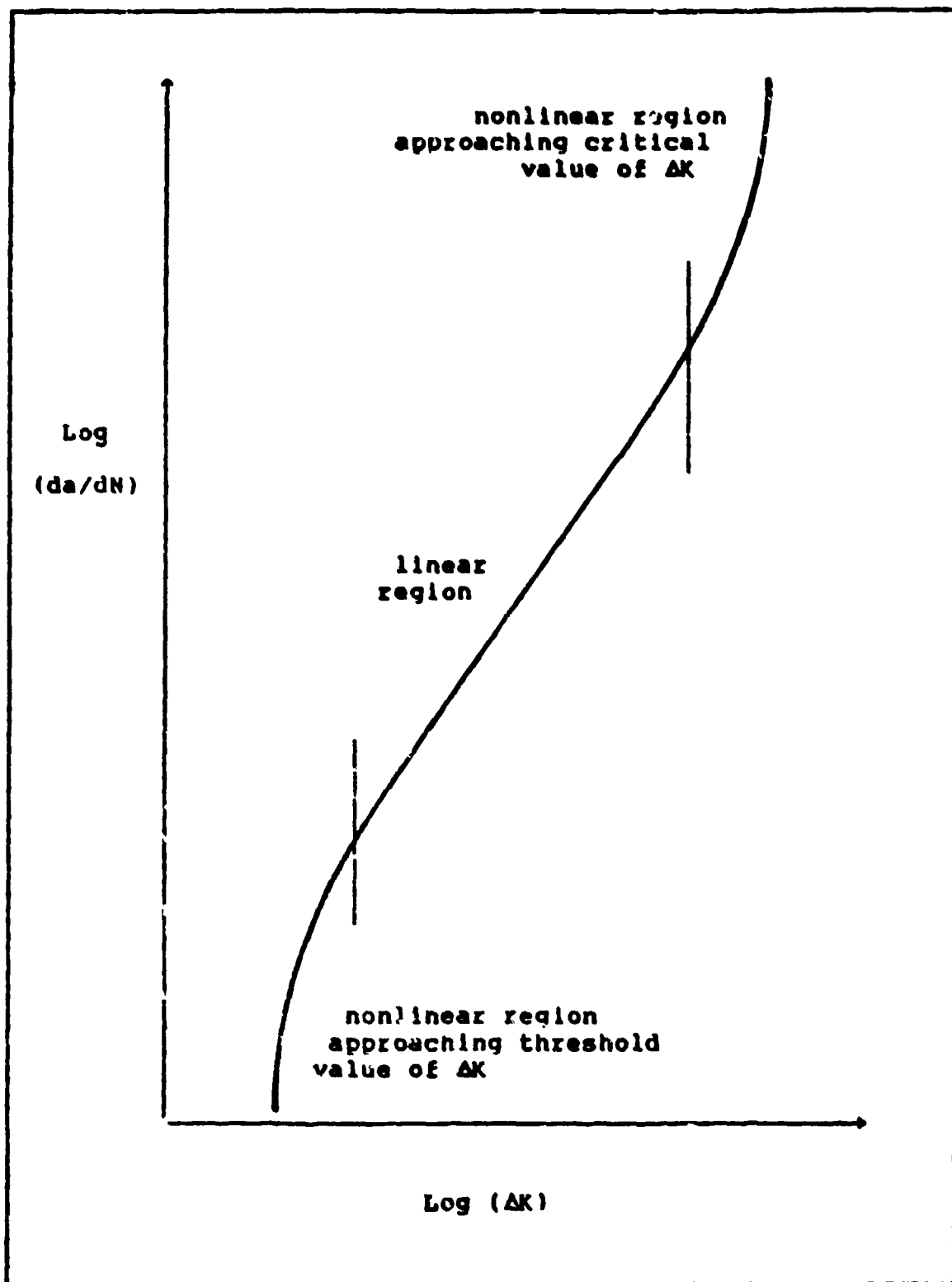


Figure 2. Typical Crack Growth Rate Curve

deformation could retard crack growth (17:95). In tests on Inconel 718, Dibiene and Pineau found that fatigue tests which included a one minute hold time resulted in crack growth rates which were twice the growth rates measured under continuous cycling (4:146).

In studies on Inconel 718 Nicholas et al. found that creep growth following a fatigue cycle can be faster or slower depending on the amplitude and frequency of the fatigue cycle. When creep growth precedes a fatigue cycle, the fatigue growth rate is usually decreased because "steady state" conditions are not achieved before the cycle (13:168). These factors can complicate attempts to model crack growth behavior since a summation of the cycle and time-dependent processes cannot generally describe crack growth under combined loading conditions accurately.

### III. Description of Test Equipment

The objective of this study was to investigate crack growth in  $Ti_3Al$  at elevated temperatures. Standard compact tension (CT) specimens of the alloy were tested using the facilities at the Materials Laboratory (AFWAL), Wright-Patterson Air Force Base, Ohio. The equipment used to test the specimens is described in this section.

The sustained load tests were conducted using an automated creep testing system. Crack length measurements for the sustained load tests were generated manually with visual measurements using traveling microscopes. For the hold time tests, the visual measurements were complemented with data collected from transducers, extensometers, and thermocouples using the automated creep testing system. Since the creep testing system was unable to run a pure fatigue test, the .1 Hz fatigue test was conducted using an MTS test stand. A schematic of the creep system is included in Figure 3 and consisted of the following components:

- 1.) Swedish Creep test frame
- 2.) Link-type load cell transducer
- 3.) Daytronics 9000 Signal Conditioner
- 4.) Digital PDP-11 Microcomputer
- 5.) Clamshell-type resistance furnace with West Controller
- 6.) Two K-type chromel-alumel thermocouples
- 7.) Two Gaertner traveling microscopes
- 8.) MTS extensometer (modified for creep frame)
- 9.) Two Linear Variable Differential Transducers (LVDT)



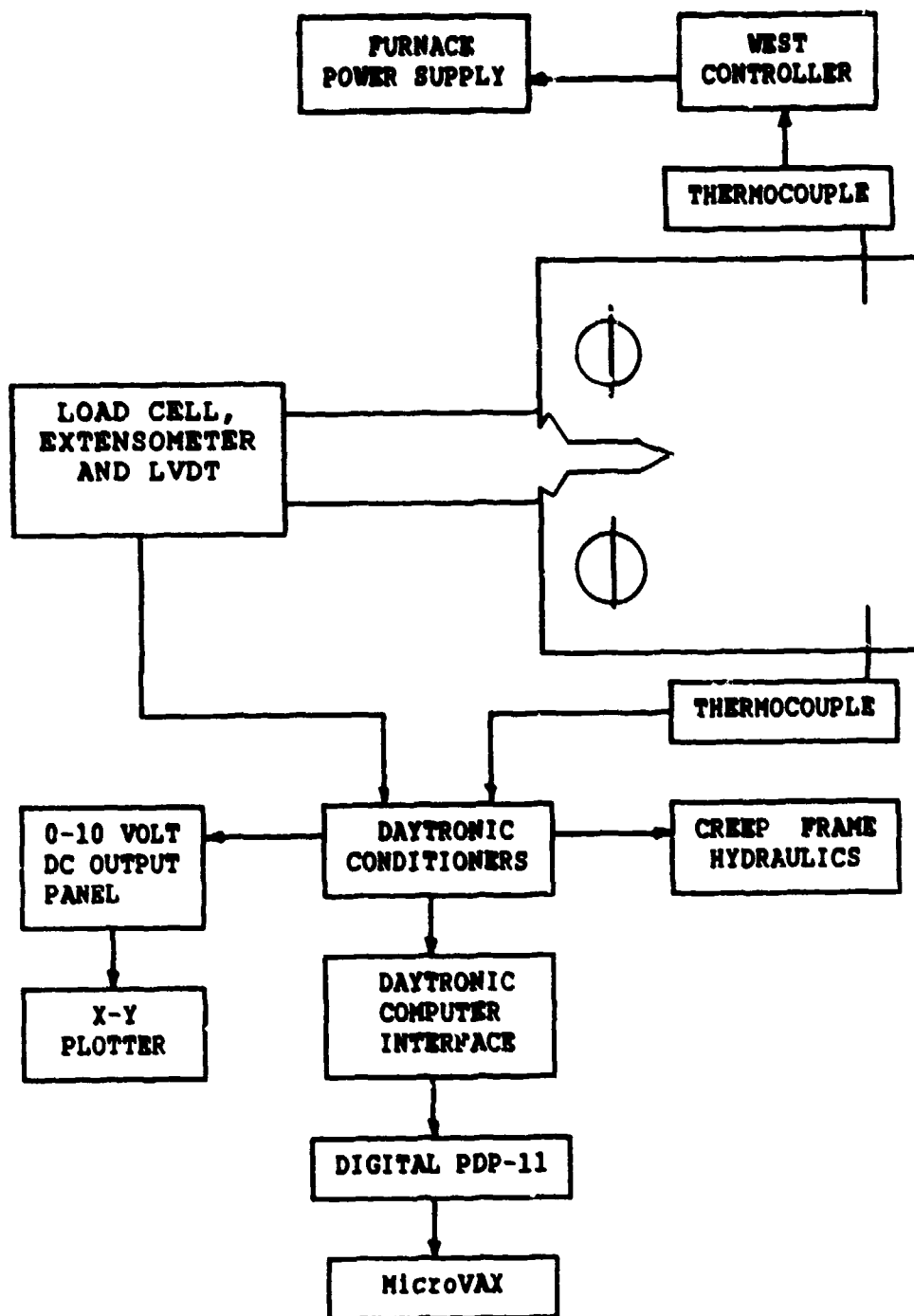


Figure 3. Test System Diagram

For the sustained load (creep) and hold time tests, a 12,000 pound capacity Swedish creep frame was used to periodically load and unload the specimens. The frame has a 20 to 1 lever arm loading ratio with weights suspended on one end and the load train on the other. A hydraulic ram is used to load or unload the specimen by supporting the suspended weights or allowing them to hang freely. The hydraulics can be controlled manually or by signals from the Daytronics 9000 signal conditioner. The load train consisted of two pull bars with grips to hold the specimen, and the specimen. The lower pull bar has a load cell mounted on it to measure the load on the specimen. The creep frame also has mounts for the furnaces and traveling microscopes (Figure 4).

The Daytronics 9000 signal conditioner was essential for the test control and data acquisition. It was the interface between the Digital PDP-11, which monitored and controlled the tests, and the test instrumentation. It amplified the raw test data and provided the necessary instrumentation calibrations. It also sends a 5-volt output signal to the creep frame servo-hydraulics to load and unload a test specimen at the desired time intervals. The Daytronics conditioner scans the data channels at a rate of 15,000 measurements per second and converts the data to -5 V to +5 V analog input for the Digital microcomputer. The Daytronics conditioner is also used to calibrate the instrumentation. For the hold time tests, the following calibrations were used:

LVDT	1 V = 0.025 inches
MTS Extensometer	1 V = 0.0125 inches
load cell	1 V = 2500 pounds
thermocouple	2.17 mV = 1° F



Figure 4. Swedish Creep Frame

The Digital PDP-11 microcomputer was programmed to control and record data for the automated tests. It provides control for and records data from all of the eight creep frames in the creep lab. It can be programmed to periodically unload and load the specimens to apply fatigue cycles or to determine crack length. The microcomputer collects and records test data at regular intervals. It also records data if a measurement changes by a significant (set by user) amount. It does not,

however, calculate crack length from compliance real-time, so visual measurements must be taken at regular intervals to supplement the automated data collection process. Instrument calibration parameters are also preprogrammed, allowing real-time evaluation of a test in progress. Once a test has completed, the data can be stored on disk or transferred directly to the MicroVAX for further processing.

A clamshell-type resistance oven was used to heat the specimens to the desired temperature. The oven has four distinct heating elements powered by a West temperature controller. The power to individual zones could be controlled manually and was typically set at 3 amperes per zone and 130 volts AC. The temperature was monitored by the West controller through one of two K-type chromel-alumel thermocouples welded to the specimen prior to test. The second thermocouple was wired to the Daytronics signal conditioner for direct readout and, if desired, its readings could be stored on the Digital microcomputer. The oven placement on the creep frame can be adjusted to center the specimen.

The oven was equipped with viewing ports on each side to allow visual measurements of the crack length. Gaertner traveling microscopes were mounted on each side of the oven. The clamshell oven and traveling microscope placement can also be seen in Figure 4. Crack lengths were read from a digital readout device wired to the microscopes. While the display showed crack lengths to within a tenth of a mil, readings were generally reproducible to only one mil.

Titanium-aluminide Compact Tension (CT) specimens (Figure 5) were used for all the tests. The chemical composition and material properties for the alloy are included in Appendix A. The exact dimensions

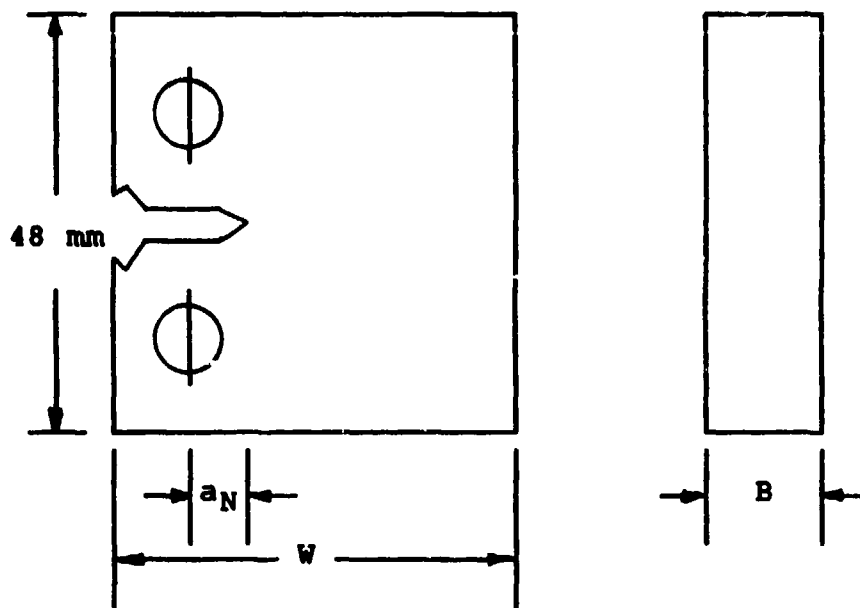


Figure 5. Compact Tension Specimen

Table I. Compact Tension Specimen Dimensions (mm)

Specimen No.	Width (W)	Thickness (B)	Notch Length ( $a_N$ )
88-102	40.03	9.91	6.609
88-104	40.12	9.86	6.789
88-105	40.09	9.81	6.873
88-112	40.23	9.72	6.784
88-113	40.38	9.87	6.731
88-114	40.33	9.73	6.746
88-115	40.53	9.86	6.932
88-116	40.17	9.83	6.840
88-117	40.26	9.69	6.962

for the specimens tested is included in Table I. The specimens were mounted between the load train pull bars with Inconel grips and secured with Inconel pins.

Two types of extensometers were used to determine displacement at various points on the test specimens during the tests, an MTS extensometer measured front face displacements, while an LVDT was used to measure load line displacements. A schematic of the extensometer mounting provisions is included in Figure 6 below. Both extensometers were wired directly into the Daytronics signal conditioner. A mount for the MTS extensometer was attached directly to the creep frame. Seven-inch long quartz rods extended from the extensometer to holes drilled in the front

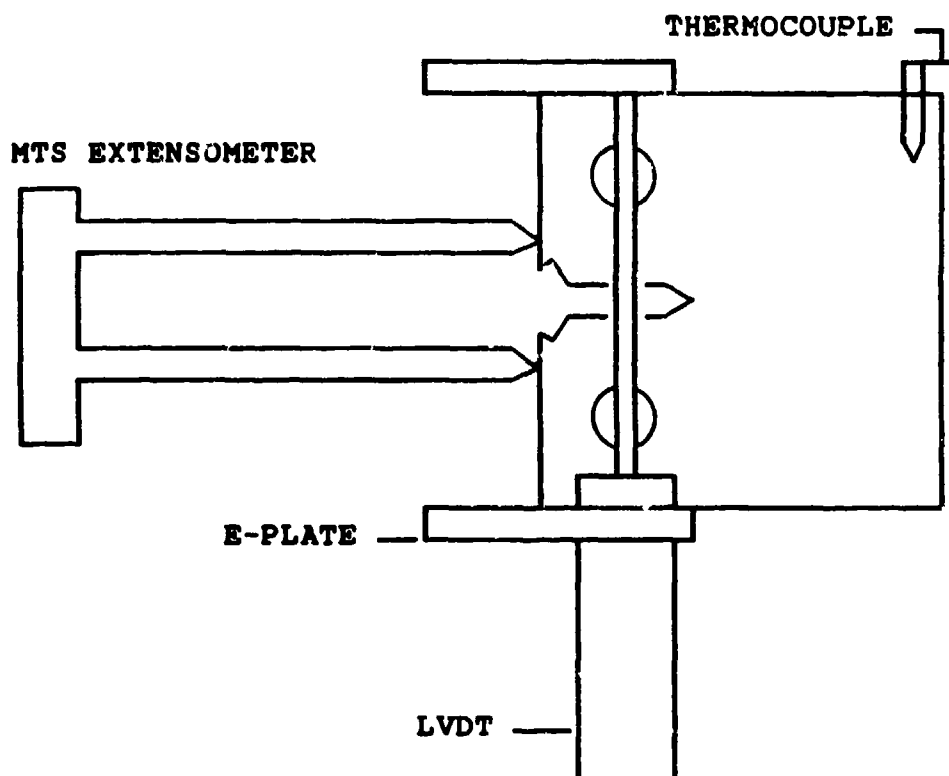


Figure 6. Instrumentation Placement

face of the specimen. The extensometer was air-cooled and held in place by spring tension provided by its mount.

Two more holes were drilled and tapped in the top and the bottom of test specimens along the load line to attach Inconel E-shaped plates which held two stainless steel rod-in-sleeve extension arms with LVDTs mounted at the bottom. The extension rods were required to protect the LVDTs from high temperature. Although LVDTs were mounted on both sides of the test specimen, the automated creep testing could only record data from one because only two channels are available for extensometers for each creep frame. LVDTs have been used extensively in sustained load tests and are a proven method for accurately determining load line displacement (20:I-3). The MTS extensometer, however, has been used primarily in fatigue tests and has not been previously tested on the Swedish creep frames.

Since the creep testing system was unable to perform continuous fatigue cycles, the fatigue baseline test used an MTS servohydraulic system to provide the desired load and frequency spectrum. The MTS system was required because the hydraulics on the Swedish creep frame cannot provide continuous fatigue cycles. The MTS test system used the same clamshell-type oven and traveling microscopes as the creep frame, but used only a single MTS front face extensometer to determine crack lengths from compliance measurements. The MTS system was monitored by a Zenith Z-248 computer. Its software could calculate crack length real-time from compliance measurements, so visual crack length measurements were not required as often as they were for the creep testing system.

#### IV. Test Procedures

##### General

Before the titanium-aluminide specimens could be tested, they required polishing, thermocouple installation, precracking, and extensometer modifications. The titanium-aluminide specimens were polished to a 3 micron finish using successively finer grades of diamond paste to polish them on a polishing wheel. Polishing was required to make the crack tip easier to see so it could be measured optically. Once polished, two K-type thermocouples were welded to the specimen (Figure 6). These were later connected to the West temperature controller and to the Daytronics signal conditioner. Small clamps also were welded to the back of the specimen to secure the thermocouple wires. The specimens were then fatigue precracked using an MTS servohydraulic control system. Precracking parameters are included in Appendix B. For the extensometer, two small indentations were drilled about 10 millimeters apart on the front face of the specimens (Figure 6). These indentations kept the quartz rods from shifting and detaching during the periodic fatigue cycles. Two small holes were also drilled on the top and bottom of the specimen along the load line to secure the E-plates which held the LVDTs.

Three types of tests were conducted; they included sustained load tests, a fatigue baseline test, and sustained load tests with periodic fatigue cycles (hold time tests). Typical load versus time profiles for each are included in Figure 7. Table II contains a complete list of the tests performed on each specimen and the test parameters used.



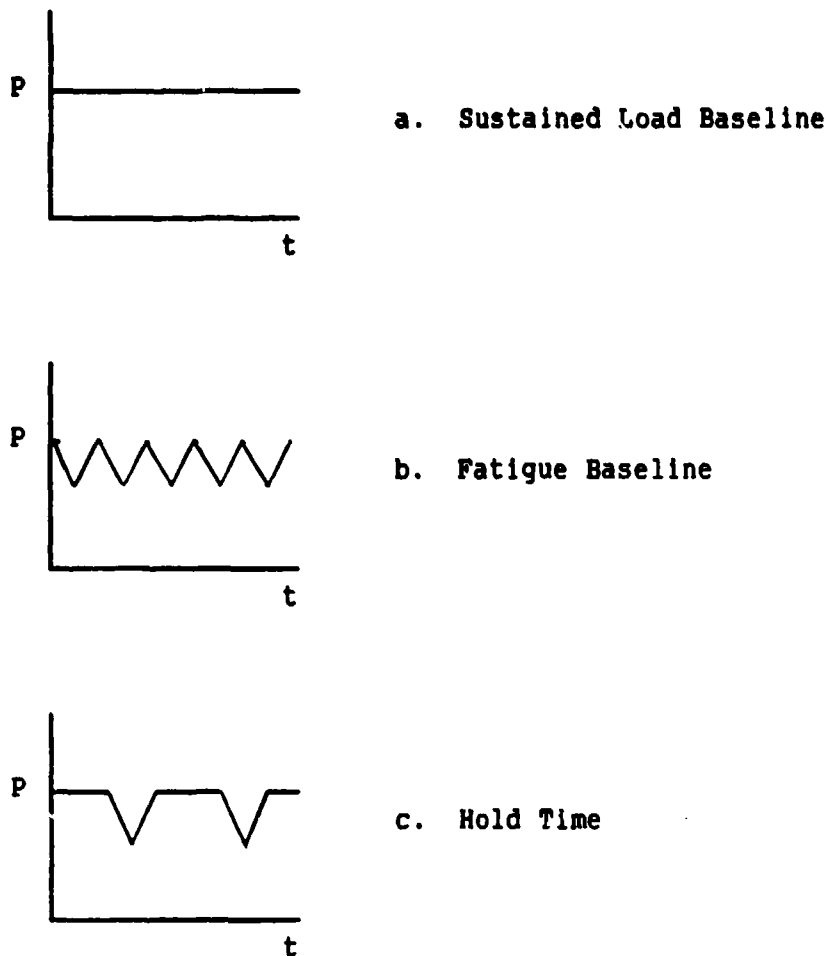


Figure 7. Types of Tests

Crack lengths were measured using two methods: direct optical measurements and from crack opening displacement compliance relations. The optical measurements were made using Gaertner traveling microscopes on each side of the specimen. Measurements were made using the notch as a reference point; the crack length from the notch was read directly from a digital display connected to the microscope. Visual measurements are undesirable since they require personal supervision throughout the

Table II. Test Matrix

Specimen No.	Temperature °C	Comments
88-102	750	Creep 22 MPa/ $\sqrt{a}$ start
88-104	800	Creep 22 MPa/ $\sqrt{a}$ start
88-105	700	Creep 25 MPa/ $\sqrt{a}$ start <sup>1</sup>
88-112	700	Creep 25 MPa/ $\sqrt{a}$ start
88-113	750	.1 Hz R=0.3 2 minute hold
88-114	750	.1 Hz R=0.3 5 minute hold
88-115	750	.1 Hz Fatigue R=0.3
88-116	750	.1 Hz R=0.3 10 minute hold
88-117	750	.1 Hz R=0.3 10 Minute hold <sup>2</sup>

**Notes**

1. Thermocouple failed 10 hours into test. Specimen reached 850°C before anomaly discovered and corrected. Repeated test on Specimen 88-112.
2. Hydraulic failure 11 hours into test. Extensometer misranged, no usable data recovered.

test to insure data is collected. Crack opening displacement (COD) compliance relations, on the other hand, can be collected and stored by a computer thus reducing the need for personal supervision (11:1).

Compliance is the crack opening displacement per unit load. For the hold-time tests, the crack opening displacement was measured along the load line using LVDTs and along the front face with the MTS extensometer. The load versus crack opening displacement curves are generated by periodically unloading and reloading the specimen during the test. A typical load versus displacement curve is shown in Figure 8. The figure shows that the crack opening displacement doesn't immediately return to the displacement measured prior to the unload cycle. This occurred every time the load-displacement curves were plotted during the tests, and is attributed to crack closure. For this reason, the slope of the unload curve is used to calculate compliance. Compliance is the inverse of the slope of the curve (11:9). The mathematical relations used to calculate crack length from compliance are presented later in this section.

A third method for determining crack length, electric potential (EP) drop, is currently being evaluated for use in the creep lab. Pernot used this method to determine crack lengths in CT specimens during thermal-mechanical fatigue testing (14:12). In this method, a constant current is applied to the specimen. As the crack gets longer, the voltage across the specimen drops. This voltage drop can be calibrated as a function of crack length. This method, too, requires less supervision than the visual method, since the voltages can be measured and stored on computer.

Only one previous sustained load crack growth test had been conducted using  $Ti_3Al$ . Dr. M. Khobaib, UDRI, had tested one specimen at  $650^{\circ}C$  but no creep crack growth was evident even at high stress intensity. Based on this data,  $700^{\circ}C$ ,  $750^{\circ}C$ , and  $800^{\circ}C$  were chosen as baseline test temperatures. Results from these tests were then used to determine the temperature for the baseline fatigue test and hold time tests.

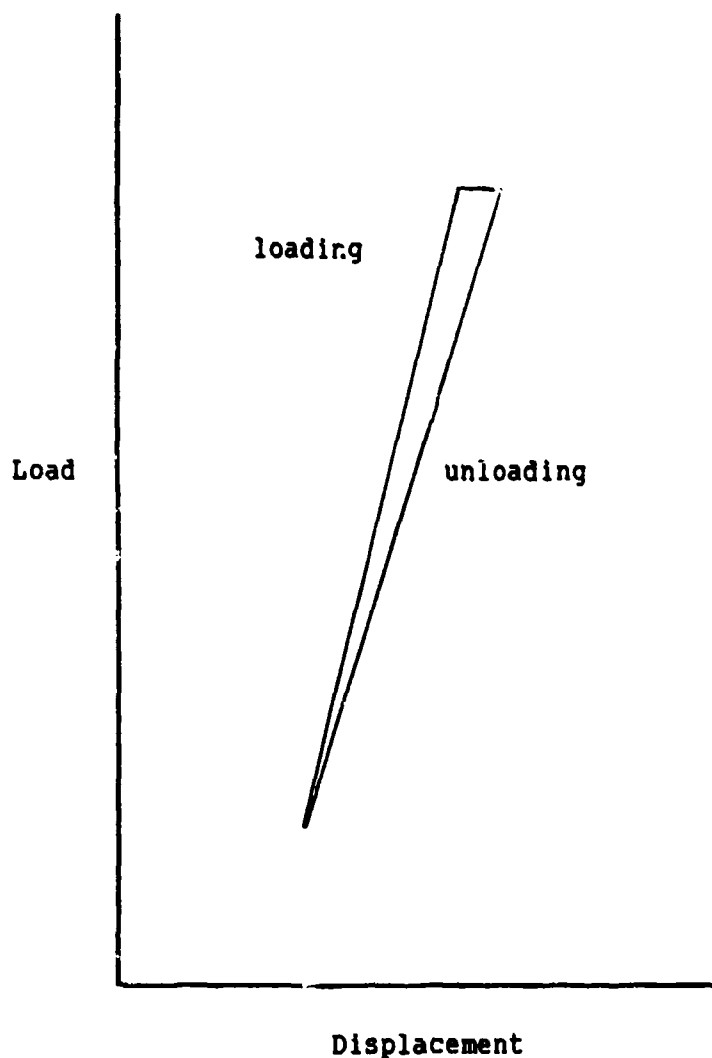


Figure 8. Typical Compliance Curve

### Sustained Load Tests

Once a specimen was prepared, it was mounted on the load train and the oven was secured around it. Before the oven was turned on, each thermocouple was tested using the Daytronic signal conditioner to insure proper operation. The power for each zone was then adjusted to provide three amps current to each zone. The sustained load tests did not use the LVDTs or the extensometer since crack length measurements from compliance would require fatigue cycles which could bias the crack growth rate data. Instead, crack lengths were measured optically using traveling microscopes on each side of the test specimen.

At the end of each day, the specimen temperature was reduced to 500° C and the load was removed. These steps insured crack length measurements could be made for all stress intensities. The initial stress intensity levels, also based on Dr. Khobaib's results, are contained in Table II. The desired stress intensity level was required to determine the load suspended on the creep frame. The relation between stress intensity, crack length, and load for a standard compact tension specimen (3:181) is:

$$K = \frac{P(2+a/W)}{B\sqrt{W(1-a/W)^{3/2}}} \left[ 0.886 + 4.64 \frac{a}{W} - 13.32 \left( \frac{a}{W} \right)^2 + 14.72 \left( \frac{a}{W} \right)^3 - 5.6 \left( \frac{a}{W} \right)^4 \right] \quad (1)$$

where

K = Stress Intensity Factor

P = Applied Load

B = Specimen Thickness

W = Specimen Width

a = Total Crack Length

The total crack length,  $a$ , is the sum of the notch length,  $a_N$ , the optically measured crack length from the notch,  $a_{opt}$ , and the tunneling correction,  $a_t$ . At the end of each test, the specimens were examined for signs of crack tip tunneling (Figure 9). This could be easily measured since heat tinting of the crack surface made the tunneling effect clearly visible.

Using the correction factor recommended in ASTM E872 (1), five measurements were made from the notch to the tinted regions on the specimens. Usually, two or three clearly defined regions could be measured on each specimen starting, on average, 12 mm from the notch. The tunneling which occurred during the fatigue precrack could also be easily measured since the surface of the precrack was much smoother than the fracture surface formed by sustained load crack growth. The tunneling correction was then determined using the following equations:

$$a_{opt} = \frac{a_1 + a_5}{2} \quad (2)$$

$$a_{avg} = \frac{a_{opt} + a_2 + a_3 + a_4}{4} \quad (3)$$

$$a_t = a_{avg} - a_{opt} \quad (4)$$

As with tests on Inconel 718 (7:19-21), the tunneling correction did not vary through the thickness after the first measurable tinting, nor did it vary significantly with test temperature. The average measured tunneling correction during sustained load crack growth was 2.286 mm, which was very significant since the correction measured for the fatigue precrack was less than 0.1 mm. The correction for Inconel 718 was only .68 mm (7:21). Since only the surface crack could be measured using the traveling microscope, there was no way to determine how the tunneling proceeded from the precrack to the 2.29 mm correction measured 12mm from the notch, so only the 0.1 mm fatigue correction is reflected in the data. This problem is discussed further in section 5.

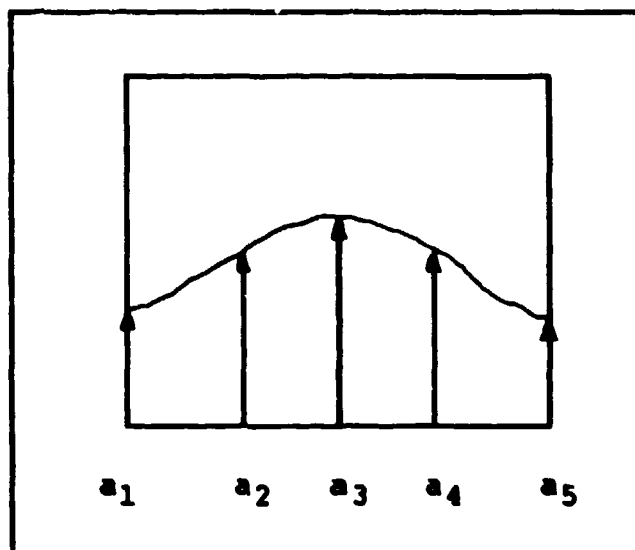


Figure 9. Crack Tip Tunneling

ASTM E647 (1:708,709) recommends the following intervals for crack length measurements:

$$\Delta a \geq 0.002 W \text{ for } 0.25 \leq a/W \leq 0.60$$

$$\Delta a \geq 0.001 W \text{ for } a/W > 0.60$$

Visual measurements were normally taken every 30 minutes during a test, but this frequency changed depending on crack growth rates. During periods of very slow growth, usually at the start of the test, measurements would be recorded an hour apart; near the end of a test, when crack growth was more rapid, measurements would be made as close as 10 minutes apart. These time intervals usually conformed the ASTM recommendations. Time and crack length data were then transferred to disk for further processing. Plots of crack length versus time for each of the specimens tested is included in Appendix C. Data analysis is discussed later in this section.

The 800° C baseline sustained load test resulted in extensive deformation of the test specimen, so 800° C was ruled out as a candidate for the fatigue and hold time tests. The tests performed at 700° C and 750° C showed no such problems. Since only a limited number of specimens were available, 750° C was selected for the fatigue baseline and hold time tests.



### Fatigue Baseline Test

A fatigue test was needed to determine the crack growth rate in  $Ti_3Al$  when subjected to cyclic loading at elevated temperatures. Data from this test would then be used for the cycle dependent portion of the linear cumulative damage model. Test procedures for the fatigue baseline test are explained below.

The fatigue baseline test was performed on an MTS servohydraulic test system since the Swedish creep frame is unable to perform a continuous fatigue cycle. The load reduction and frequency spectrum were also chosen to meet the capabilities of the creep frame. The load ratio was chosen at 0.3 because lower load ratios could cause shifting in the creep frame load train, dislodging the front face extensometer. The 0.1 Hz frequency was chosen because it can match the time required for the creep frame hydraulics to load and unload a specimen.

The specimen was placed in the load cell and instrumented with a single front face extensometer. The MTS extensometer has been used extensively in this configuration, so LVDTs were not required. The initial stress intensity selected was a  $12 \text{ MPa}\sqrt{m}$  load and then it was slowly shed during the test to  $8 \text{ MPa}\sqrt{m}$  to help determine the threshold stress intensity,  $K_{th}$ ; thereafter, the test was continued at a constant maximum load. The software monitoring the test calculated crack length directly from compliance measurements, so only occasional visual measurements were required. The relation used to calculate crack length from compliance measured on the front face of a standard CT specimen is (11:12-13):

$$a = W(1.001 - 4.6695U^{-1} + 18.46U^{-2} - 236.82U^{-3} + 1214.9U^{-4} - 2143.6U^{-5}) \quad (5)$$

where:

a = crack length

W = specimen width

U = (E\*B\*C)<sup>h</sup>

E = effective modulus at test temperature

B = specimen thickness

C = compliance

The MTS software could record crack lengths at specific time or at crack length intervals; for this test, crack lengths were recorded for every 2 mils of crack growth. At the same time, load, number of cycles, compliance, specimen identification, and effective modulus were also recorded. Once the test was completed, the data file was transferred to the microVAX for further processing. Since crack lengths calculated from compliance account for tunneling, no correction was needed.

#### Hold Time Tests

The hold time tests performed two functions. They provided a measure of the interaction between creep and fatigue crack growth in Ti<sub>3</sub>Al at elevated temperature, and they could be used to verify the linear cumulative damage model. The test procedures used to conduct hold time tests on Ti<sub>3</sub>Al are explained below.

The hold time tests were conducted using the Swedish creep frame. The specimens were mounted the same manner as they were for the creep

tests, except E-plates were now mounted on the specimen to support the LVDTs. Small rectangular holes needed to be cut in the front and back of the oven to allow for installation of the MTS extensometer. The front hole allowed two quartz rods to extend to the specimen from the extensometer. The hole in the back was needed to install another quartz rod which would maintain pressure against the back of the specimen. This pressure reduced the horizontal motion of the specimen during unload cycles so the extensometer wouldn't slip off. The mount holding the MTS blocked one of the viewing ports in the side of the oven, so visual measurements could only be made from one side of the oven.

Once the specimen was installed, the extensometer, an LVDT, and the thermocouples were connected to the Daytronics signal conditioner and the oven was heated to 750° C. Once at temperature, the automated creep test program was started and the first fatigue cycle was commanded. The duration of unload and load cycles were measured to insure a 0.1 Hz frequency with a triangular waveform to match the fatigue baseline test. Adjustments were made, as necessary, to valves controlling the creep frame hydraulic actuator to change the duration of the unload and load cycles. These cycles were checked periodically during a test to insure subtle changes in the hydraulic pressure supply did not alter the desired response.

The automated program recorded temperature, load, and compliance (both front face and load line) at ten minute intervals for all the hold time tests. In addition, the compliance was calculated and recorded each time the specimen was unloaded and loaded. Three different hold times were evaluated: 2, 5, and 10 minutes. These durations were chosen

to evaluate relatively short, intermediate, and long hold times. Crack length from compliance on the front face was still calculated using equation 5. For compliance measured on the load line the polynomial expression for crack length is (11:12-13):

$$a = W(1.0002 - 0.632U^{-1} + 11.242U^{-2} - 106.04U^{-3} + 464.33U^{-4} - 650.68U^{-5}) \quad (6)$$

where:

a = crack length

W = specimen width

U =  $(E \cdot B \cdot C)^{1/2}$

E = effective modulus at test temperature

B = specimen thickness

C = compliance

The material properties for  $Ti_3Al$  as a function of temperature are included in Appendix A. As mentioned earlier, the automated creep program did not calculate crack length real-time, so visual measurements were made as frequently as they were for the sustained load tests to verify the compliance data collected. The hold time tests, however, were allowed to run overnight since the visual measurements only needed to supplement the compliance measurements. Once the tests were completed, the data was transferred to the VAX where it was sorted and analyzed.

## Data Analysis

Post test data analysis was hampered by problems involving the calculation of crack length from compliance. Load line compliance data was scattered for crack lengths less than 16 millimeters and front face compliance measurements produced no usable data.

A number of factors can make crack length determination difficult for short crack lengths; these factors include transducer range, signal noise, and instrumentation limitations. Any or all of these factors can combine to cause experimental scatter in compliance measurements, thus degrading the accuracy of the calculated crack length.

The load cell on the creep frame is rated for a 12,000 pound capacity load. During the tests, the maximum load used was just under 1,800 pounds; compliance measurements reduced the load to 30 percent of the maximum weight. This meant the load cell was measuring data in the lower 15 percent of its operating range for all of the tests. The lowest weight during a compliance was only 300 pounds or 2.5 percent of the cell's rated limit. The load cells are calibrated for the limit loads, in this case, 2500 pounds per volt, during the experiments, the weight measured by the load cell was typically in error by as much as 10 percent. Signal noise also adds to the error.

Load information on the PDP-11 terminal was displayed and updated constantly during the testing. During some periods, the calculated load (based on the load cell signal) would shift as much as 100 pounds from one update to the next, only seconds apart. While such dramatic shifts in the data were not common, shifts of 20 to 30 pounds in the displayed load were much more frequent and represent nearly 10 percent of the

lower load limit when the specimen is unloaded. Some additional error can also be attributed to the LVDT.

Previous testing with LVDTs has shown that frictional effects occur when an oxide layer builds up on the extension rods at high temperatures (4:29). This effect is most noticeable at shorter crack lengths since shorter displacements occur and the effects of friction are more pronounced. Figure 10 shows a comparison of calculated crack length from compliance with visual measurements for the 10 minute hold time test. The effect of experimental scatter can clearly be seen at the shorter crack lengths where the calculated crack length is shorter than the visual crack length. The plot also shows that occasionally, the calculated crack length gets shorter with time. Since the crack growth rate is calculated from the slope of the crack length curve, the experimental scatter effects the calculated crack growth rate even more. The MTS extensometer had more serious problems, due more to its installation than to its operation.

The MTS extensometer provided no usable data in any of the tests using it. While some of its inaccuracies can be attributed to the problems with the load cell mentioned above, the primary problem was due to the difference between the creep frame and the MTS servohydraulic system. The load train on the MTS system is rigid, allowing only one degree of freedom for the test specimen. The load train on the creep frame is over 10 feet long and supported by knife edges at both ends, allowing a horizontal and rotational degree of freedom in addition to the vertical (COD). The Horizontal component was eliminated by spring tension provided by the extensometer on the front face and a counter

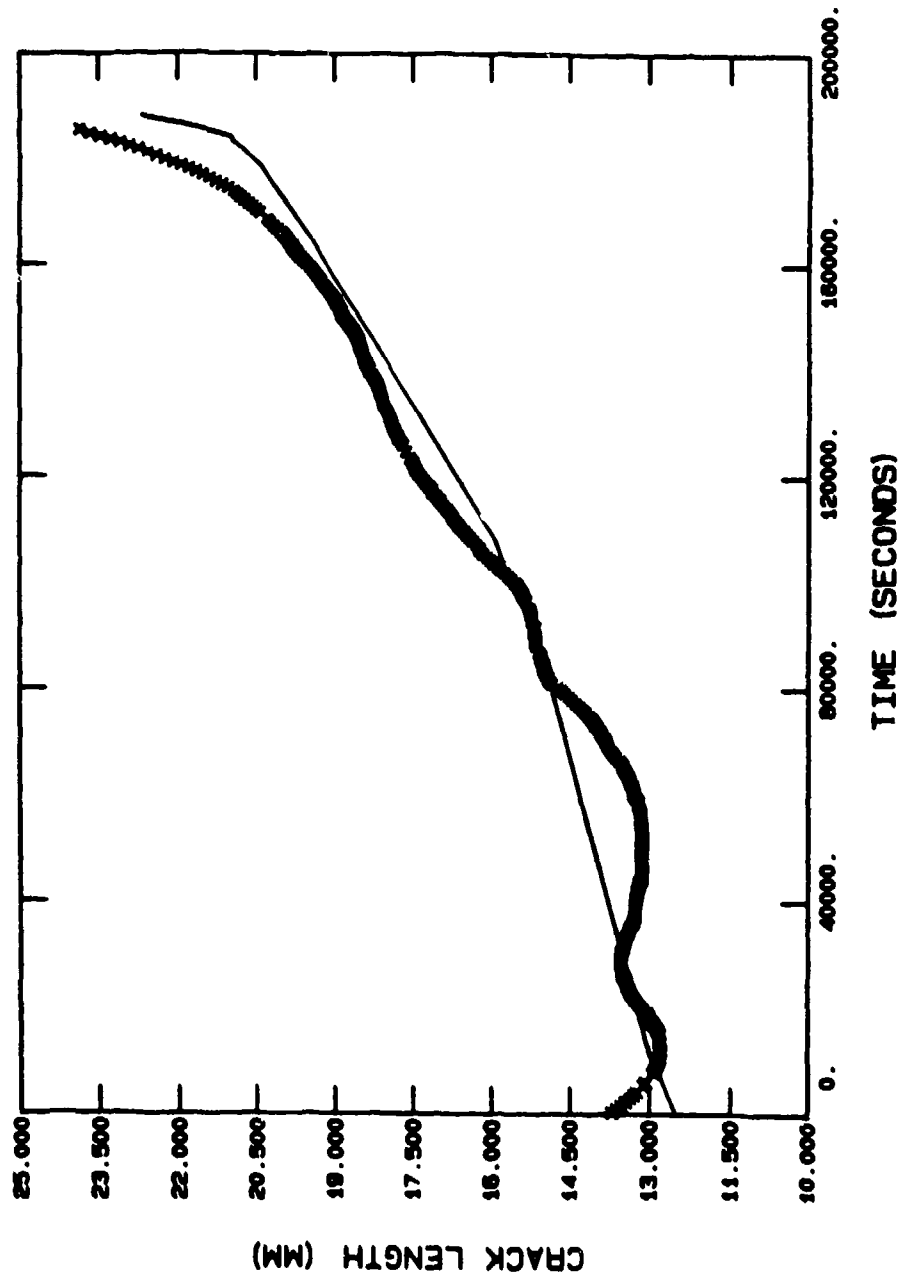


Figure 10. Comparison of Crack Length Calculated from Compliance with Visual Measurements

force on the rear. The rotational effect, clearly visible during compliance, effectively masked front face crack displacement readings.

Error caused by experimental scatter was reduced by editing out obvious outlying points in the data file and by smoothing the remainder of the data with a sliding least square polynomial fit. This method is also used to smooth data from visual measurements as well. The most common polynomial fit is similar to the seven-point polynomial recommended in ASTM E-647. The equation for the polynomial is:

$$a_i = b_0 + b_1(N_i - C_1)/C_2 + b_2((N_i - C_1)/C_2)^2 \quad (7)$$

with

$$-1 \leq (N_i - C_1)/C_2 \leq 1$$

where

$a_i$  = fitted crack length at time or cycle  $N_i$

$b_0, b_1, b_2$  = regression parameters determined by least squares

$N_i$  = current cycle or time

$C_1 = (N_{i-n} + N_{i+n})/2$

$C_2 = (N_{i+n} - N_{i-n})/2$

3 for 7-point fit

$n = 7$  for 15-point fit

10 for 21-point fit

Since comparison of crack growth rates both as a function of time and frequency were desired, the recorded time or cycle data had to be adjusted to include both the number of cycles and the elapsed time in the test. For the fatigue test, the elapsed time was calculated by



dividing the number of cycles by the frequency. For the hold time tests, the number of cycles was calculated by dividing the elapsed time by the time between cycles.

The crack growth rate can be determined by differentiating the least squares polynomial generated to smooth the crack length data. The resulting crack growth rate equation is:

$$\frac{da_i}{dN} = \frac{b_1}{C_2} + \frac{2b_2(N_1 - C_1)}{C_2^2} \quad (8)$$

where

$$\frac{da_i}{dN} = \text{crack growth rate (time or cycle) at } a = a_i$$

Figure 11 compares the crack growth rate for the 750° C sustained load test calculated with a 3 and 15 point sliding polynomial, showing how the scatter is reduced by the polynomial. The stress intensity factor for a given crack length is calculated using equation 1 restated below and the results are plotted on a log-log scale. Figure 11 shows crack growth rate versus stress intensity plotted for the three sustained load tests. Because experimental scatter induced a significant amount of error into the crack lengths calculated from compliance, all future graphs are based on visual crack length measurements unless stated otherwise.

$$K = \frac{P(2+a/W)}{B\sqrt{W}(1-a/W)^{3/2}} \left[ 0.886 + 4.64 \frac{a}{W} - 13.32 \left(\frac{a}{W}\right)^2 + 14.72 \left(\frac{a}{W}\right)^3 - 5.6 \left(\frac{a}{W}\right)^4 \right] \quad (1)$$

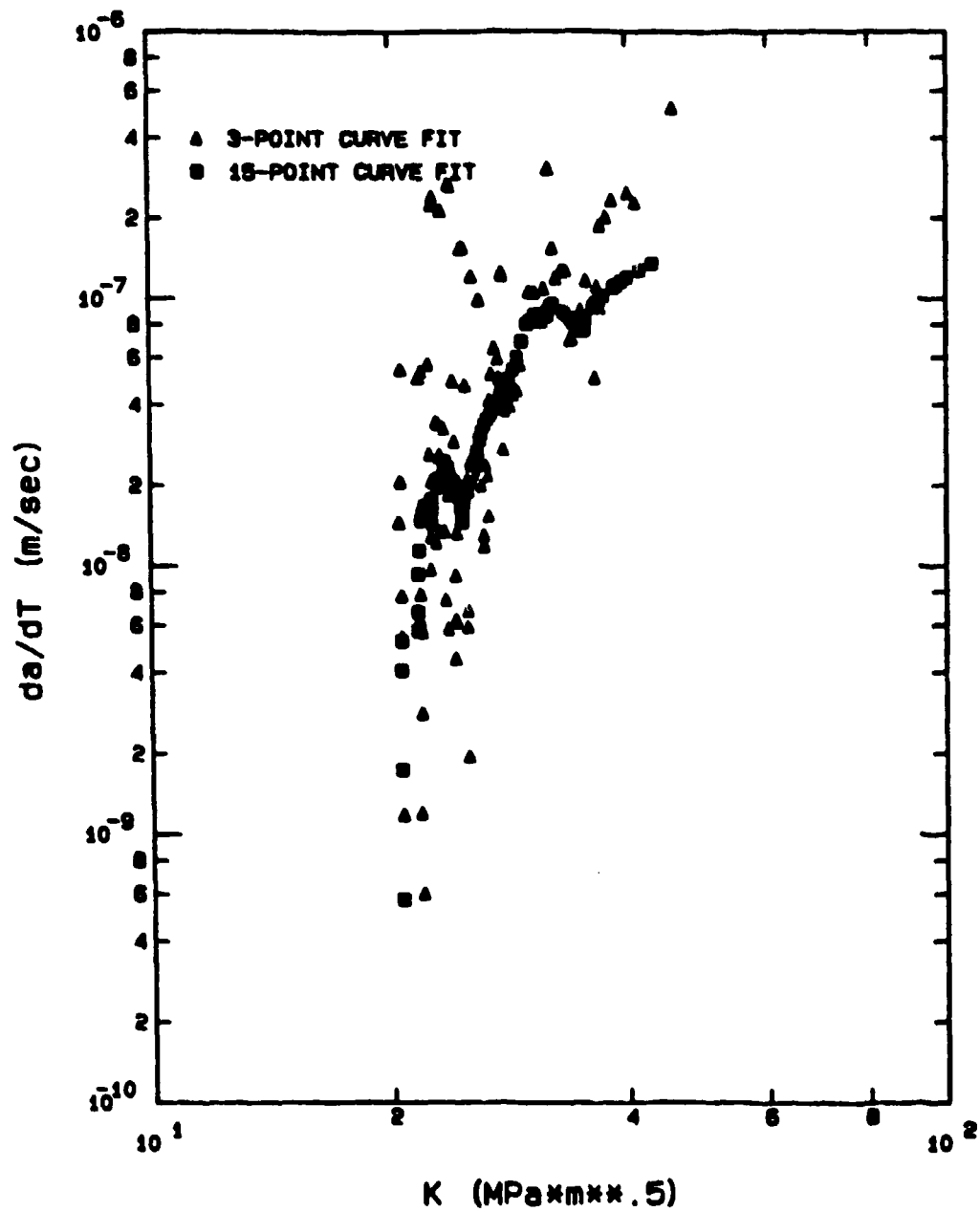


Figure 11. Reduction of Data Scattering with Polynomial Curve Fit

Since all the fatigue cycles used the same load ratios, the crack growth rate per cycle versus maximum stress intensity could be used to compare the different tests. If different load ratios had been used, the crack growth per cycle versus delta stress intensity would be required. The delta stress intensity is calculated using the following equation:

$$\Delta K = \frac{\Delta P(2+a/W)}{B\sqrt{W}(1-a/W)^{3/2}} \left[ 0.886 + 4.64 \frac{a}{W} - 13.32 \left(\frac{a}{W}\right)^2 + 14.72 \left(\frac{a}{W}\right)^3 - 5.6 \left(\frac{a}{W}\right)^4 \right] \quad (9)$$

where

$$\Delta K = \text{delta stress intensity } K_{\max} - K_{\min}$$

$$\Delta P = P_{\max} - P_{\min}$$

While they were not used for this investigation, plots of crack growth rate per cycle versus delta stress intensity were prepared for the fatigue and hold time tests and are included in Appendix C for reference purposes. The evaluation of the analyzed data continues in the next section, experimental results and discussion.

## V. Experimental Results and Discussion

This study investigated crack growth in  $Ti_3Al$  at elevated temperatures. The objectives were to characterize sustained load (creep) crack growth at elevated temperatures and to determine the applicability of linear cumulative damage modeling to the  $Ti_3Al$  alloy at elevated temperatures. Nine tests were conducted on compact tension specimens of the  $Ti_3Al$  alloy using the equipment described in section 3 and the procedures developed in section 4. The results of those tests are presented in this section.

Sustained load crack growth was studied at three different temperatures: 700° C, 750° C, and 800° C. The lower limit was chosen because a previous test had shown that sustained load crack growth did not occur at 650° C; 800° C was considered the maximum practical test temperature for the alloy. Crack lengths were measured optically and crack growth rates were determined using the polynomial routines found in the last section. Sustained load crack growth has been described as balance between high stress intensities at the crack tip which result in crack growth, and plastic deformation which blunts the crack tip retarding growth (16:449). This description most certainly applies to  $Ti_3Al$ .

Figure 12 shows the sustained load crack growth rate in  $Ti_3Al$  at 750° C. The plot shows very slow growth at lower stress intensities. Crack growth initially increases steadily, but then slows down as creep effects blunt the crack tip. During the sustained load tests, there were occasionally periods of an hour or more when no noticeable crack growth would occur. After a period of time, the environmental effects

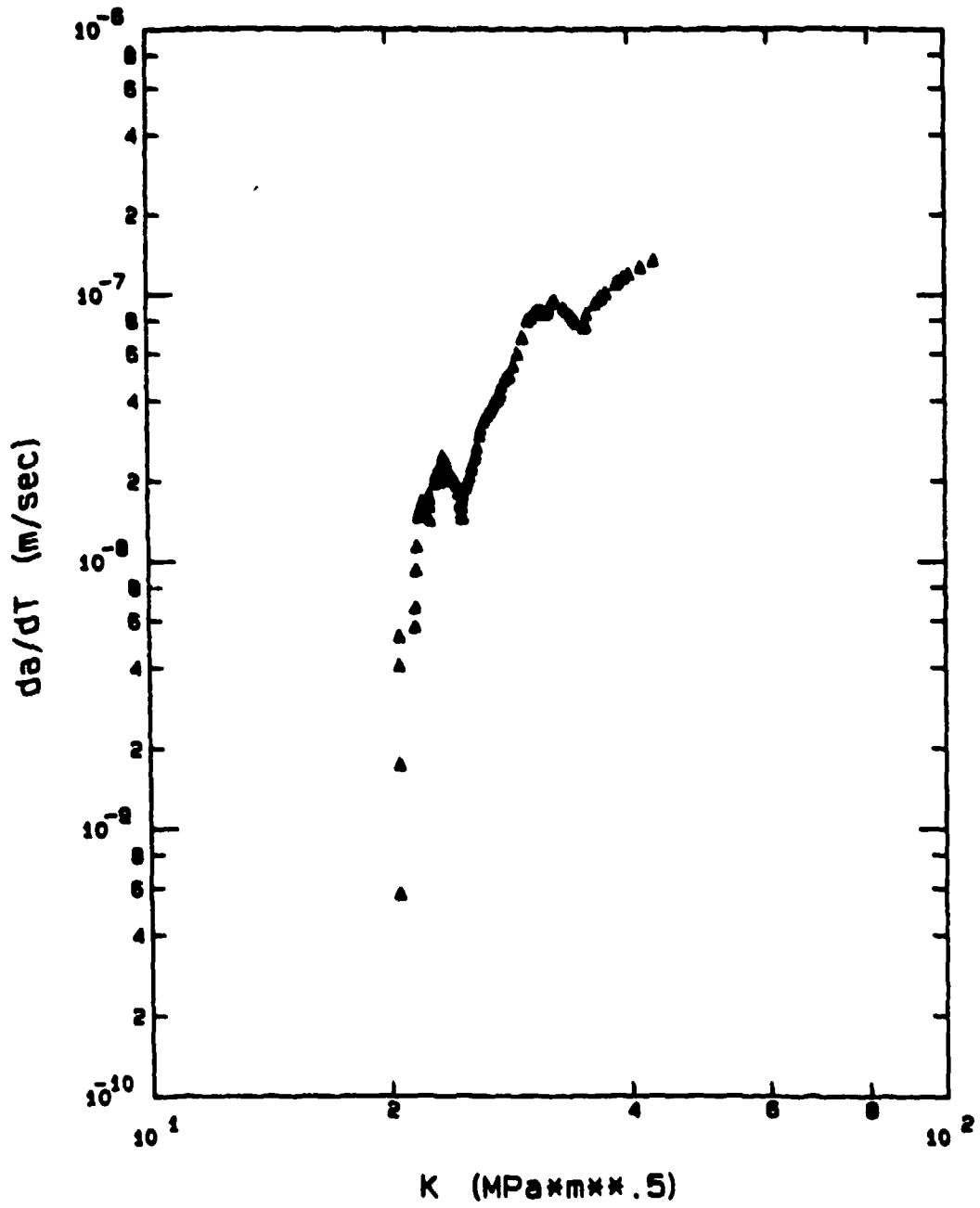


Figure 12. Sustained Load Crack Growth Rate for 750 C

cause steady crack growth to return until creep effects begin to blunt the crack tip again, retarding growth. Crack tip blunting could clearly be seen through the microscope while measuring the crack length. Eventually, the stress intensity at the tip was high enough to resist blunting and steady crack growth continued until failure. The crack growth rates at 700° C and 800° C also showed similar behavior during the tests. Individual crack growth rate curves for these tests are contained in Appendix C.

The effect of temperature on sustained load crack growth can be seen by plotting all three crack growth rate curves on a single graph. The resulting sustained load crack growth rates as a function of stress intensity,  $K$ , are shown in Figure 13. Sustained load crack growth rates usually increase with increased temperature since increased temperature lowers the elastic modulus, but the plot of the crack growth rates shows that temperature had very little effect on crack growth rate in the alloy. For 95 percent of the data, the difference between the slowest growth and the fastest is less than a factor of five apart over the entire stress intensity range tested. This range is shown by the dashed lines, and is within the possible experimental scatter for the experiments. These results are in sharp contrast with tests conducted on Inconel 718, which showed crack growth rate changes of as much as 100 times for a 100° C temperature difference (12:17). The results would indicate that the creep effects retarding the crack growth are as sensitive to temperature as the environmental effects increasing crack growth, resulting in no net difference in the crack growth rate at higher temperatures. The critical and threshold stress intensities

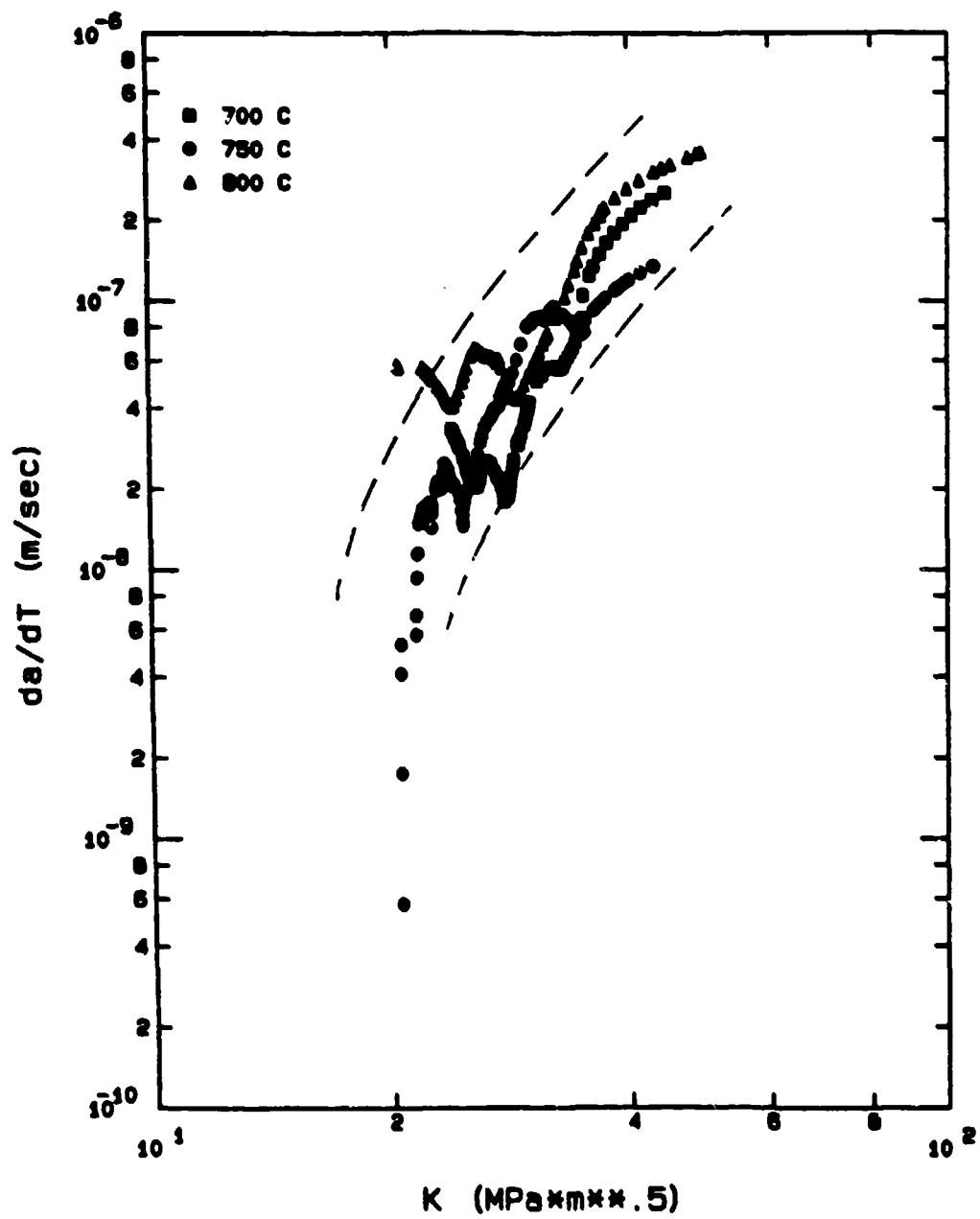


Figure 13. Sustained Load Crack Growth Rate Curves

calculated from the test data also showed very little temperature dependence.

The stress intensity at failure,  $K_{IC}$ , was determined by measuring the crack length just prior to failure and using equation 1. As was the case for crack growth rates,  $K_{IC}$  also showed very little temperature dependence. The difference between the highest and the lowest  $K_{IC}$  measured was less than 10 percent. The calculated stress intensities at failure were  $48 \text{ MPa}\sqrt{\text{m}}$ ,  $46 \text{ MPa}\sqrt{\text{m}}$ , and  $51 \text{ MPa}\sqrt{\text{m}}$  for  $700^\circ \text{ C}$ ,  $750^\circ \text{ C}$ , and  $800^\circ \text{ C}$  respectively. No tests were specifically conducted to determine the threshold stress intensity of the alloy,  $K_{th}$ . Threshold tests take hundreds of hours to complete and that time was not available for this study. Reasonable estimates for  $K_{th}$ , however, can be made based the extremely slow growth rates encountered after initial loading in the  $750^\circ \text{ C}$  test. The test was initially started with a stress intensity factor of  $20 \text{ MPa}\sqrt{\text{m}}$ , but showed less than 0.08 mm crack growth in the first 8 hours of the test. The slow crack growth rate in addition to the general crack growth trend indicated by the crack growth rate curves would indicate that  $20 \text{ MPa}\sqrt{\text{m}}$  is probably a reasonable estimate for  $K_{th}$ .

These results show that crack growth rates and fracture toughness in  $\text{Ti}_3\text{Al}$  at elevated temperatures are insensitive to temperature, indicating that crack propagation is most likely due to corrosion of the crack tip caused by oxidation at high temperature. For the sustained load tests, the specimens typically were in a high temperature environment for two weeks and all showed signs of oxidation when they were removed. Further tests on the alloy at elevated temperatures in a vacuum or a non reactive gas would be required to test the effects of



oxidation on crack growth. Since the alloy did not exhibit crack growth at 650° C, temperature must serve as a "go or no go" criteria for sustained load crack growth.

In addition to the sustained load tests, a fatigue test and several hold-time tests were conducted at 750° C to determine the applicability of linear cumulative damage modeling to  $Ti_3Al$  at elevated temperatures. Since only a limited number of test specimens were available, all of these tests used a fatigue frequency of 0.1 Hz and a load ratio of 0.3. While results for these tests will only be applicable for the frequency and load ratio tested, the general growth rate trends should be applicable to other frequencies and load ratios. Based on Saxena and Bassani's review of factors affecting crack growth at elevated temperatures (19:360-370), two results were expected. First, the crack growth rate,  $da/dt$ , should decrease with increased hold time from the fatigue crack growth rate to the sustained load crack growth rate. The crack growth rate per cycle  $da/dN$ , however, should show a steady increase with increased hold time since sustained load crack growth occurs during the hold time. If no interaction occurs, the increase in  $da/dN$  will be proportional to the hold time, and will not occur below the sustained load threshold stress intensity.

The test results, plotted in Figure 14, show that the crack growth rate,  $da/dt$ , shows a clear and steady decrease from the fatigue crack growth rate (0 hold time) to the sustained load crack growth rate (infinite hold time). Except for the transition growth rates (caused by transition from precrack test conditions to actual test conditions) at the beginning of the test, the fatigue growth rate is almost linear,

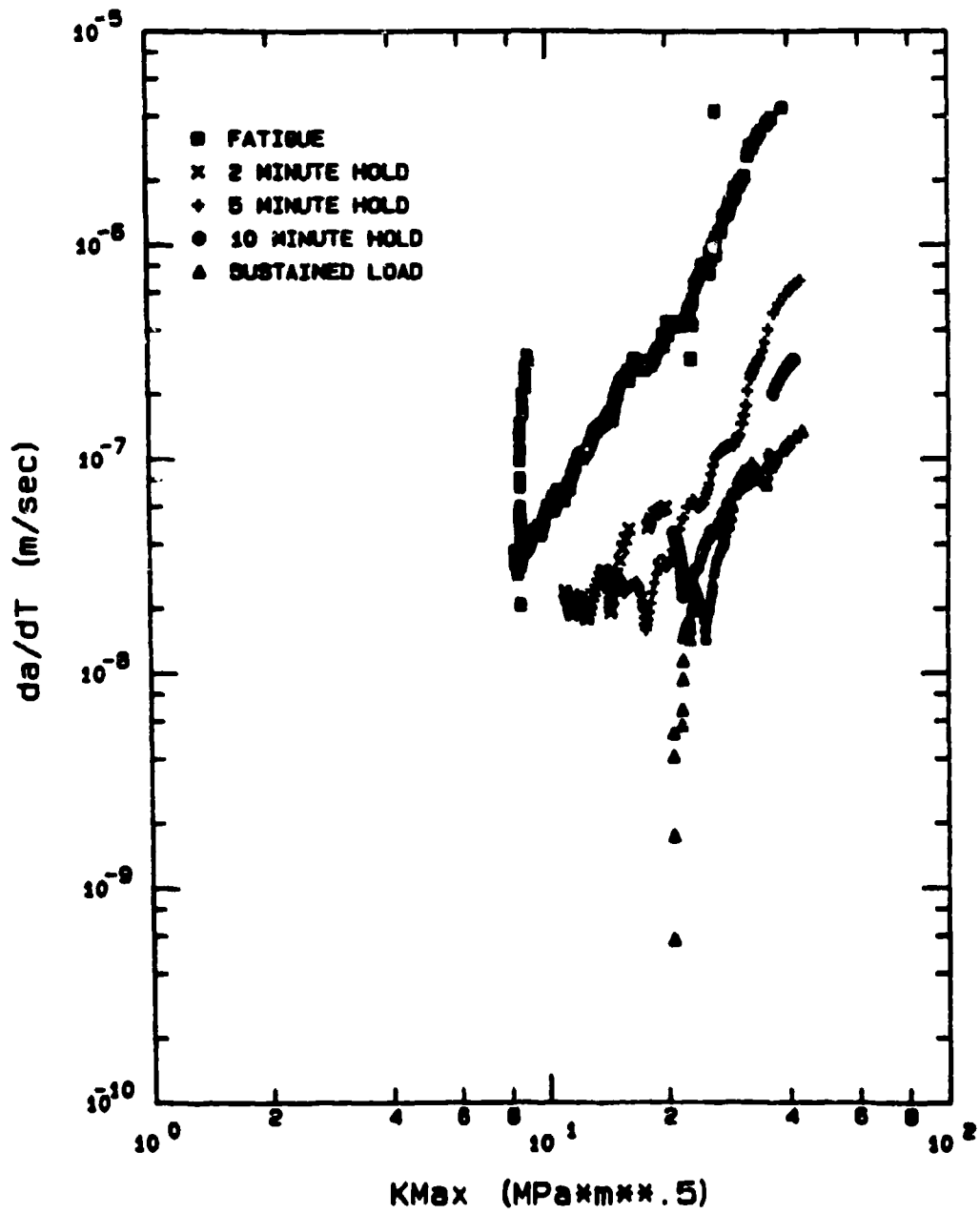


Figure 14. Crack Growth Rate Curves for 750° C

showing a clear difference between the fatigue and sustained load crack growth rate characteristics. The two and five minute hold time crack growth rate curves also resemble the fatigue crack growth rate curve, but they are not as linear. The ten minute hold-time crack growth rate curve looks more like the sustained load curves, with signs of periodic retardation in the crack growth rate. From the figure, the data from the ten minute hold-time crack growth rate is not much faster than the sustained load crack growth rate, so its data should resemble the sustained load data. The general trend in the plot from the sustained load crack growth rate to the fatigue crack growth rate indicates that linear cumulative damage modeling techniques should be able to predict crack growth in  $Ti_3Al$  at elevated temperatures. If, for instance, the crack growth rate curve for the two minute hold time test was slower than the sustained load crack growth rate, the story would be different. A damage model developed from the test data is presented in the next section. The model will be much easier to develop if there is no interaction or mixed-mode crack growth. One way to test for interaction is to compare the crack growth rates per cycle.

The plot of crack growth per cycle, Figure 15, shows the crack growth per cycle,  $da/dN$ , for all the hold-time tests was about three times faster than the fatigue test over the entire range of stress intensities; the  $da/dN$  plots for all three hold time tests fell along a single line. This indicates that there is a change in the crack growth rate during the hold times in the tests. While all the crack growth rate curves were expected to be faster than the fatigue crack growth rate curve, the ten minute hold time curve should have shown the fastest

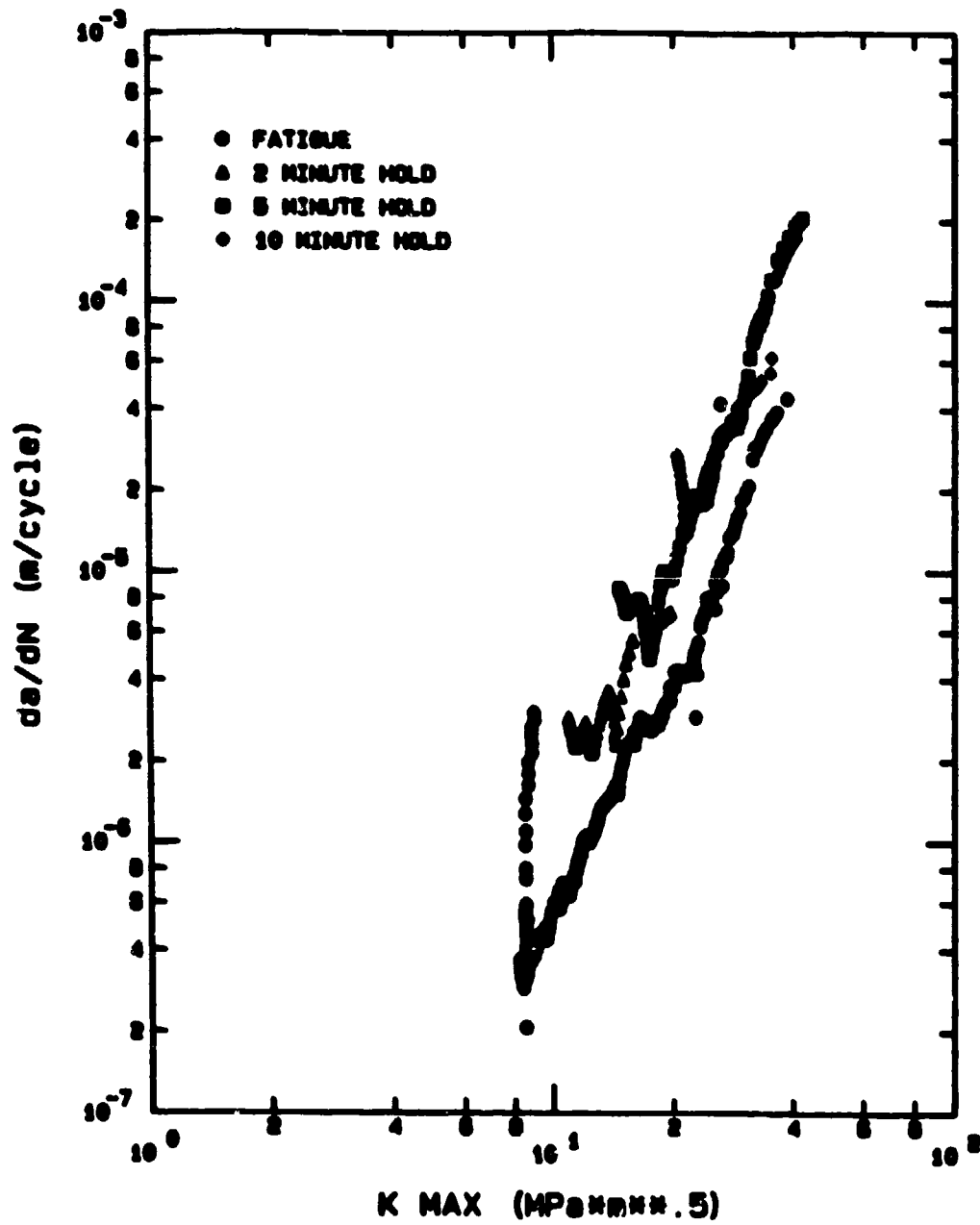


Figure 15. Crack Growth per Cycle Curves for 750° C

crack growth. The curves for five and two minute tests would still be faster than the fatigue growth rate per cycle, but slower than the ten minute hold time. An increase in  $da/dN$  was expected above  $20 \text{ MPa}\sqrt{\text{m}}$  due to creep crack growth, the increased growth rate below  $20 \text{ MPa}\sqrt{\text{m}}$  indicates that some mixed-mode crack growth occurred, increasing the crack growth rate at lower stress intensities. The model developed in the next section was useful for estimating the amount of the interaction. Those results will be presented in the next section.

The critical stress intensities for the fatigue and hold time tests, calculated by measuring the crack length just prior to failure, were within the same range of critical stress intensities measured for the sustained load tests. The calculated stress intensity at failure was  $43 \text{ MPa}\sqrt{\text{m}}$ ,  $43 \text{ MPa}\sqrt{\text{m}}$ , and  $46 \text{ MPa}\sqrt{\text{m}}$  for the fatigue, ten minute and five minute hold time tests, respectively. The two minute hold time test was not being monitored when it failed, so no calculation could be made.

Post-test inspection of the sustained load test specimens showed severe tunneling in all of the specimens. Photos of the fracture surfaces for all the specimens are shown later in this section. Crack tip tunneling was easily measured since heat tinting caused by the elevated temperatures formed colored bands at various points along the fracture surfaces starting about 12 mm from the notch. The average tunneling correction for all the specimens was 2.29 mm. This correction varied by less than ten percent between the different specimens and at different locations on individual specimens after the first measurable heat tinting. Unfortunately, there was no way to determine how the tunneling

proceeded from the fatigue precrack extending 5 mm from the notch, which had less than 0.1 mm tunneling correction, and the 2.29 mm correction measured about 12 mm from the notch. The optical measurements only could only measure the crack length at the surface of the specimens. Tests with accurate methods of determining the effective crack length would be required to determine how the crack propagates in the interior of the specimen before the tunneling correction is constant. For this reason, only the tunneling correction measured from the precrack is included in the crack length data.

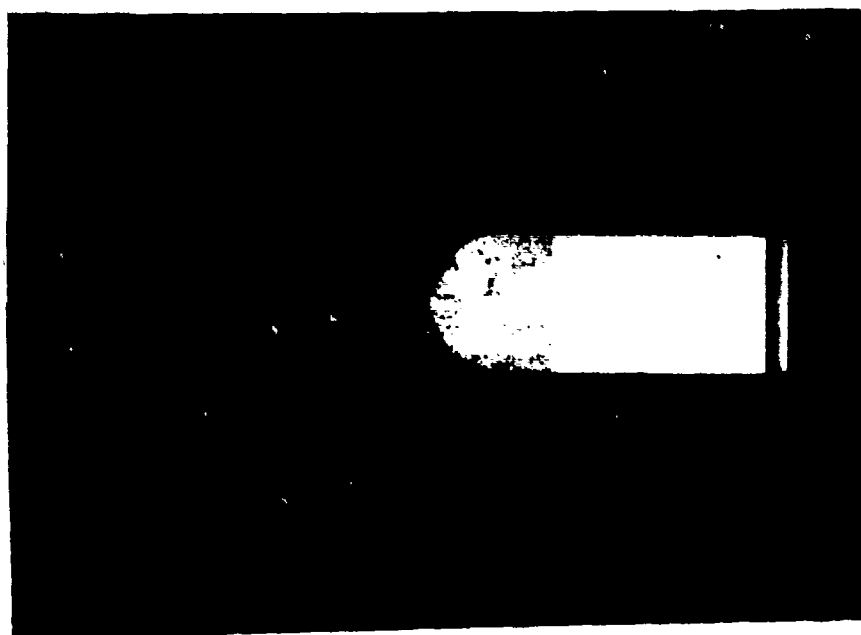
Post-test inspection of the specimens used for the fatigue and hold time tests showed less than 0.1 mm tunneling correction for the fatigue test, the two minute hold-time test, and the five minute hold-time test. The tunneling correction for the ten minute hold-time test was 2.2 mm, roughly equivalent to the correction for the sustained load tests. The transition in the tunneling correction between the fatigue precrack and the first measurable correction could not be determined from COD compliance relations because the experimental scatter at shorter crack lengths (the area of interest) was too severe to provide accurate measurements (Figure 10).

The fracture surfaces also showed other differences between the fatigue and the sustained load tests. Photos of the fracture surfaces, included in Figures 16-20, clearly show that the sustained load fracture surfaces were very rough, especially when compared to the smooth fracture surface for the fatigue test. The sustained load fracture surfaces looked more like they were torn apart. The fatigue precrack is easily distinguished from the sustained load crack growth since it had a much

smoother surface. The heat tinting regions used to measure the tunneling correction can also be clearly seen. The precrack for the specimen used in the fatigue test was not as easy to find. The fracture surface remained smooth until just prior to failure, where it looks similar to the sustained load fracture surface. The fracture surfaces for the hold time tests were not as smooth as the fatigue surface, but not as rough as the sustained load surfaces. The surface for the ten minute hold time test resembled the sustained load surfaces while the two minute hold time surface was similar to the fatigue fracture surface. The fracture surface for the five minute hold time test was between the two, but more closely resembled the fatigue fracture surface. The sustained load and the ten minute hold test specimens also showed more plastic deformation than the fatigue and other two hold time tests. The sustained load and ten minute hold test specimens show signs of "necking" soon after the precrack, while the cross sections for the other test specimens remain relatively constant until just prior to failure.



**Specimen 88-102 750° C Sustained Load**



**Specimen 88-104 800° C Sustained Load**

**Figure 16. Fracture Surfaces for Specimens 88-102 and 88-104**





Specimen 88-105 700° C Sustained Load

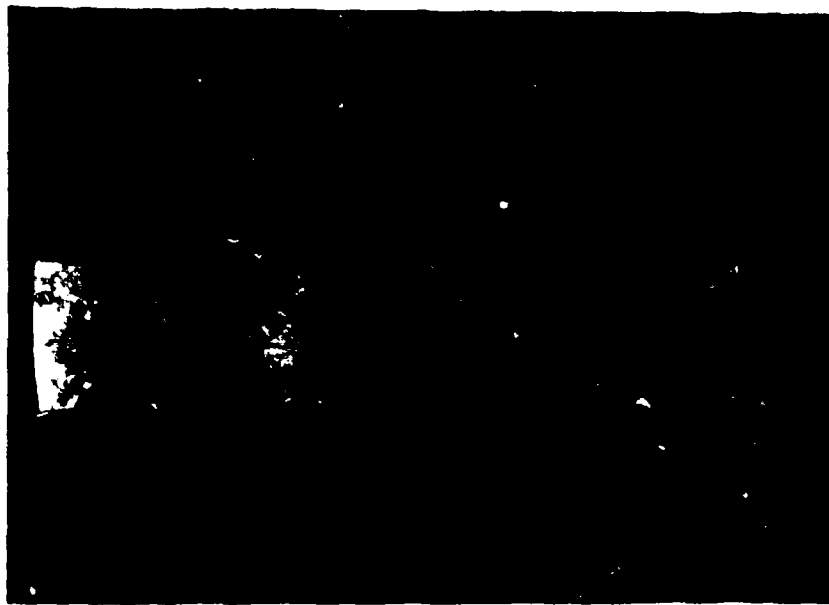


Specimen 88-112 700° C Sustained Load

Figure 17. Fracture Surfaces for Specimens 88-105 and 88-112

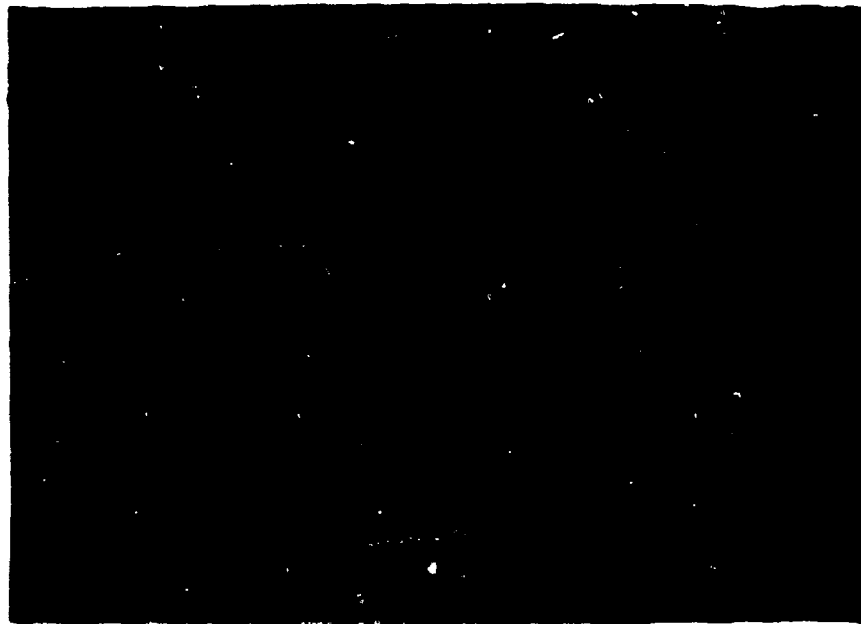


Specimen 88-113 750° C 2 Minute Hold

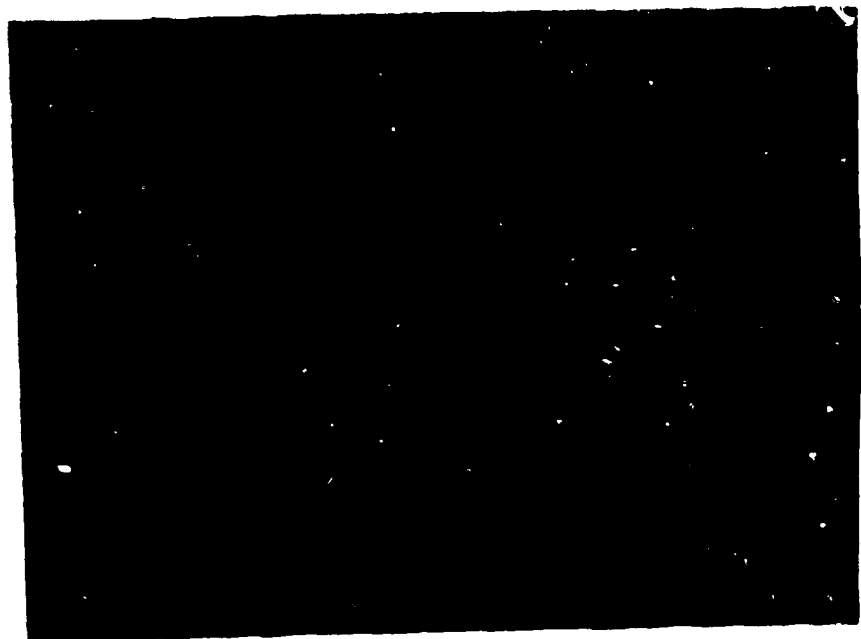


Specimen 88-114 750° C 5 Minute Hold

Figure 18. Fracture Surfaces for Specimens 88-113 and 88-114

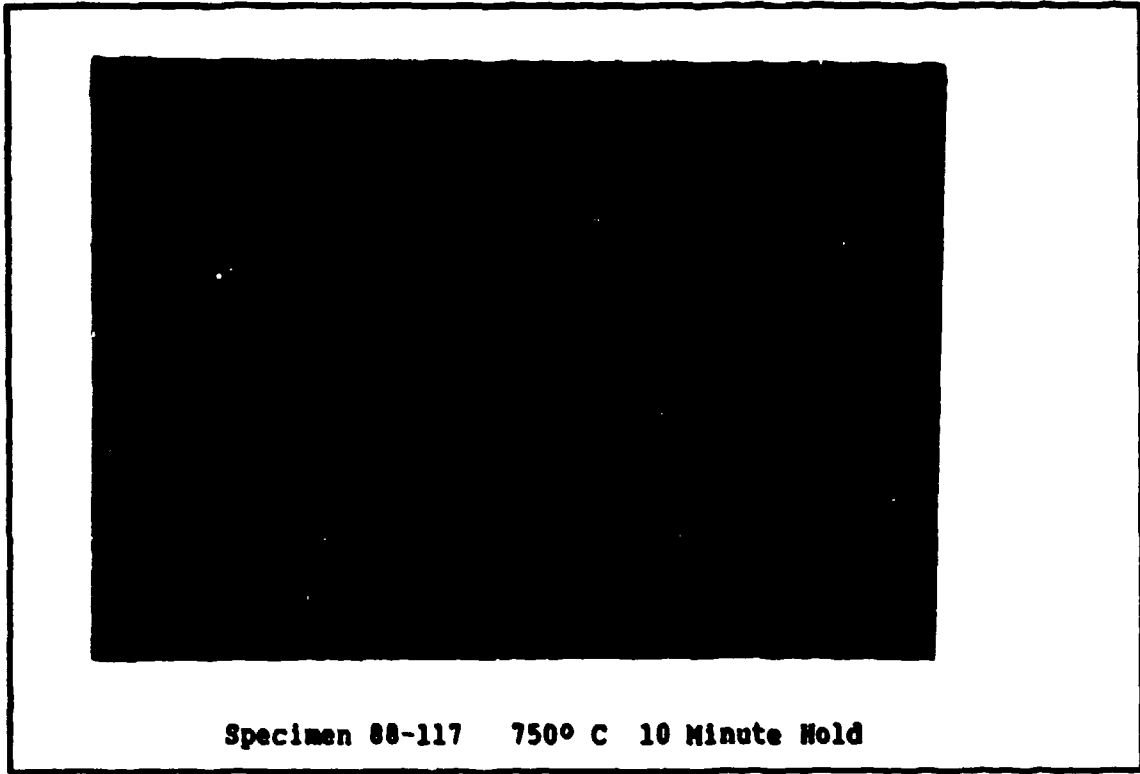


**Specimen 88-115 750° C 0.1 Hz Fatigue**



**Specimen 88-116 750° C 10 Minute Hold**

**Figure 19. Fracture Surfaces for Specimens 88-115 and 88-116**



**Specimen 88-117 750° C 10 Minute Hold**

**Figure 20. Fracture Surface for Specimen 88-117**

## VI. Model Development

In this section a linear cumulative damage model is developed to predict crack growth under sustained load conditions with periodic fatigue cycles. Damage modeling, if effective, can allow crack growth under complex loading conditions to be characterized without requiring individual tests for each possible test condition. A linear cumulative damage model involves the summation of crack growth contributions from time dependent (sustained load) crack growth, cycle dependent (fatigue) crack growth, and mixed-mode (22:6). This method of damage modeling for creep-fatigue interaction has been previously demonstrated in tests on Inconel 718 (13:179), and has also been applied to thermal fatigue analysis under sustained loads, sustained load tests with periodic overloads, and combined thermal-mechanical cycling in Inconel 718 (22:21-32, 7:34-80, 9:24-85). It has not been demonstrated on  $Ti_3Al$ . Since the mixed-mode crack growth contribution is difficult to account for, it will be assumed to have no contribution to crack growth in  $Ti_3Al$ , as first approximation.

The baseline sustained load and fatigue tests were used to develop a model combining the effects of creep crack growth with superimposed fatigue cycles. Using the methods discussed in the previous sections, the sustained load and fatigue crack growth rates were calculated and plotted as a function of the stress intensity factor,  $K$ . The baseline crack growth rate curves for sustained load and fatigue are shown in Figures 21 and 22 respectively. Although a number of different correlating parameters could have been used, the stress intensity factor has

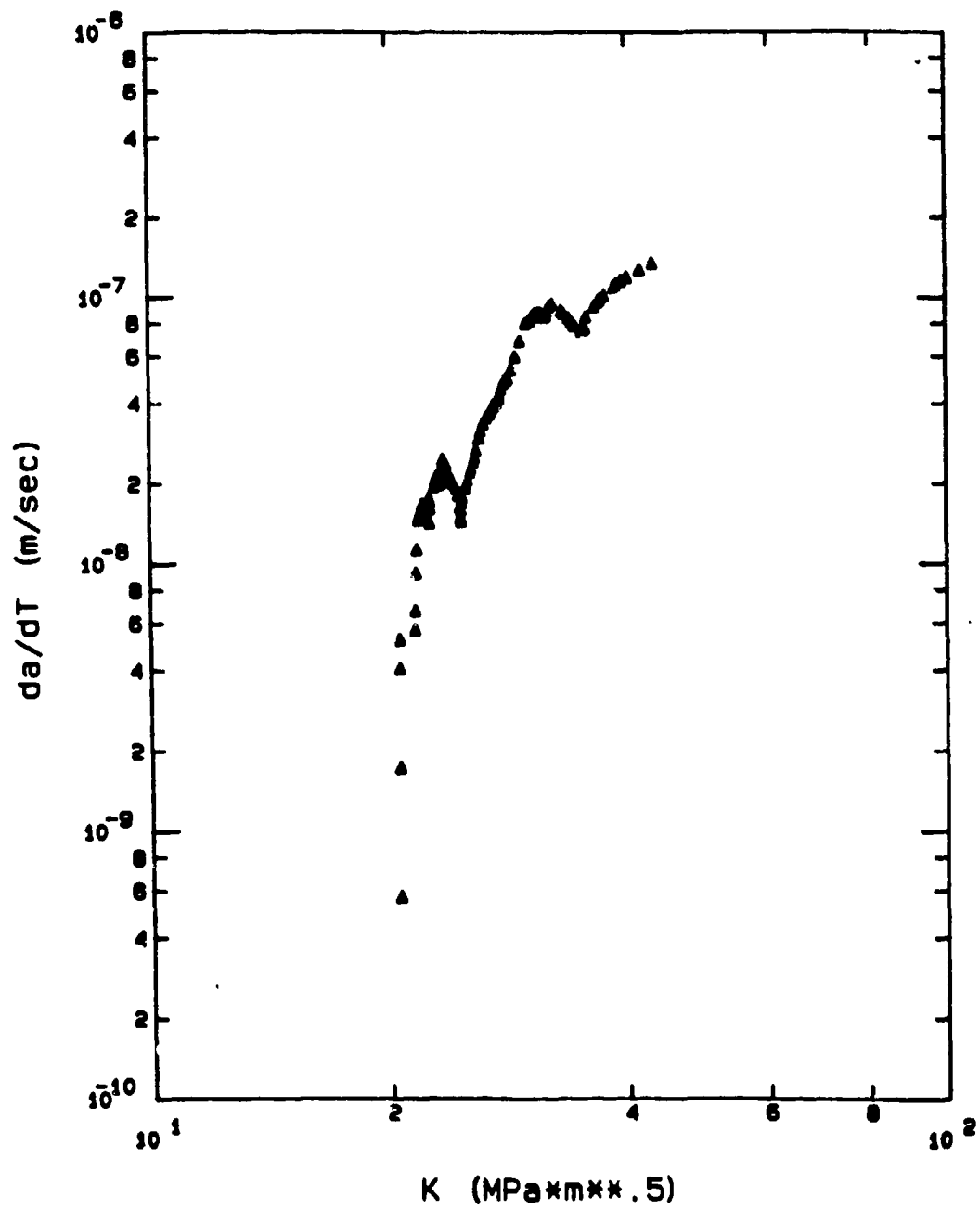


Figure 21. Baseline Sustained Load Crack Growth Rate

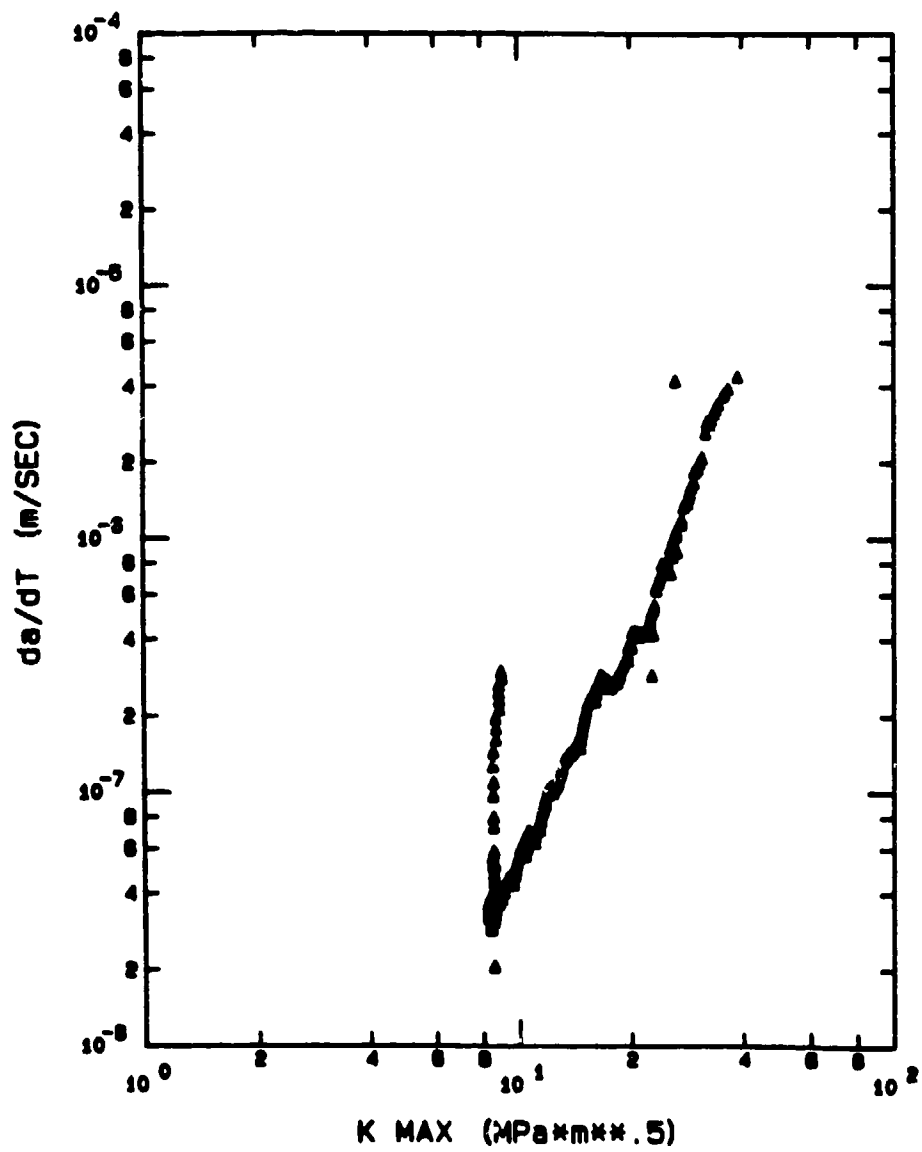


Figure 22. Baseline Fatigue Crack Growth Rate

proven quite effective for elevated temperature crack growth modeling in the models mentioned above. Using linear cumulative damage modeling, the sustained load (creep) and fatigue crack growth rates at a specific stress intensity are combined using the following relationship:

$$\left. \frac{da}{dt} \right|_{\text{total}} = \left. \frac{da}{dt} \right|_{\text{creep}} + C \left. \frac{da}{dt} \right|_{\text{fatigue}} \quad (10)$$

where the constant C depends on the fatigue frequency and the hold time and interactive effects (mixed-mode growth) are neglected.

Before the two effects can be added, they must first be characterized in some form. In cases where the crack growth rate and stress intensity factor form a straight line on the log-log plot, the following relation can be used:

$$\frac{da}{dt} = CK^n \quad (11)$$

where:

$$\frac{da}{dt} = \text{crack growth rate}$$

C = intercept of the da/dt axis

n = slope of the da/dt vs K line

K = stress intensity factor

In many cases, however, the relation between the crack growth rate and stress intensity factor do not form a straight line. General Electric developed the Modified Sigmoidal Equation (MSE) to model high



temperature crack growth rates (21). The general form of the sigmoidal curve used to model the curves is given by the following equation:

$$\frac{da}{dt} = \exp(B) \left[ \frac{K}{K_i} \right]^P \left[ \ln \left[ \frac{K}{K^*} \right] \right]^Q \left[ \ln \left[ \frac{K_c}{K} \right] \right]^D \quad (12)$$

where:

- $\frac{da}{dt}$  = crack growth rate
- $K$  = stress intensity factor
- $K_i$  = stress intensity factor at inflection point
- $K^*$  = Threshold stress intensity
- $K_c$  = Critical stress intensity
- $B, P, Q, D$  = parameters which affect the shape of the curve

A representation of the model is shown in Figure 23. Heil used the MSE to model fatigue and sustained crack growth in Inconel 718. He developed general mathematical relationships between the shape parameters to reduce the number of variables, but still had to make adjustments to allow for a best fit for the data (9:33,44,37). His relations assumed a symmetric curve about the inflection point which, in the case of  $Ti_3Al$ , did not apply. Therefore, another approach was taken.

A MathCAD template (Figure 24) was used to adjust the shape parameters to provide a best fit for the data. MathCAD is a computer program which can plot equations and data sets in the same plot. This interactive approach reduced the overall time required to produce the models,

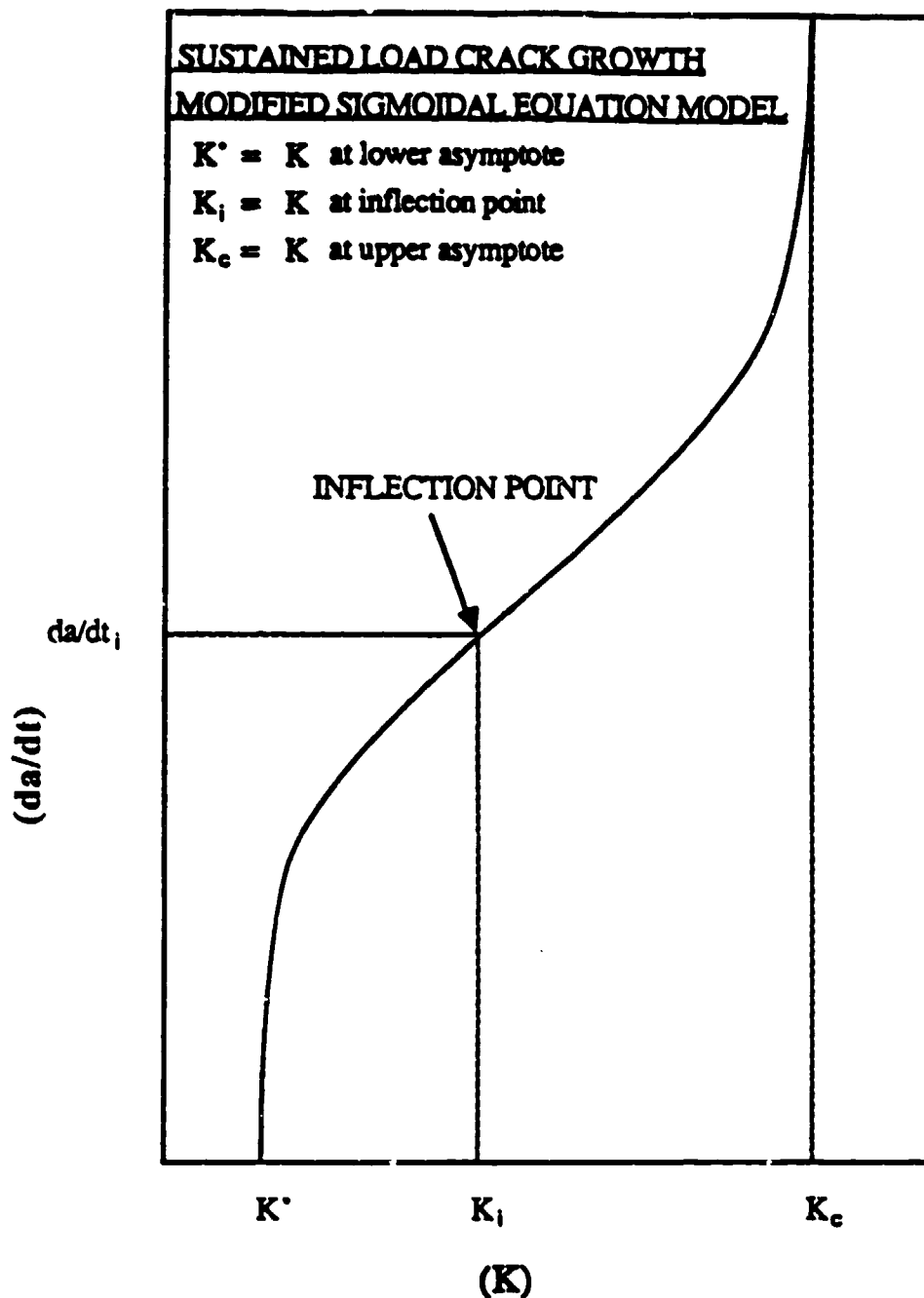


Figure 23. MSE Model Parameters

**Modified Sigmoidal Equation for thesis model**

**Test Data Input**

```

M := READPRN(Fatigue)      n := rows(M)      n = 320
                                <0>                <1>
Kt := M                    adot := .001 + 1000·M    j := 0 ..50
                                i := 0 ..n - 1
    
```

**Shape Parameters**

```

B := -12.94
P := -2.1
Q := 1.21
D := -5.88
    
```

**Test Parameters**

```

Kt := 6.2      Kj := j + 8
t      j
Ki := 20.5     Kc := 82
i      c
    
```

**MSE Equation**

$$dad_t_j := .001 + 1000 \cdot \exp(B) \cdot \left[ \frac{K_j}{K_i} \right]^P \cdot \left[ \ln \left[ \frac{K_j}{K_t} \right] \right]^Q \cdot \left[ \ln \left[ \frac{K_c}{K_j} \right] \right]^D$$

min(adot) = 0.001

min(dadt) = 0.001

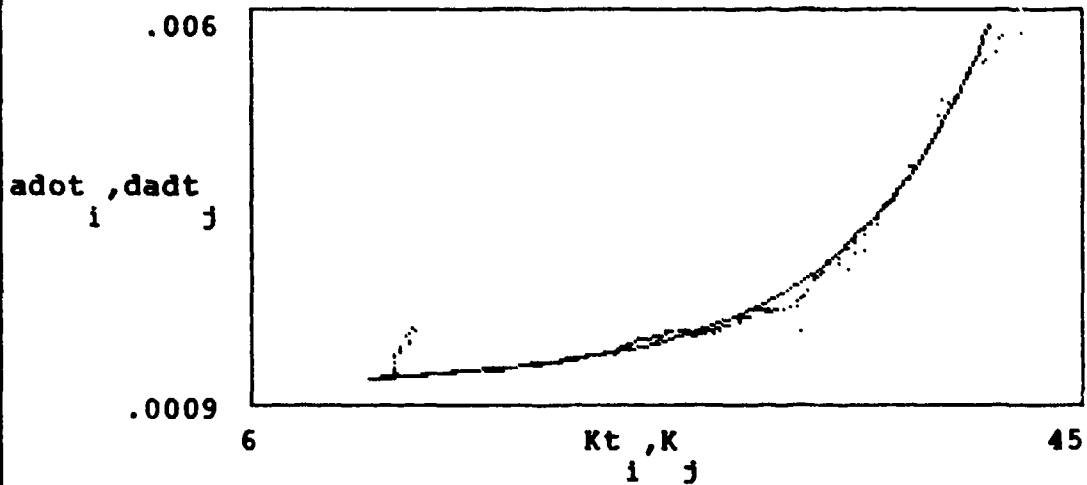


Figure 24. Sample MathCAD Template for MSE Model

since the MSE parameters could easily be adjusted and the resulting plot could be compared with the test data without additional effort. The final parameters used to model the creep and fatigue baseline data were based on a best visual fit for the data and are included in table III.

Table III MSE Model Constants

Parameter	Creep	Fatigue
$K_C$	167.00	82.00
$K^*$	19.98	6.20
$K_i$	45.50	20.50
B	-14.18	-12.94
P	-3.34	-2.10
Q	1.29	1.21
D	-4.65	-5.88

In both cases, the critical stress intensity parameter,  $K_C$  had to be adjusted to higher than the observed  $43 \text{ MPa}\sqrt{\text{m}}$  critical value observed during the testing. These changes allowed the MSE curves to fit the experimental crack growth rate data better at higher stress intensity levels. The resulting MSE model curves for sustained load and fatigue crack growth are shown in Figures 25 and 26 respectively. No attempt

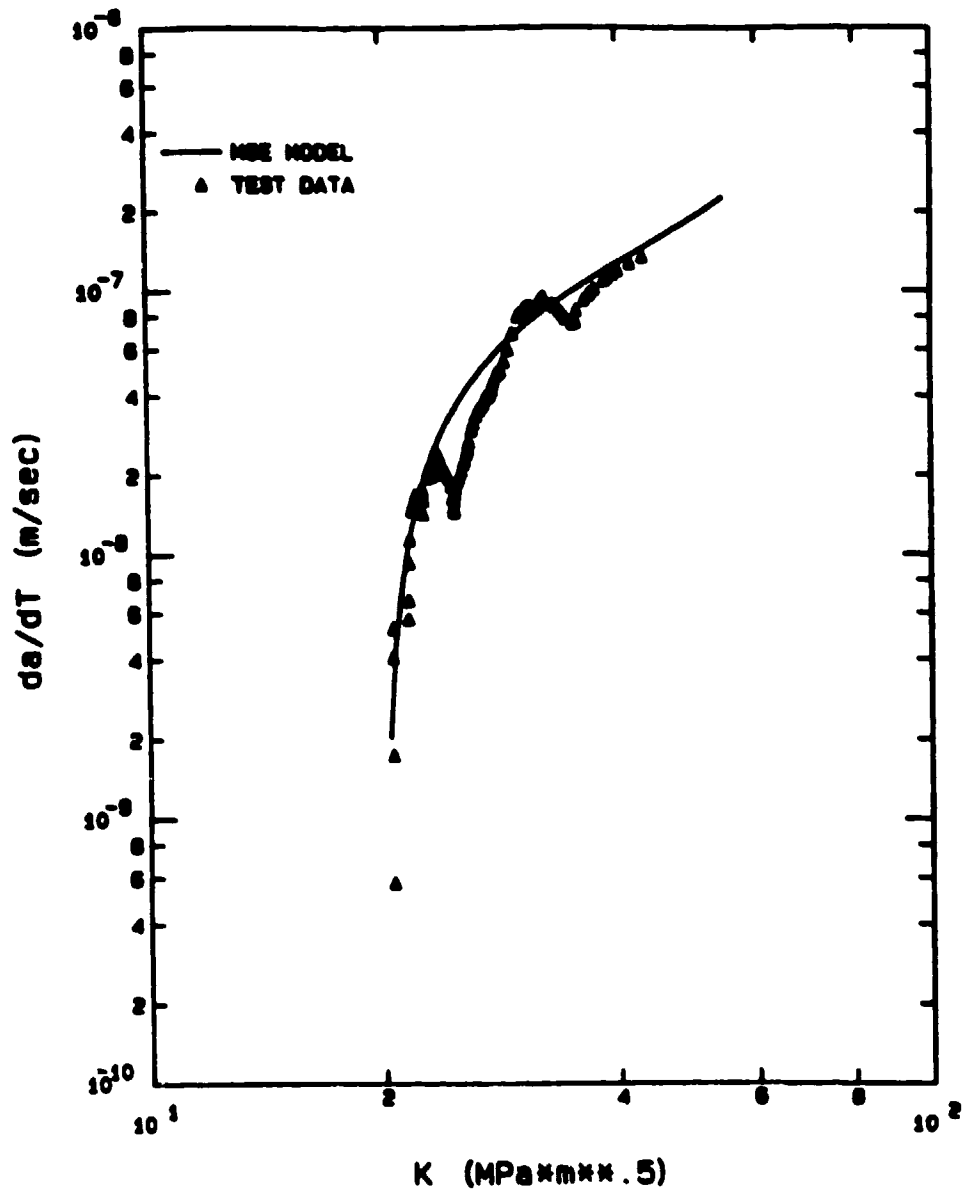


Figure 25. NSE Model for Creep Crack Growth

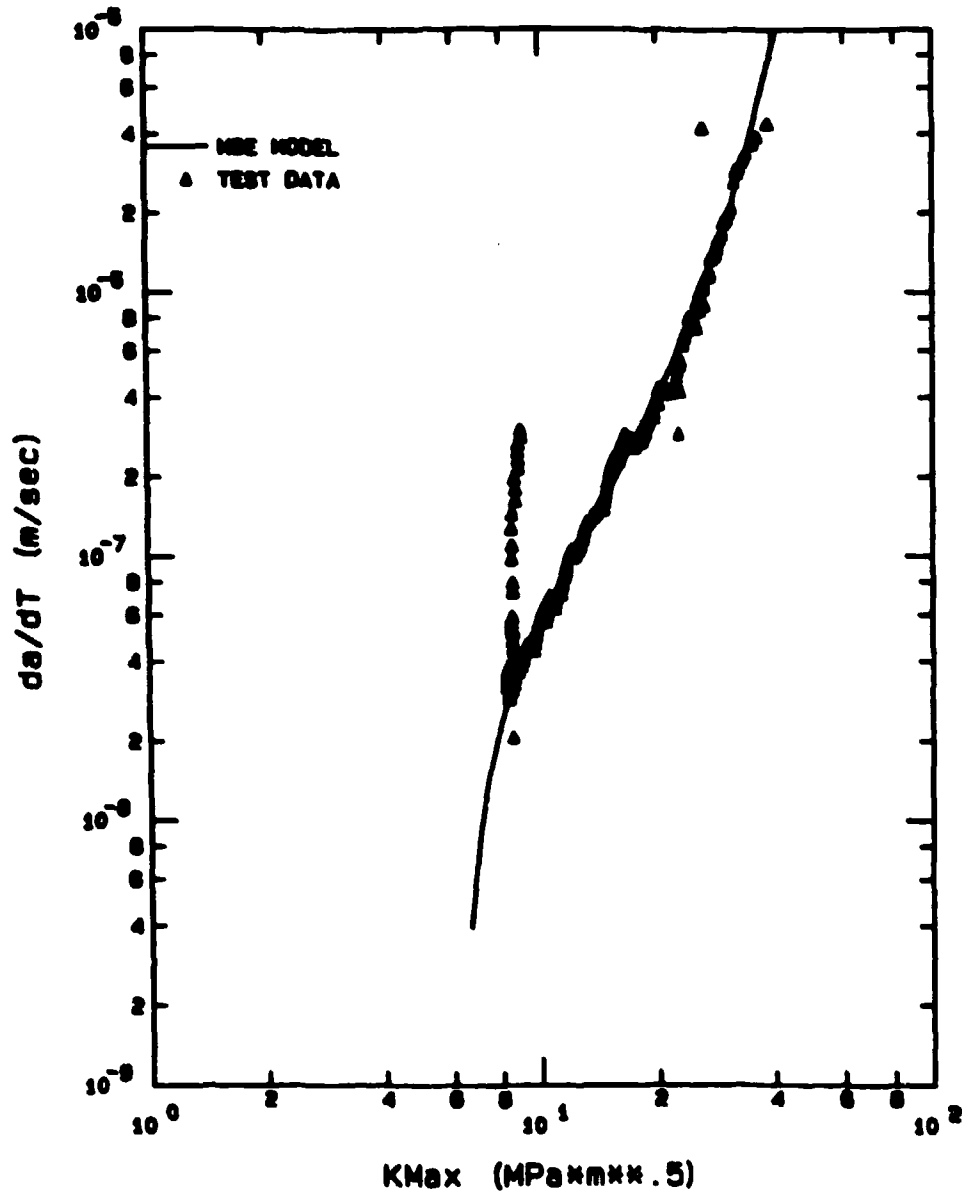


Figure 26. MSE Model for Fatigue Crack Growth

was made to model the areas of retarded crack growth for the sustained load baseline, since the MSE equation could not form such a complex shape. The region at the beginning of the fatigue test wasn't modeled either, since it caused by the fatigue precracking.

Once the MSE curves were developed they could be combined to predict crack growth rates for sustained load tests with periodic fatigue cycles. The equation used to combine the MSE curves is given by the following expression:

$$\frac{da_K}{dt} = \left. \frac{da_K}{dt} \right|_{\text{creep}} + \frac{1}{6HT} \left. \frac{da_K}{dt} \right|_{\text{fatigue}} \quad (13)$$

where:

$$\frac{da_K}{dt} = \text{crack growth rate for a given } K$$

HT = hold time in minutes

The factor of 6 in the numerator is based on the fact that for a .1 Hz frequency there are 6 cycles in one minute. Plots of the model prediction versus actual test results are provided in Figures 27, 28, and 29. These graphs clearly show that the model accurately or conservatively predicts crack growth rates for only the ten minute hold time test. The experimental data for both the two and five minute hold time tests show growth rates higher than the linear model predicts, so a simple summation of the sustained load and fatigue crack growth contributions do not adequately predict the crack growth rate for hold times under ten minutes. This indicates that some form of interaction is occurring at the hold times under ten minutes.

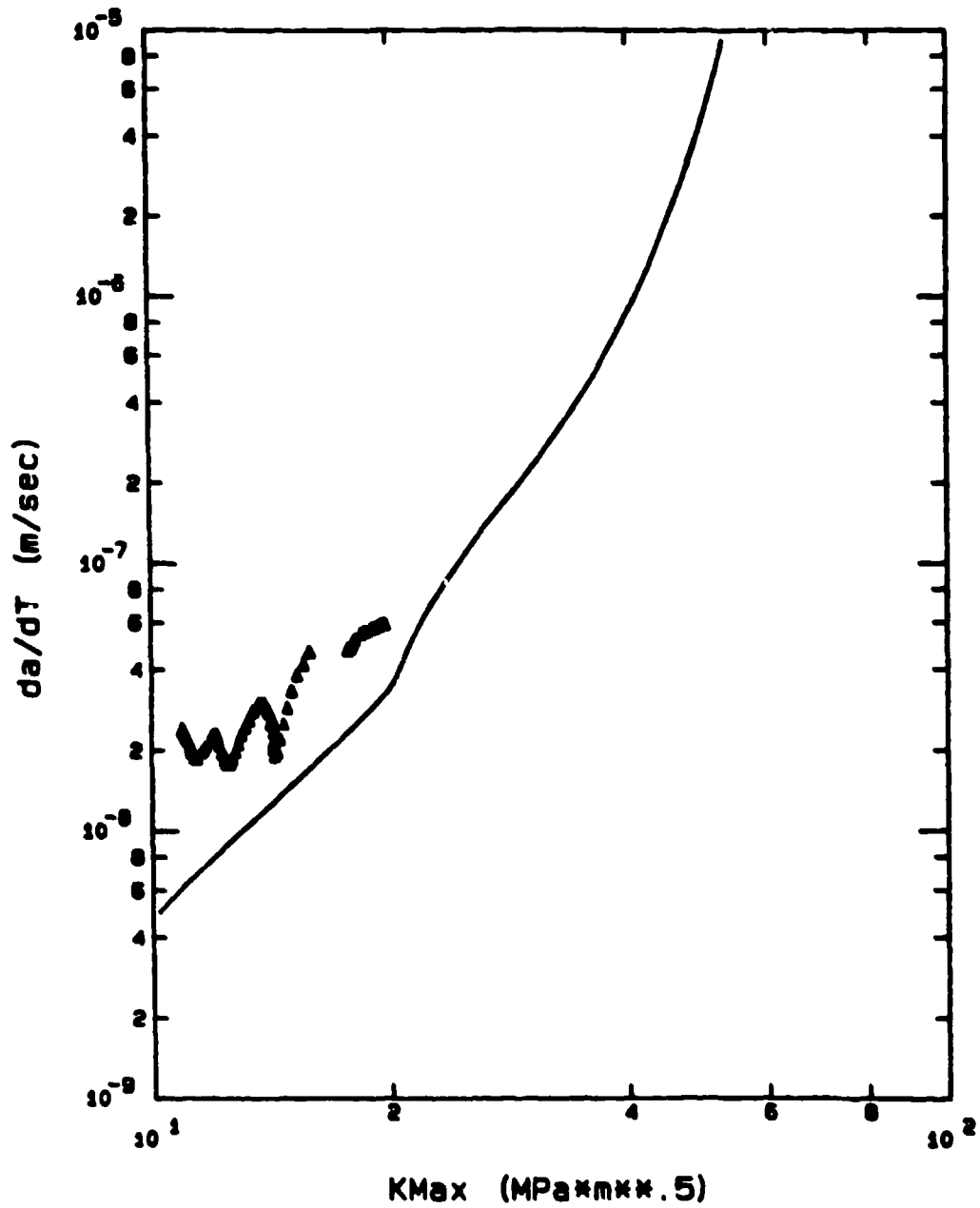


Figure 27. Model Versus Actual Crack Growth Rate for 2 Minute Hold Test



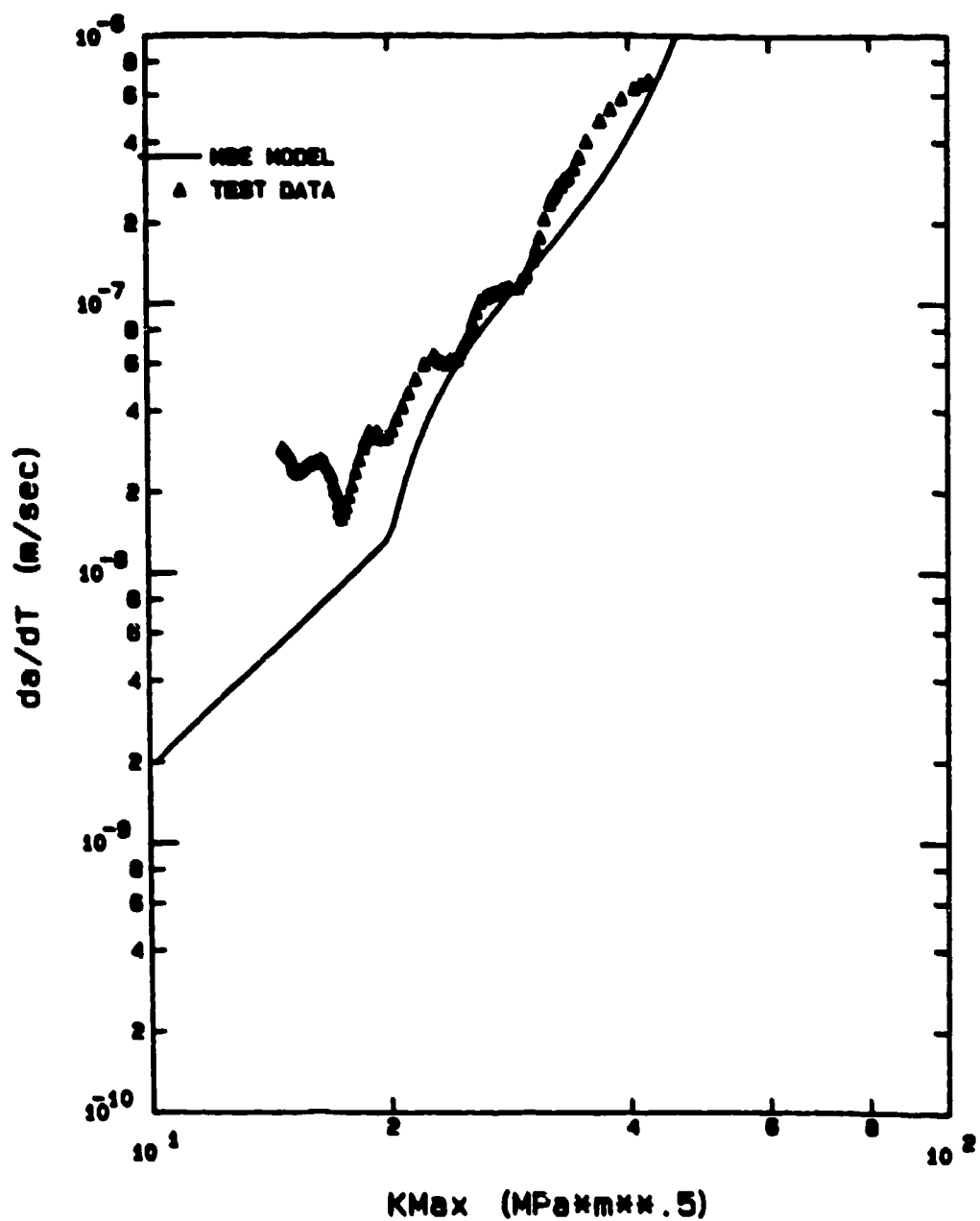


Figure 28. Model Versus Actual Crack Growth Rate for 5 Minute Hold Test

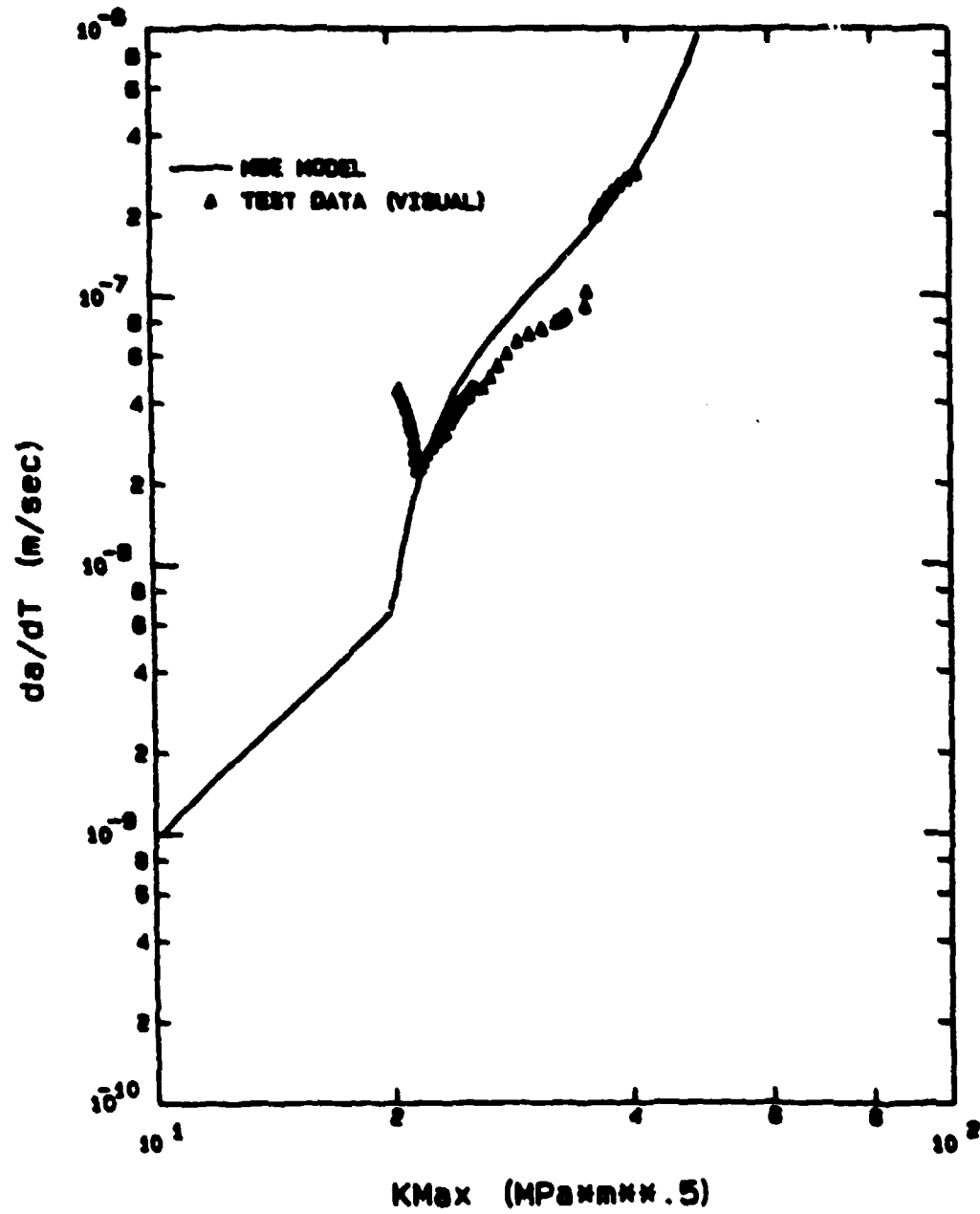


Figure 29. Model Versus Actual Crack Growth Rate for 10 Minute Hold Test

To account for the interactive effects, the crack growth rates for the hold-time tests were divided by the crack growth rates predicted by the model at a constant stress intensity. The results, shown in Figure 30, were used to develop a mixed-mode correction to the original model. The figure shows that the difference between the actual and the modeled crack growth rates increases linearly as the hold time decreases, so the assumed correction was a linear function of the hold time. The mixed-mode correction also assumes that the crack growth rate will not exceed the fatigue crack growth rate. This assumption may not be valid, so tests with hold times under two minutes will be needed to provide any additional adjustments. A quadratic equation could also be used to provide a smoother curve, but again, additional tests would be needed to assure accuracy at hold times under two minutes.

For hold times under ten minutes, the crack growth rate is multiplied by the bilinear correction to predict the new growth rate, resulting in the following adjusted model equation:

$$\frac{da_K}{dt} = \frac{da_K}{dt} \Big|_{\text{creep}} + \frac{F(HT)}{6HT} \frac{da_K}{dt} \Big|_{\text{fatigue}} \quad (14)$$

where

$$\begin{aligned} F(HT) &= \text{Bilinear Correction} \\ &= 6*HT \quad \text{for } HT < 0.522 \\ &= 3.25 - 0.225*HT \quad \text{for } 0.552 \leq HT \leq 10 \end{aligned}$$

Again, the bilinear correction assumes that the crack growth rate during a hold time test will not exceed the fatigue crack growth rate.

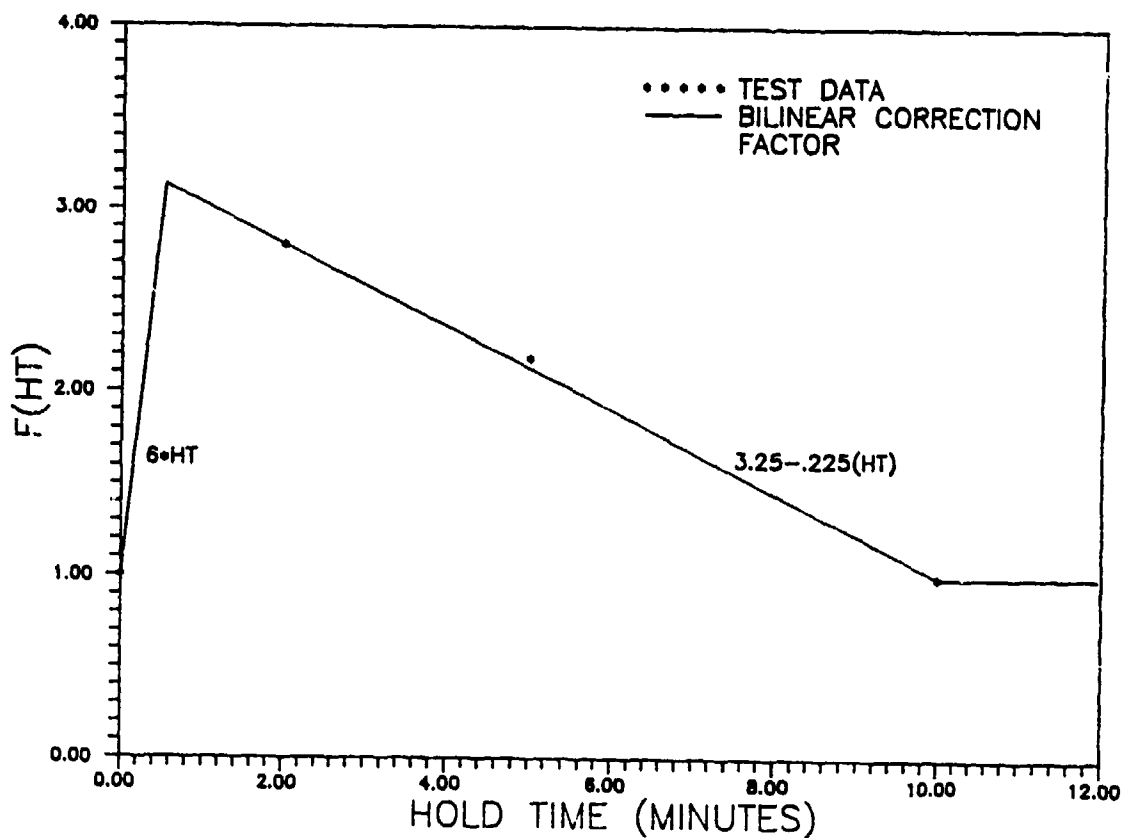


Figure 30. Comparison of Test Data with Linear Model at Constant Stress Intensity (maximum difference indicated by \*)

Additional tests with hold times under two minutes would be required to prove or further modify the model. The original model and the adjusted model are shown schematically in Figure 31 as a function of hold time at constant stress intensity. The figure also shows the sustained load and fatigue crack growth rate contributions. The mixed-mode contribution is the additional growth resulting from the bilinear correction. The predictive models for the two and five minute hold-time tests were

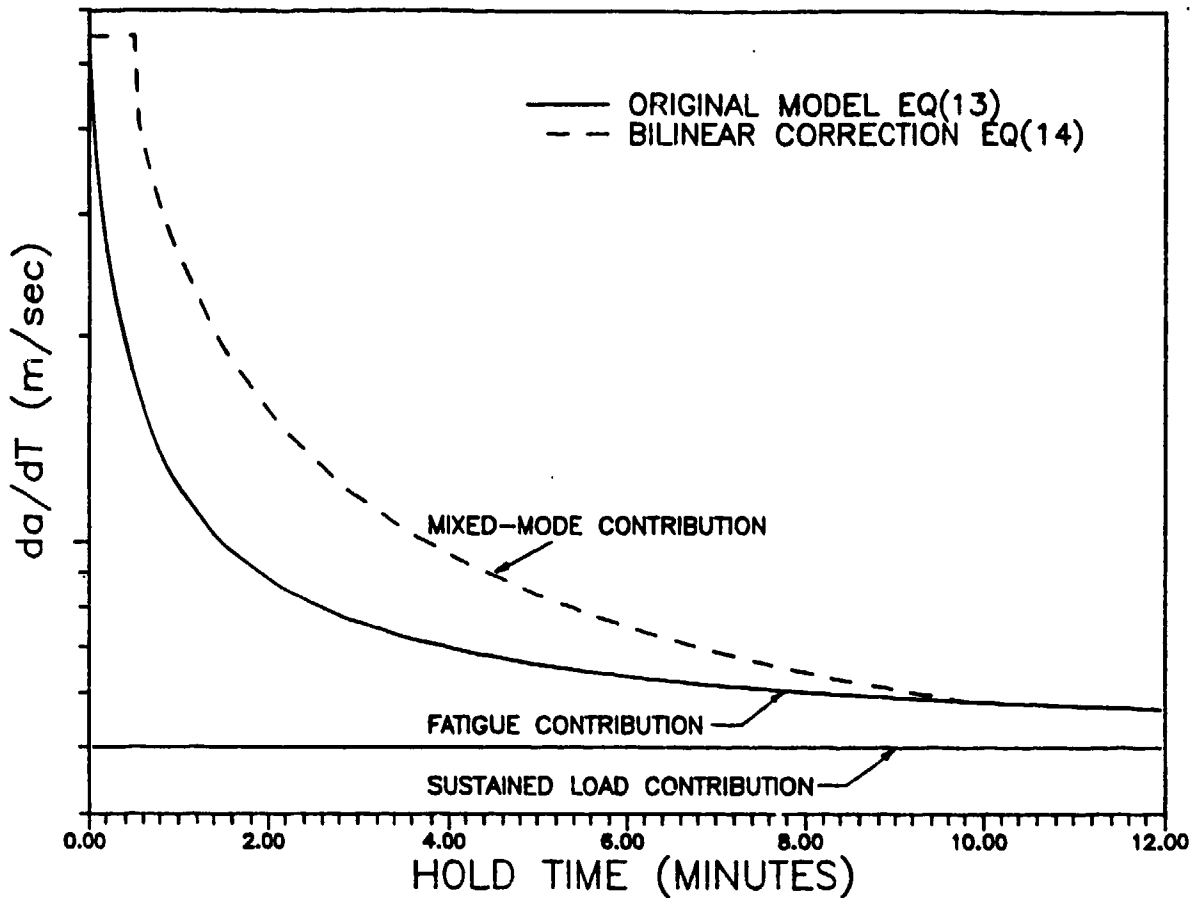


Figure 31. Schematic Representation of Crack Growth Rates at Constant Stress Intensity

recalculated using the bilinear correction. The resulting modified predictive models for the two and five minute hold-time tests are shown in Figures 32 and 33. The ten minute hold-time model was not affected by the bilinear correction.

The modified model provides a much better visual fit to the experimental data, but, this is expected since the modification was based on the test data. Additional testing and perhaps further modifications would be required before it would actually be used to predict time-to-failure for a component, especially at shorter hold times.

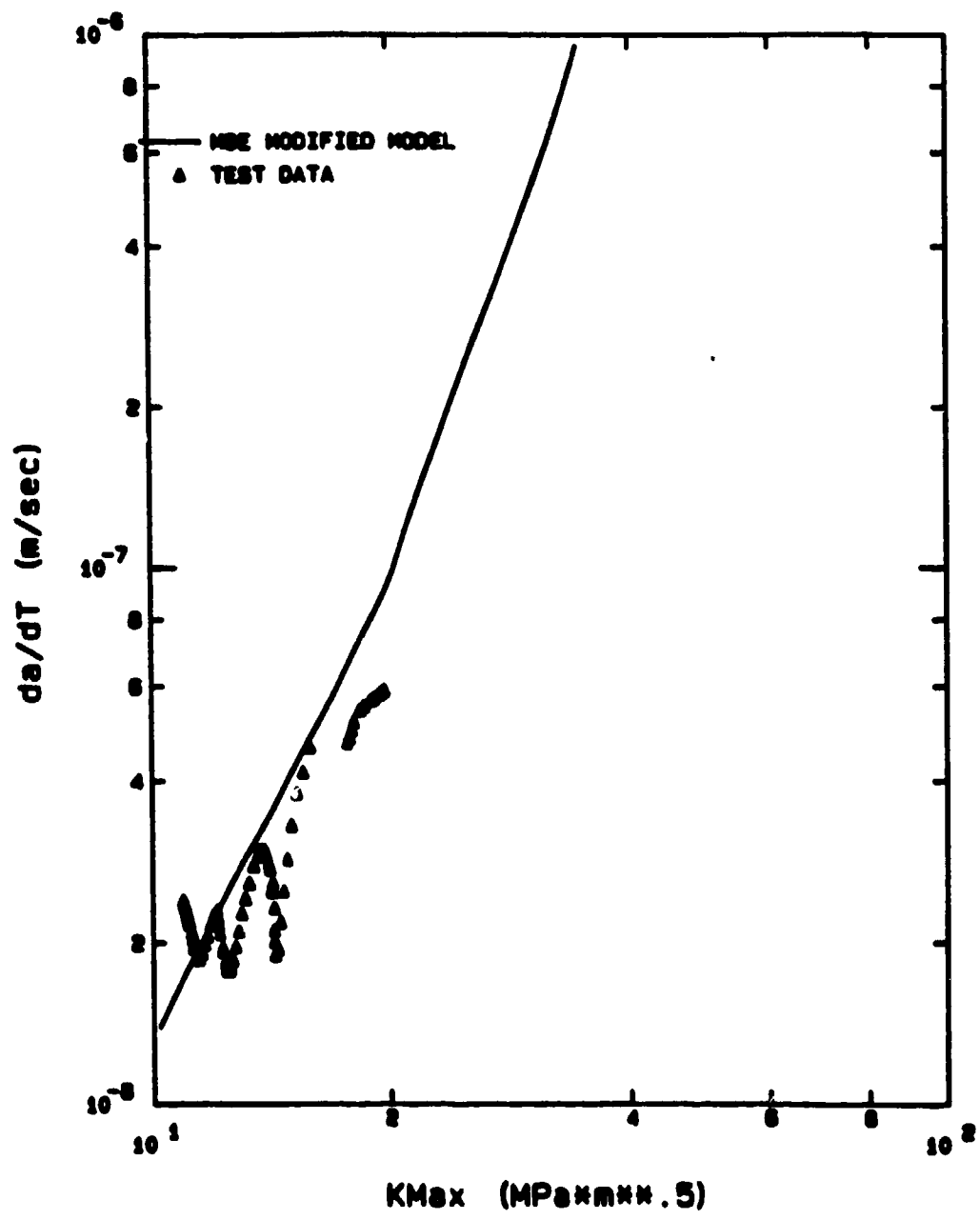


Figure 32. Modified Model Model for 2 Minute Hold Test

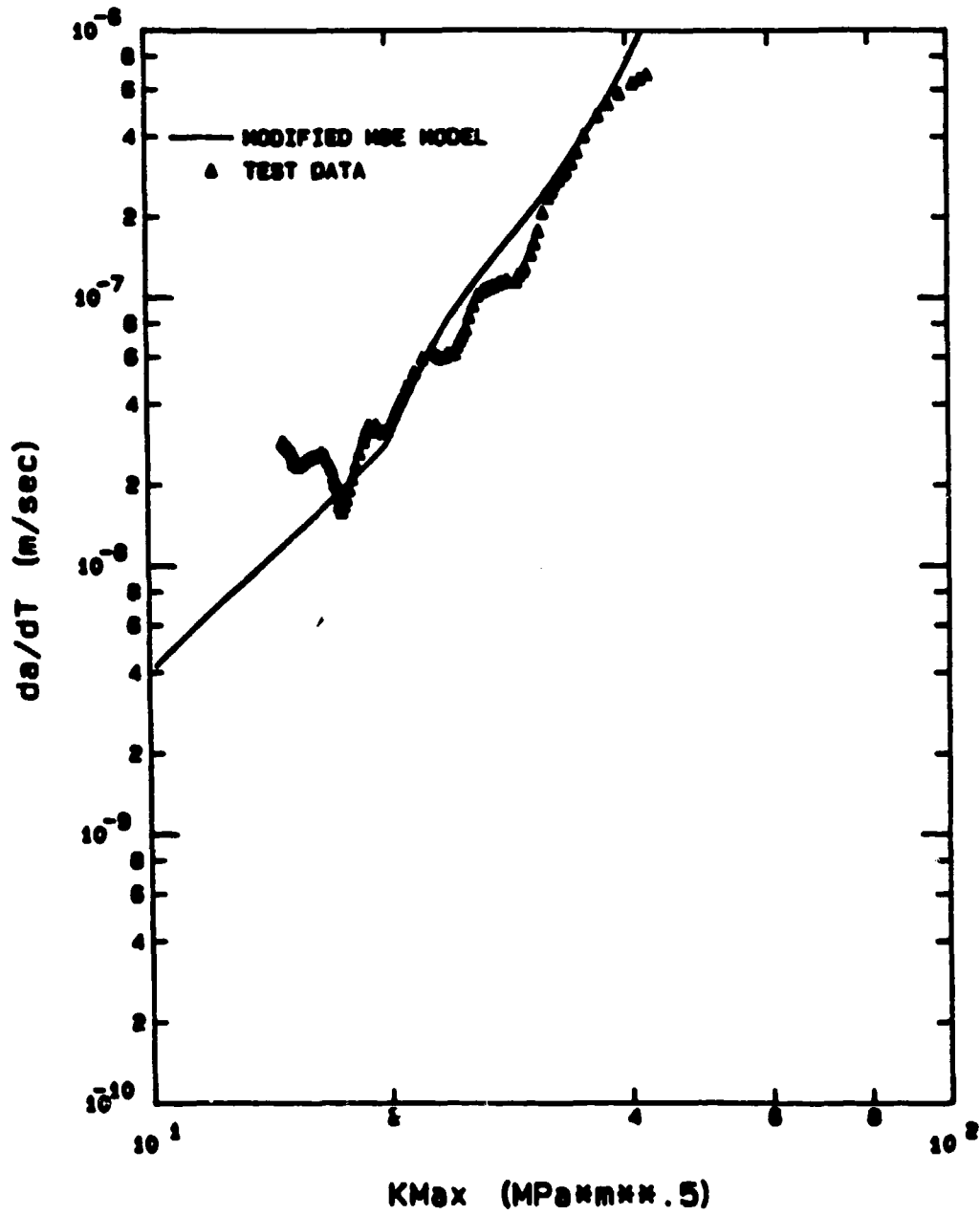


Figure 33. Modified Model Model for 5 Minute Hold Test

Once the crack growth rate for a given hold time has been established, the crack length as a function of time can be evaluated by integrating the crack growth rate, resulting in the following equation.

$$a_t = a_0 + \int_0^t \frac{da}{dt} dt \quad (15)$$

where:

$a_t$  = crack length at time  $t$

$a_0$  = initial crack length

The program used to calculate the hold time curves based on the MSE models is included in Appendix D. A simple iterative routine to calculate crack length as a function of time is also included in the program.



## VII. Conclusions and Recommendations

The purpose of this investigation was to characterize sustained load crack growth and to determine the applicability of linear cumulative damage modeling in  $Ti_3Al$  at elevated temperatures. Test results for 700° C, 750° C, and 800° C showed that sustained load crack growth rates were relatively insensitive to temperature with the difference between the slowest and the fastest growth rates only a factor of five apart for 95 percent of the data. The threshold and critical stress intensities were insensitive to temperature as well. The estimated threshold stress intensity was  $20 \text{ MPa}\sqrt{m}$  and the calculated critical stress intensity was  $46 \text{ MPa}\sqrt{m} \pm 6$  percent for all the tests. Since no sustained load crack growth occurred at 650° C, temperature serves primarily as a "go or no go" constraint for sustained load crack growth.

Data from the fatigue and hold time tests conducted at 750° C indicated that there was creep-fatigue interaction even below the estimated threshold for sustained crack growth and that this interaction appeared to be a function of the hold time. The crack growth rates per cycle for all the hold-time tests was twice as fast as the fatigue baseline data. Comparing the growth rates in the time domain, the trend, in general, was to faster crack growth with shorter hold times, indicating that crack growth in  $Ti_3Al$  can be modeled using linear cumulative damage modeling.

A damage model was developed based on a linear summation of the sustained load and fatigue crack growth contributions and it showed accurate or conservative crack growth rate estimates for only the ten

minute hold-time test. The linear model crack growth rates were a factor of two to three less than the growth rates calculated for the two and five minute hold time tests. Though still within the possible experimental scatter for the experiments, a mixed-mode crack growth correction was developed which produced more accurate predictions for the two and five minute hold-time tests.

These conclusions, of course, are based on only a very narrow band of testing conditions. Further tests on the alloy at different frequencies and with different hold times and load ratios would be required to get a more accurate understanding of the alloy's behavior at elevated temperatures. Shorter hold times should be investigated to determine the extent and range of creep-fatigue interaction between the fatigue baseline and the two minute hold-time data already collected. Since the Swedish Creep frame cannot test hold times under two minutes, these test would have to be conducted with other equipment.

The specimens used for the sustained load tests and the ten minute hold-time test were severely tunneled. Equipment limitations did not allow for accurate measurement of the transition between the fatigue precrack which showed less than 0.1 mm tunneling and the first measurable correction of 2.29 mm. Additional tests will be required to accurately measure the transition.

Appendix A

History of Test Specimens

### Specimen History

The specimens used for these experiments were provided to the Air Force Materials Laboratory by the Allison Gas Turbine Division of General Motors(10:5-7). The composition of the alloy in atomic percent is Ti-24Al-11Nb. The weight composition and heat treatment of the alloy are given in the tables below. Once delivered, the Materials Laboratory tested the alloy at several temperatures to determine its material properties. The properties for  $Ti_3Al$  are shown in the figures on the next three pages.

Table IV Compact Tension Specimen Composition

Element	Ti	Al	Nb	Fe	O <sub>2</sub>	N
Weight %	63.462	14.1	22.3	0.071	0.058	0.009

Table V Heat treatment of the  $Ti_3Al$  Alloy

- 1) Forged at 2300°F
- 2) Cross rolled at 1900°F
- 3) Beta annealed at 2150°F for 30 minutes
- 4) Air cooled to room temperature

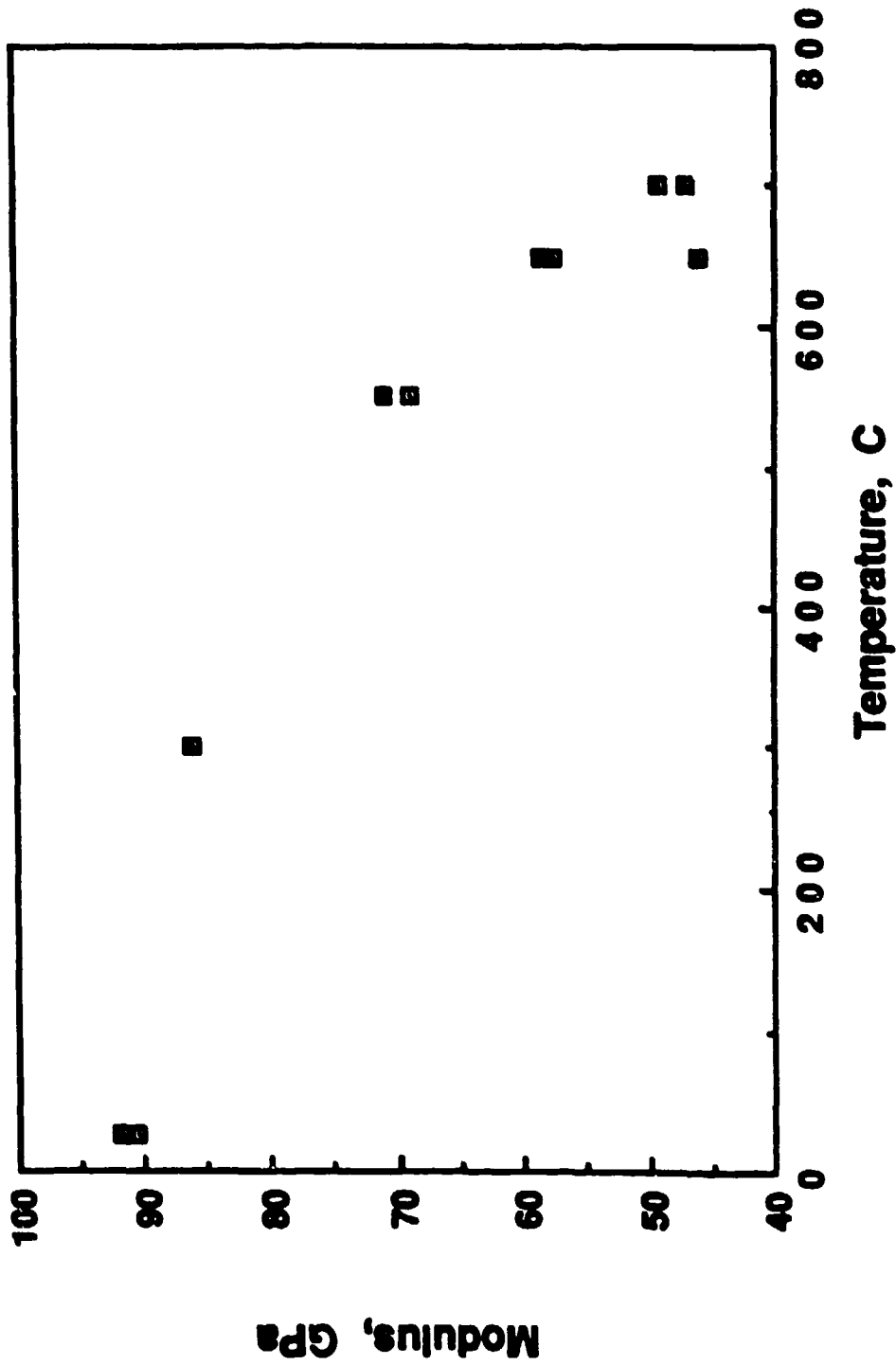


Figure 34. Modulus Versus Temperature for Ti<sub>3</sub>Al

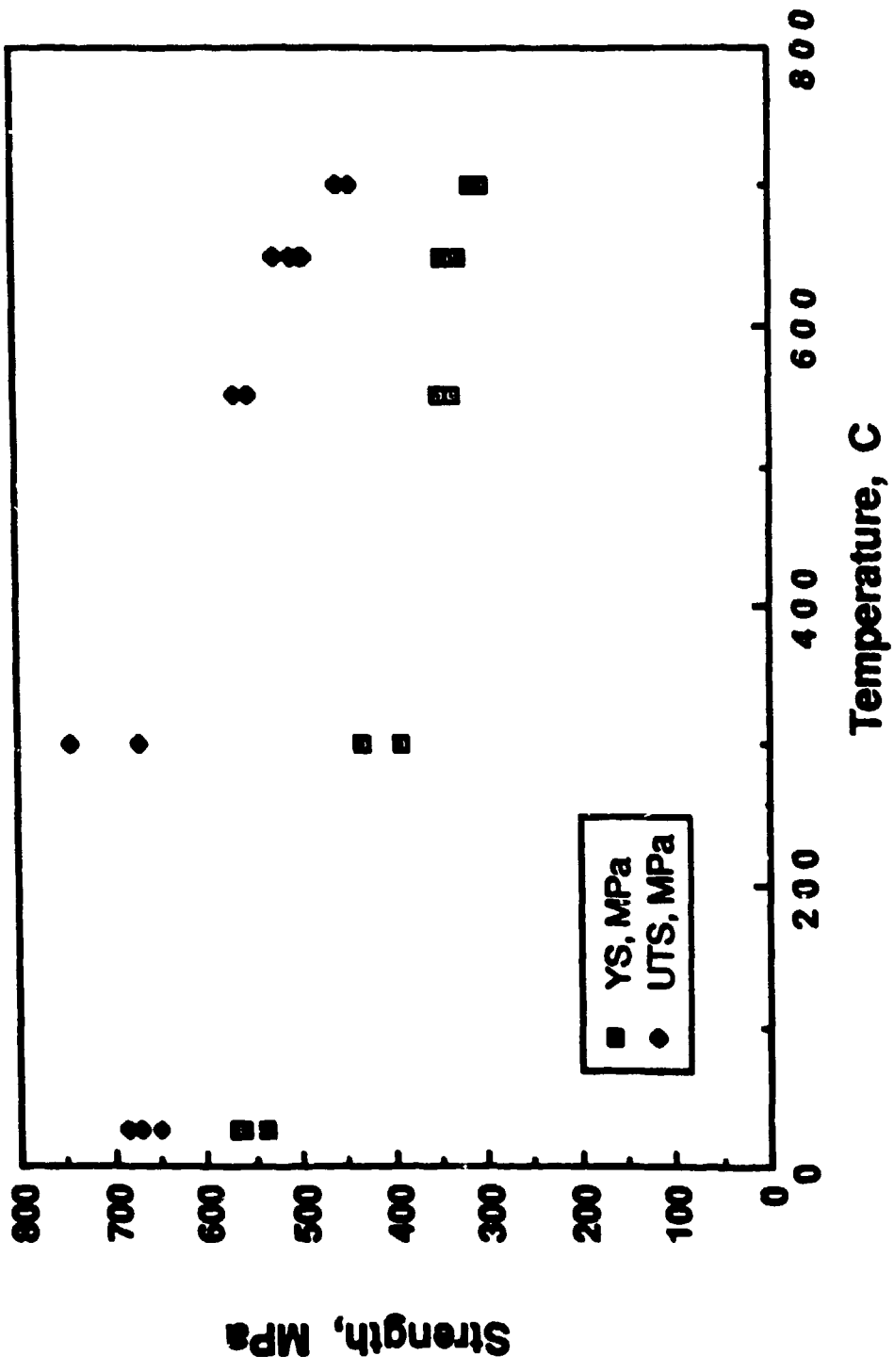


Figure 35. Strength Versus Temperature for Ti<sub>3</sub>Al

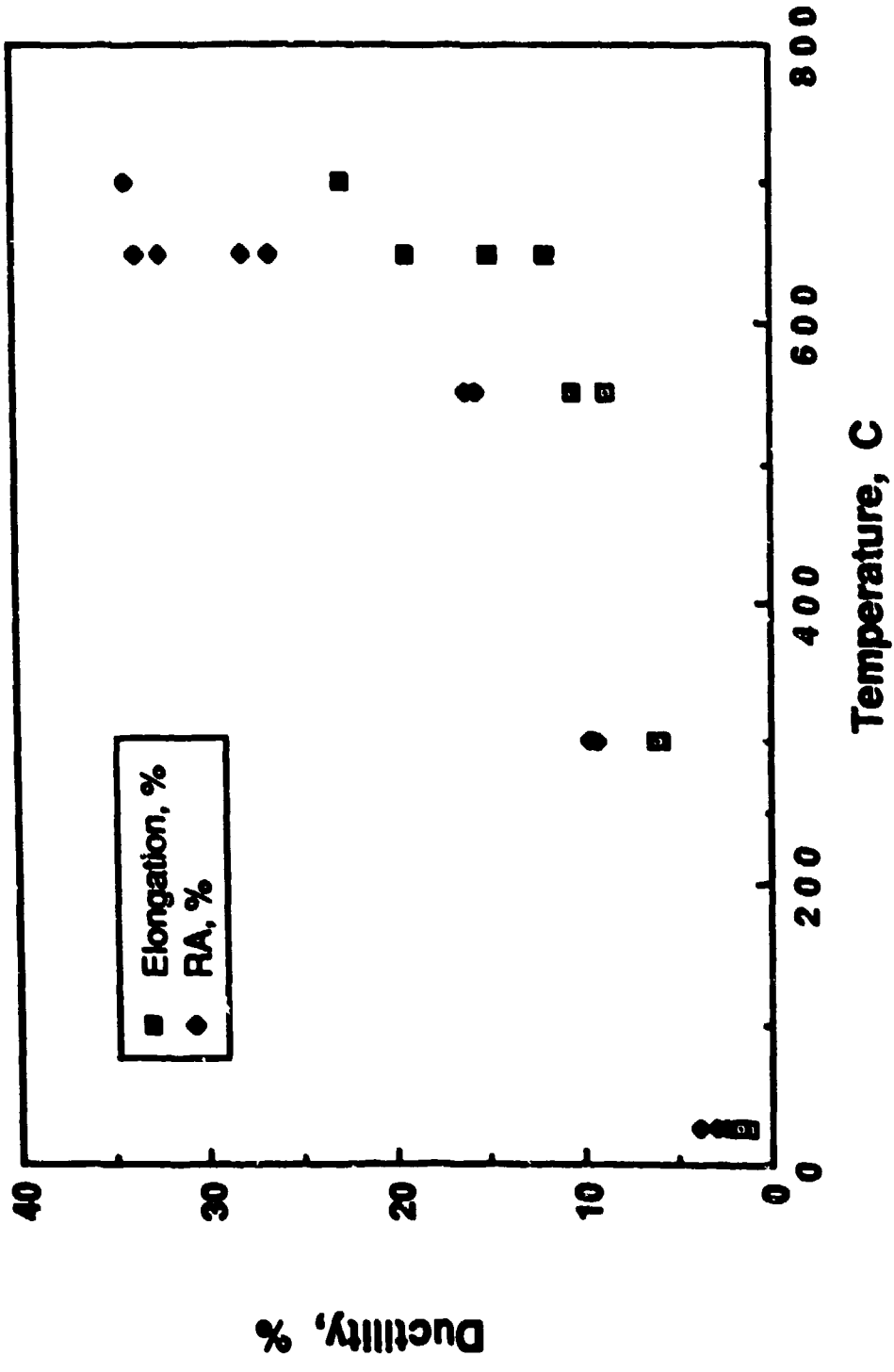


Figure 36. Ductility Versus Temperature for Ti<sub>3</sub>Al

**Appendix B**

**Fatigue Precracking of Test Specimens**



Prior to test, each CT specimen was fatigue precracked on an MTS. The table below contains the parameters used to fatigue precrack the specimens.

Table VI Specimen Precrack Parameters

1) Test Temperature	1000°F (538° C)
2) Frequency	2 Hz
3) Initial Stress Intensity ( $K_0$ )	13 ksi/ $\sqrt{\text{in}}$ (14.3 MPa/ $\sqrt{\text{m}}$ )
4) Final Maximum Stress Intensity	9 ksi/ $\sqrt{\text{in}}$ (9.89 MPa/ $\sqrt{\text{m}}$ )
5) Load Shed during Fatigue Cycle	90 %
6) Desired Crack Length (in)	.4740 (12 mm)

**Appendix C**

**Crack Growth Curves for Specimens**

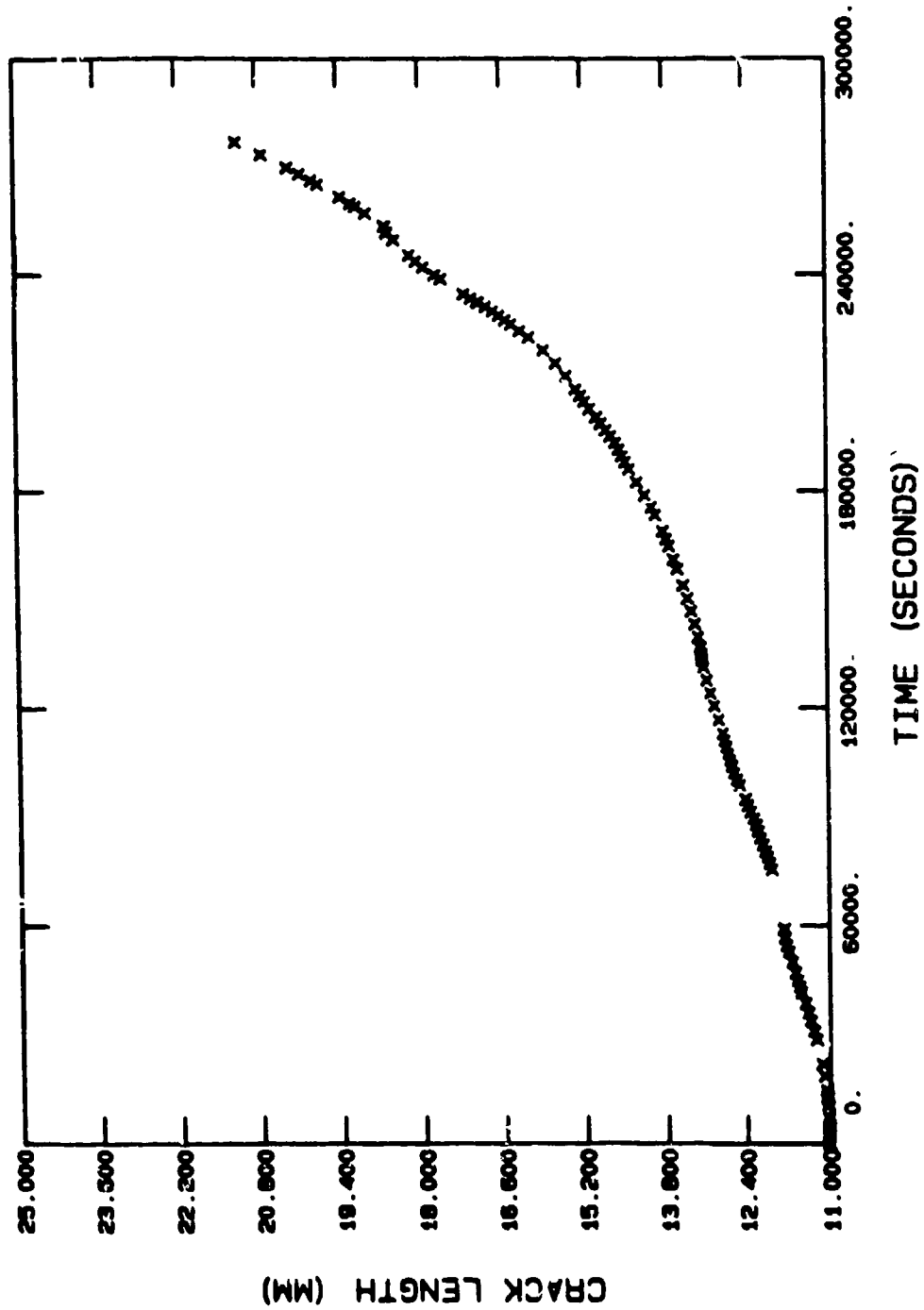


Figure 37. Crack Growth Versus Time for Specimen 88-102

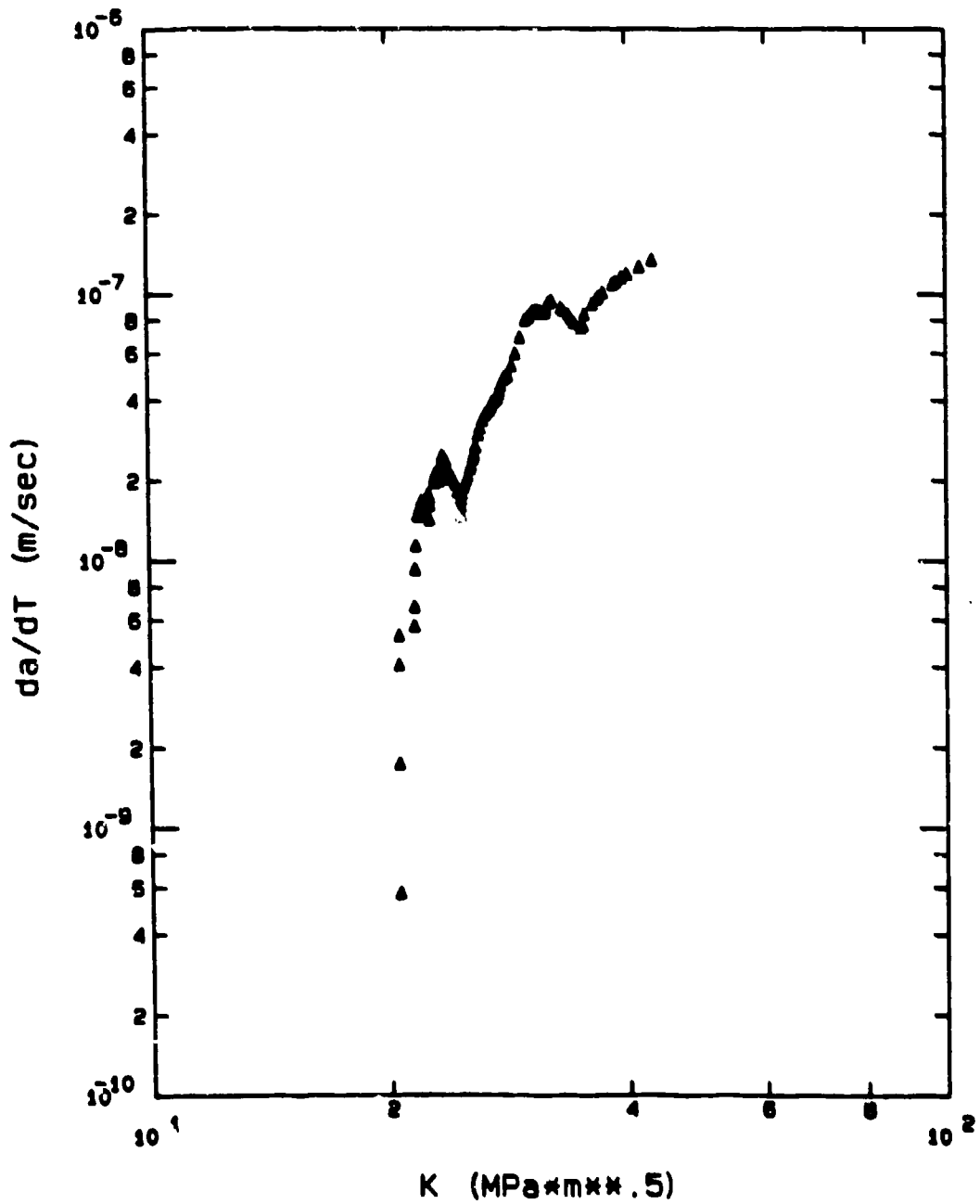
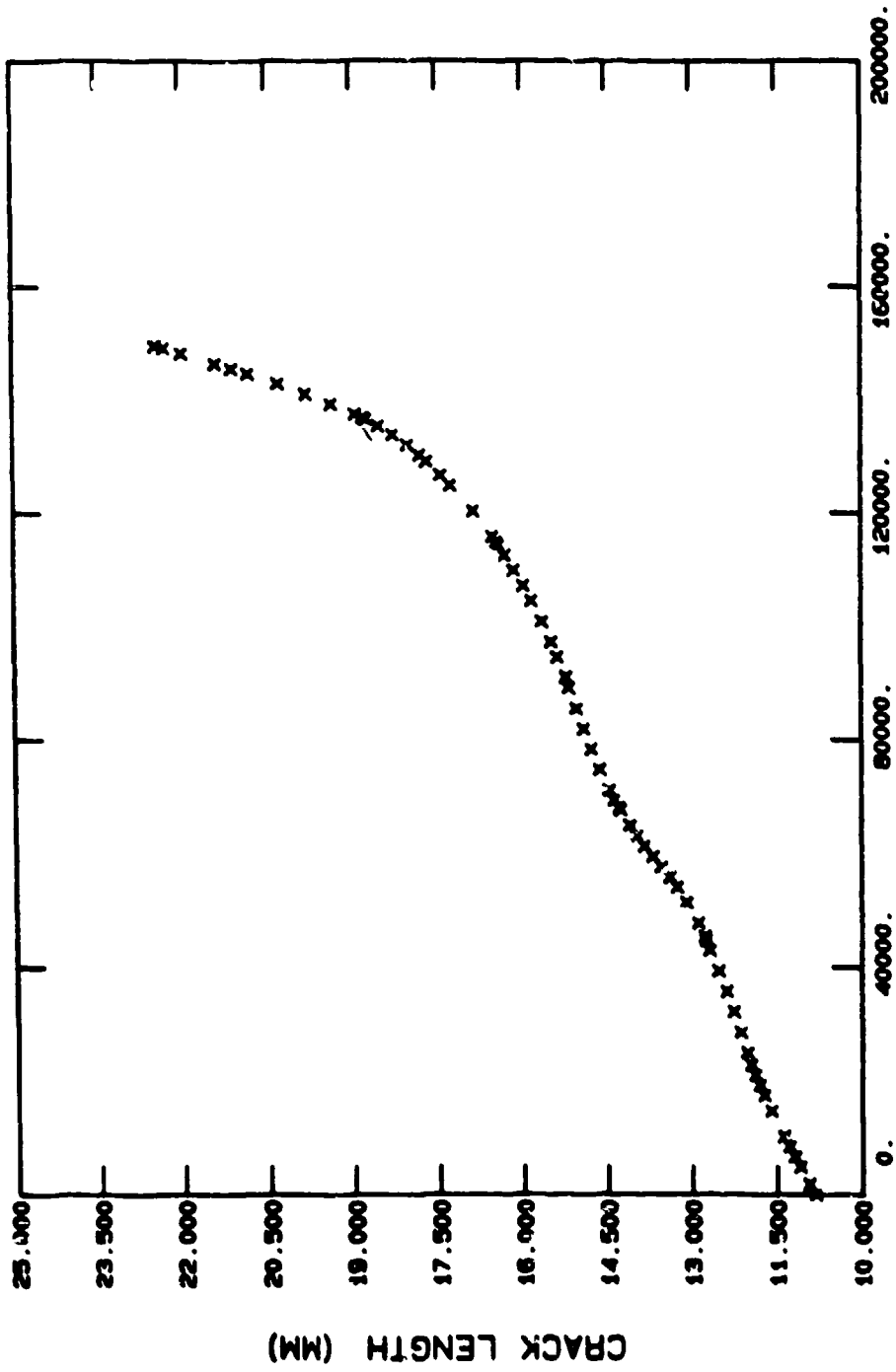


Figure 38. Crack Growth Rate Versus Stress Intensity for Specimen 88-102



TIME (SECONDS)

Figure 39. Crack Growth Versus Time for Specimen 88-104

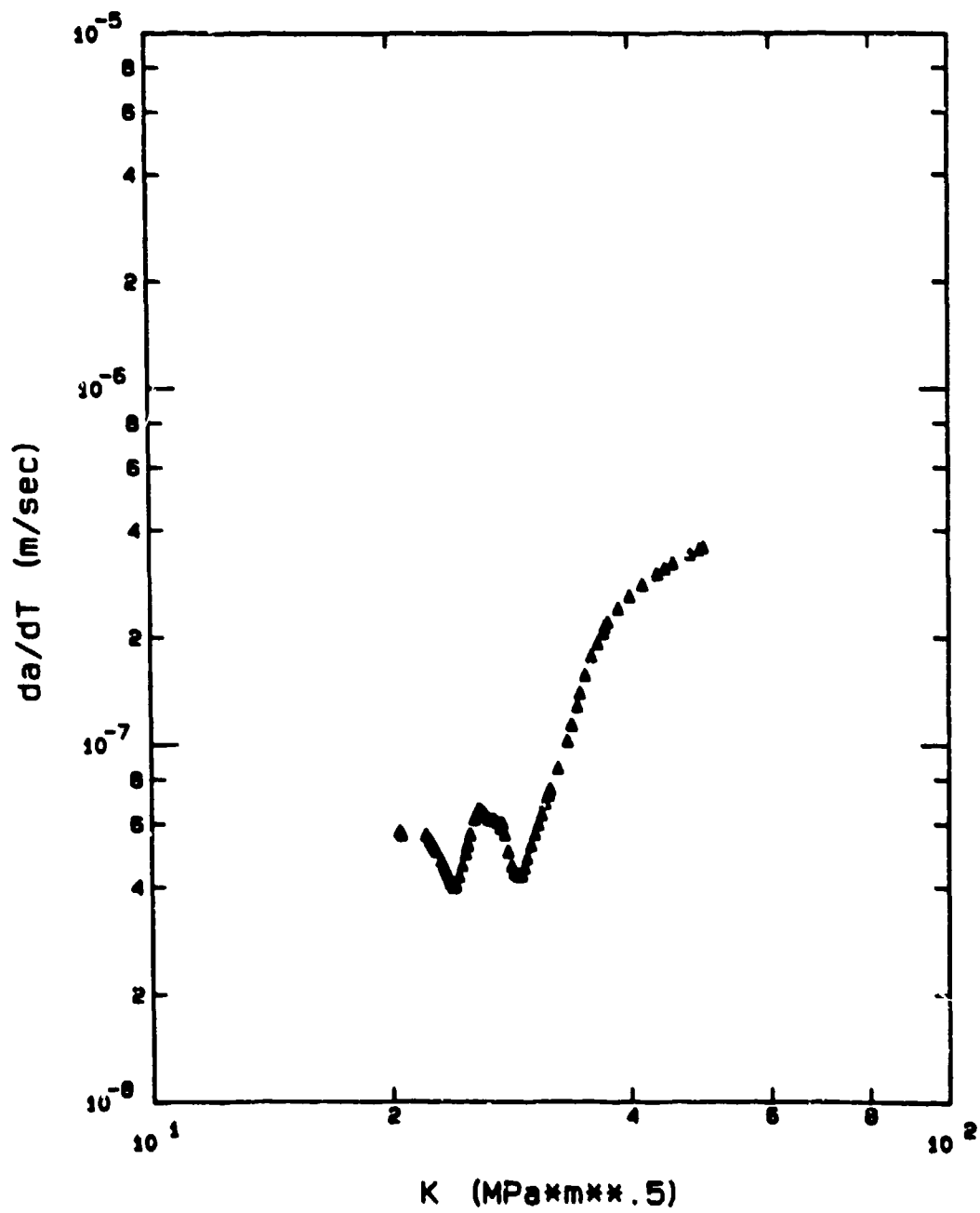


Figure 40. Crack Growth Rate Versus Stress Intensity for Specimen 88-104

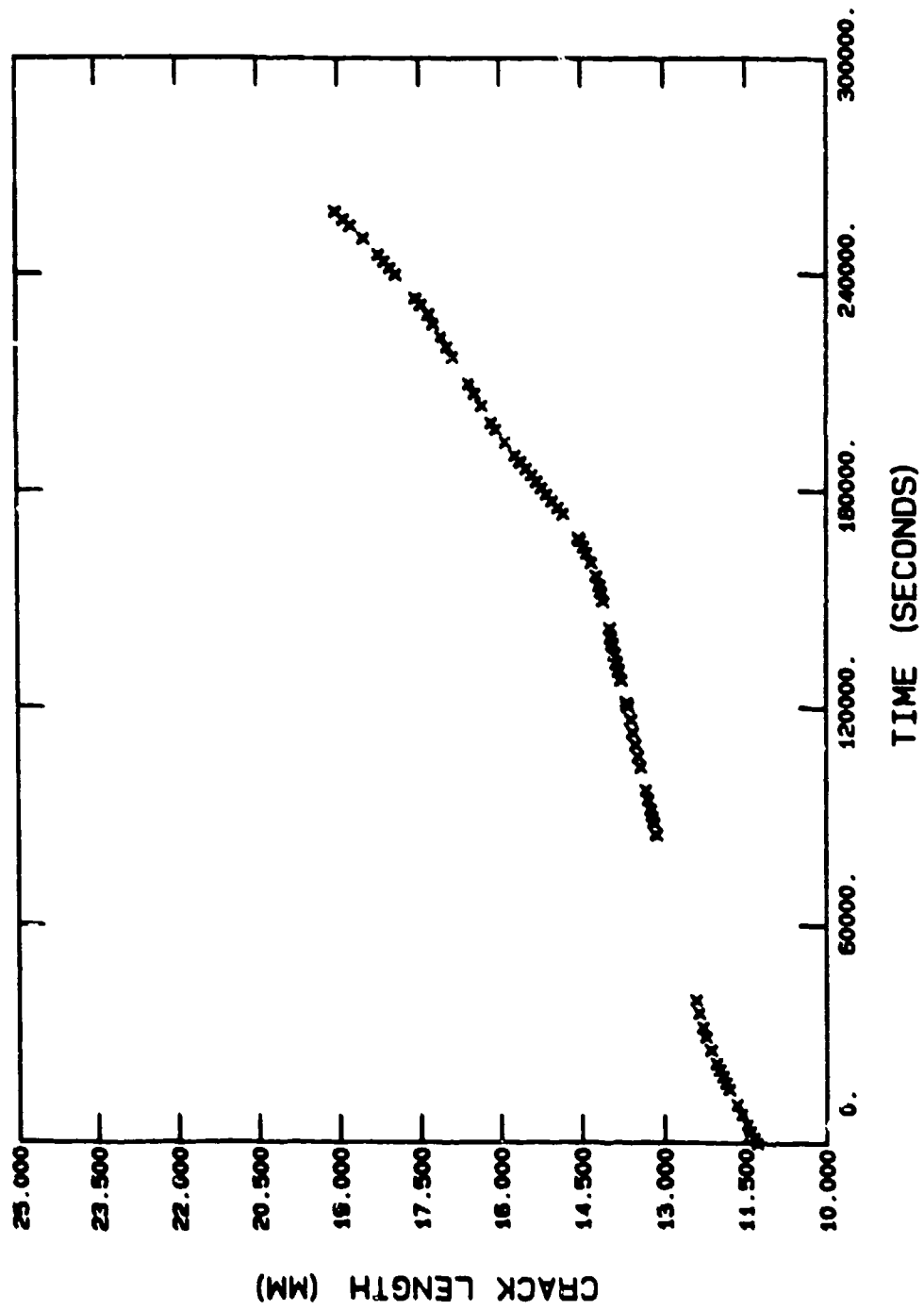


Figure 41. Crack Growth Versus Time for Specimen 88-105

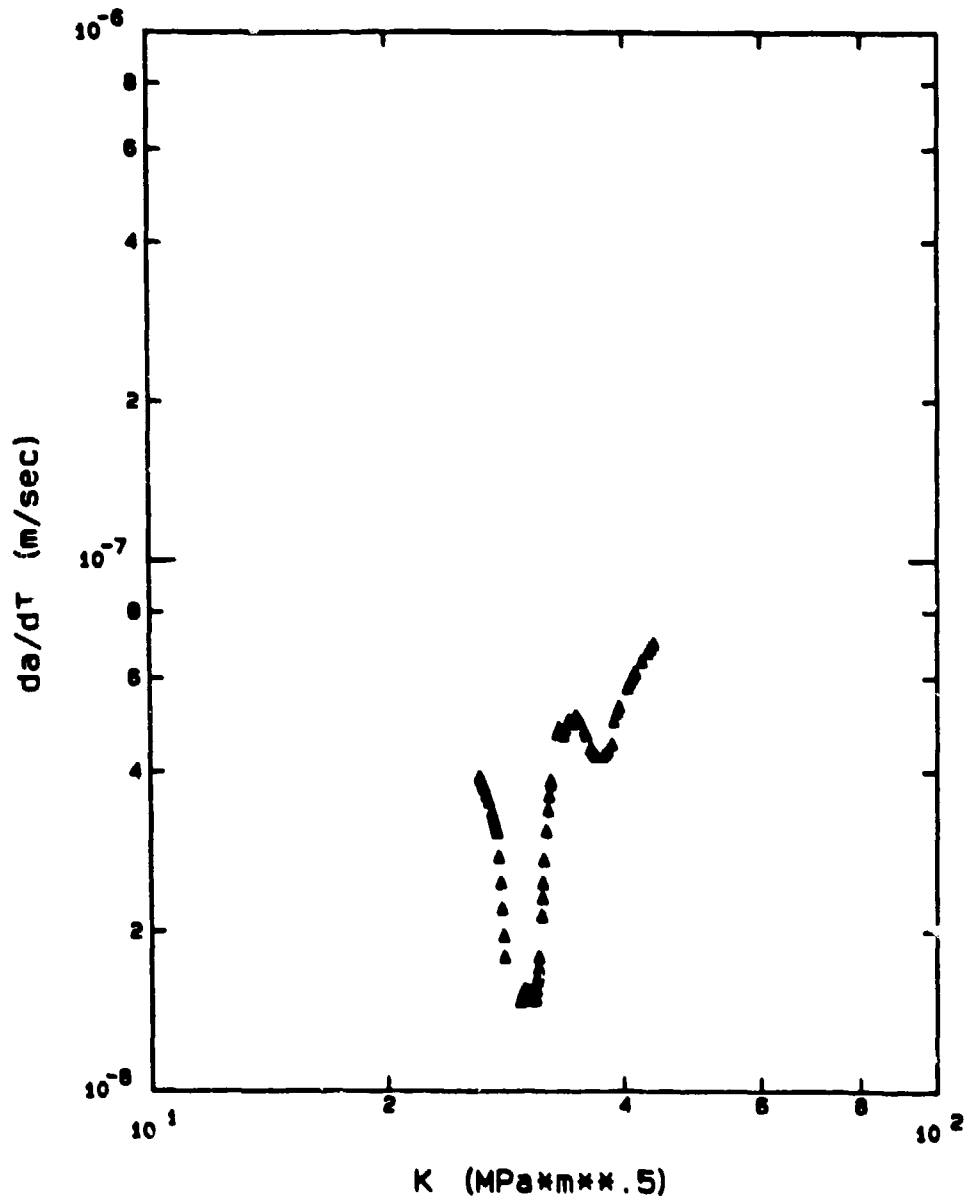


Figure 42. Crack Growth Rate Versus Stress Intensity for Specimen 88-105



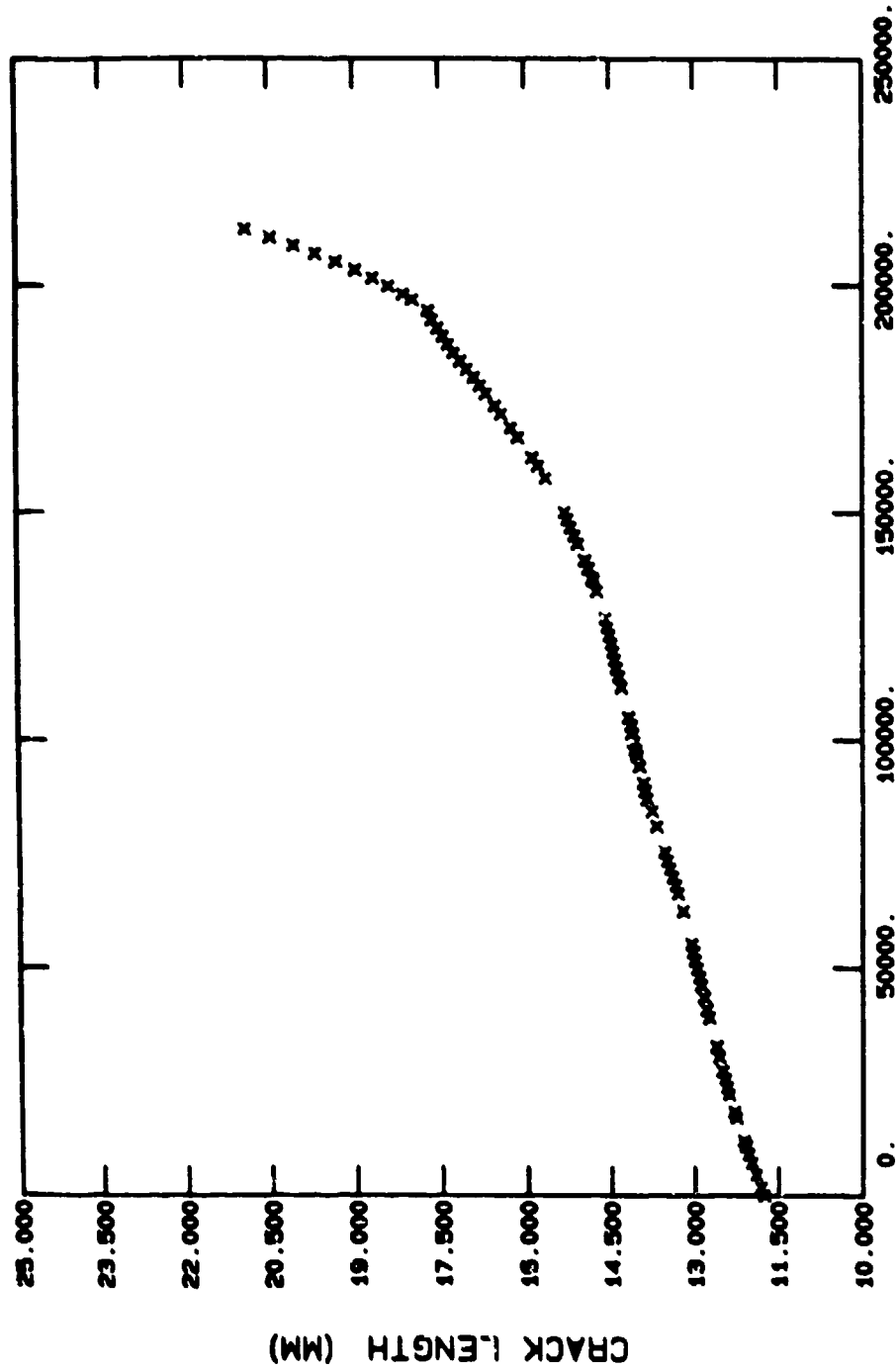


Figure 43. Crack Growth Versus Time for Specimen 88-112

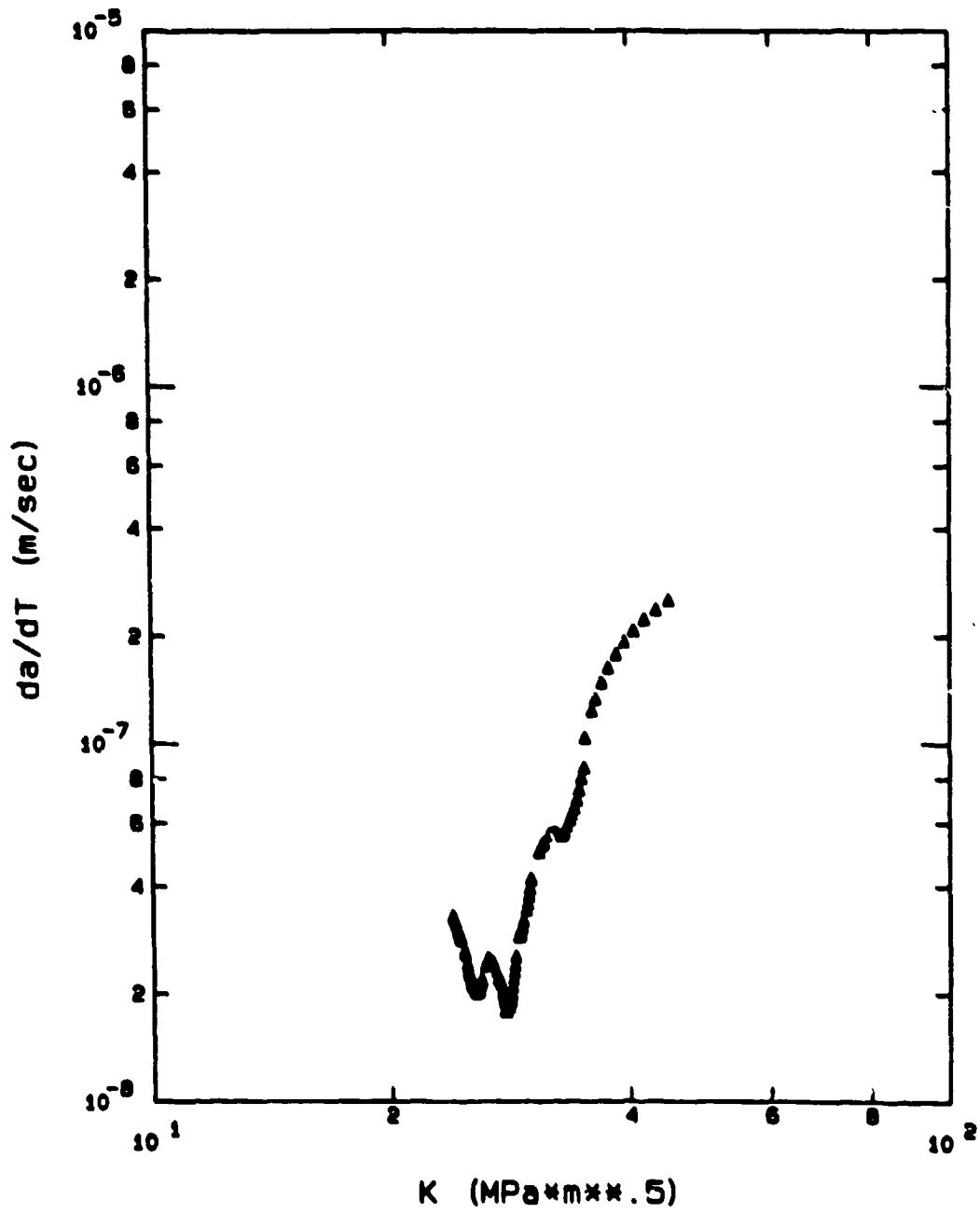
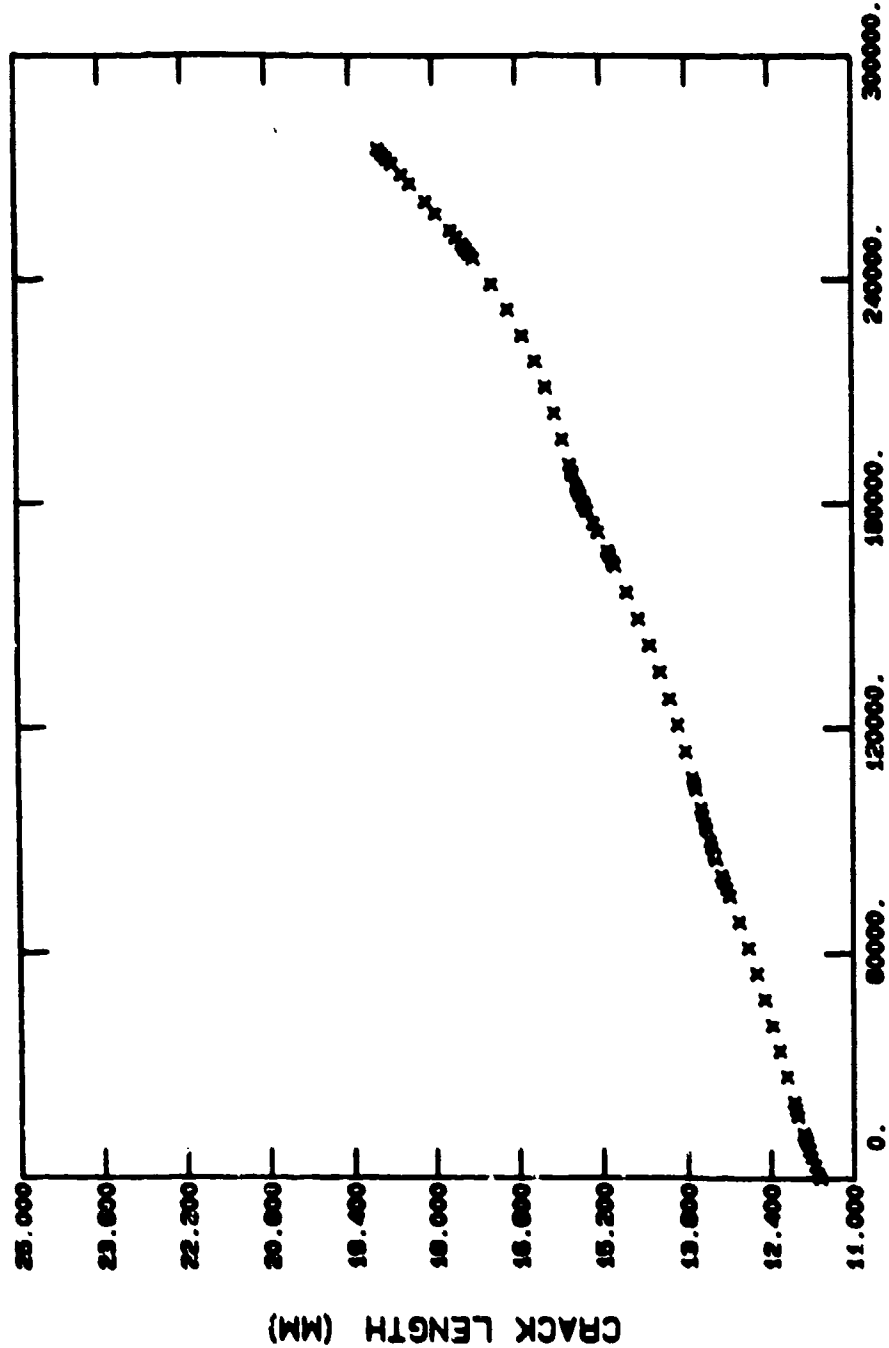


Figure 44. Crack Growth Rate Versus Stress Intensity for Specimen 08-112



TIME (SECONDS)

Figure 45. Crack Growth Versus Time for Specimen 88-113

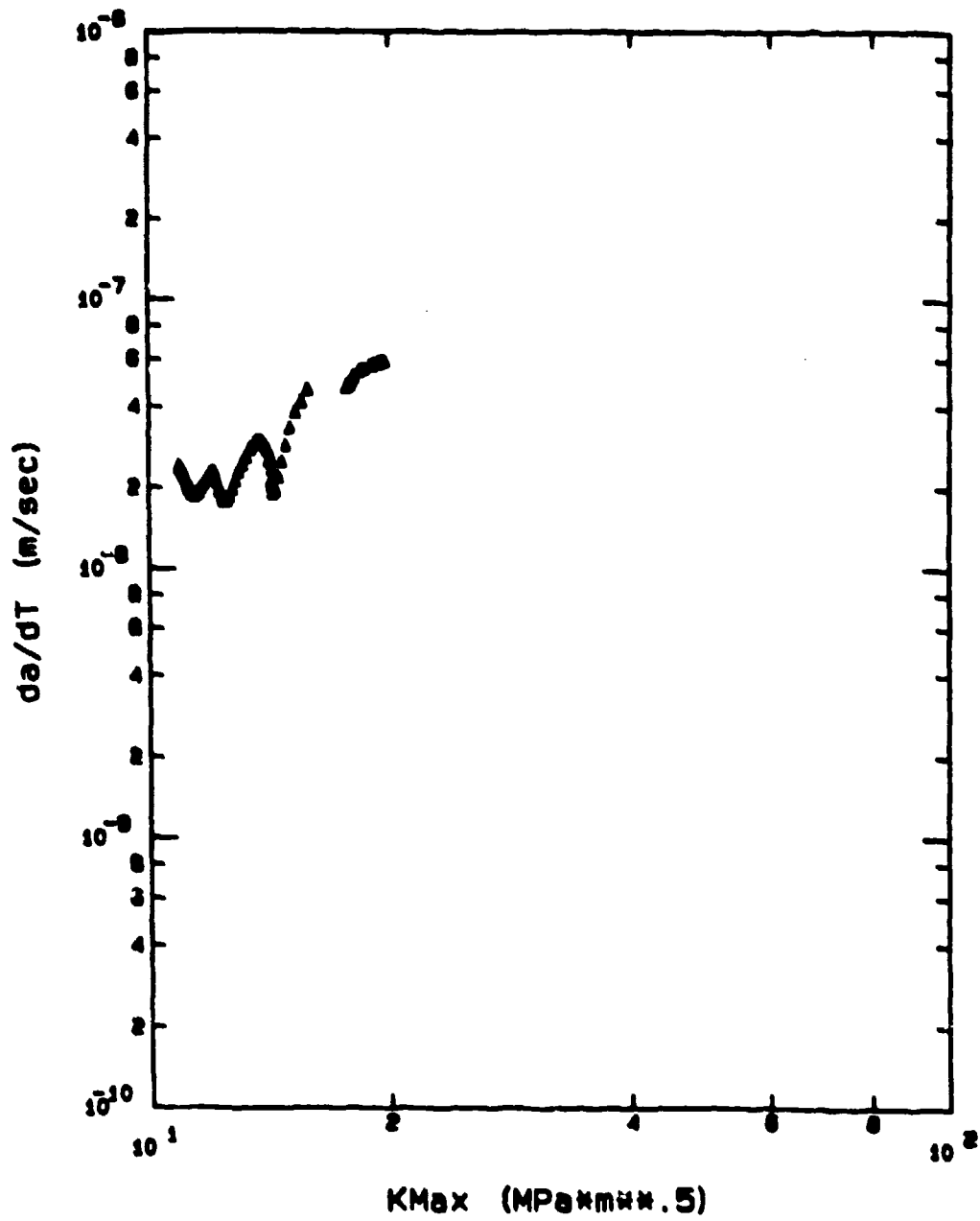


Figure 46. Crack Growth Rate Versus Stress Intensity for Specimen 88-113

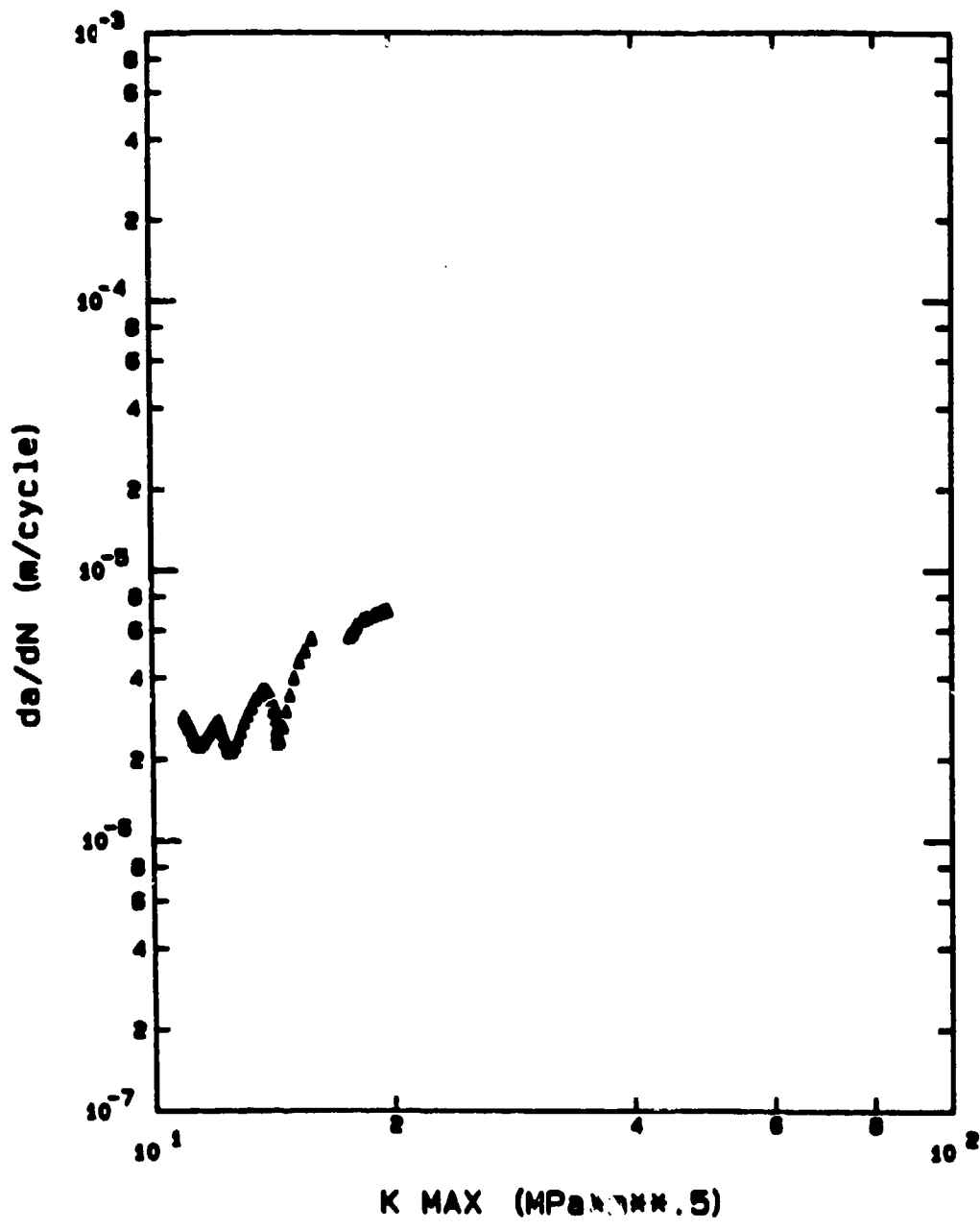


Figure 47. Crack Growth per Cycle Versus Maximum Stress Intensity for Specimen 88-113

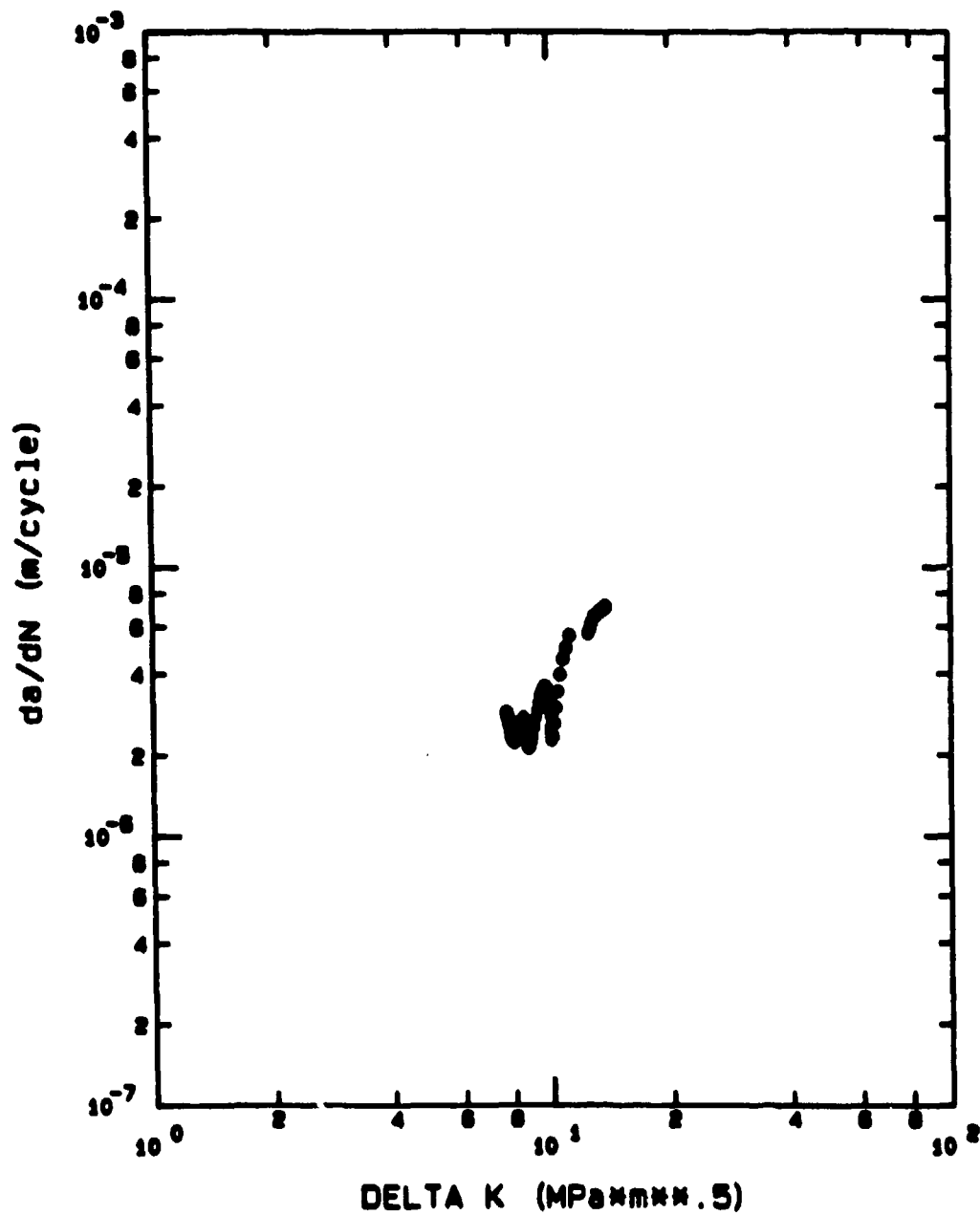


Figure 48. Crack Growth per Cycle Versus Delta Stress Intensity for Specimen 88-113

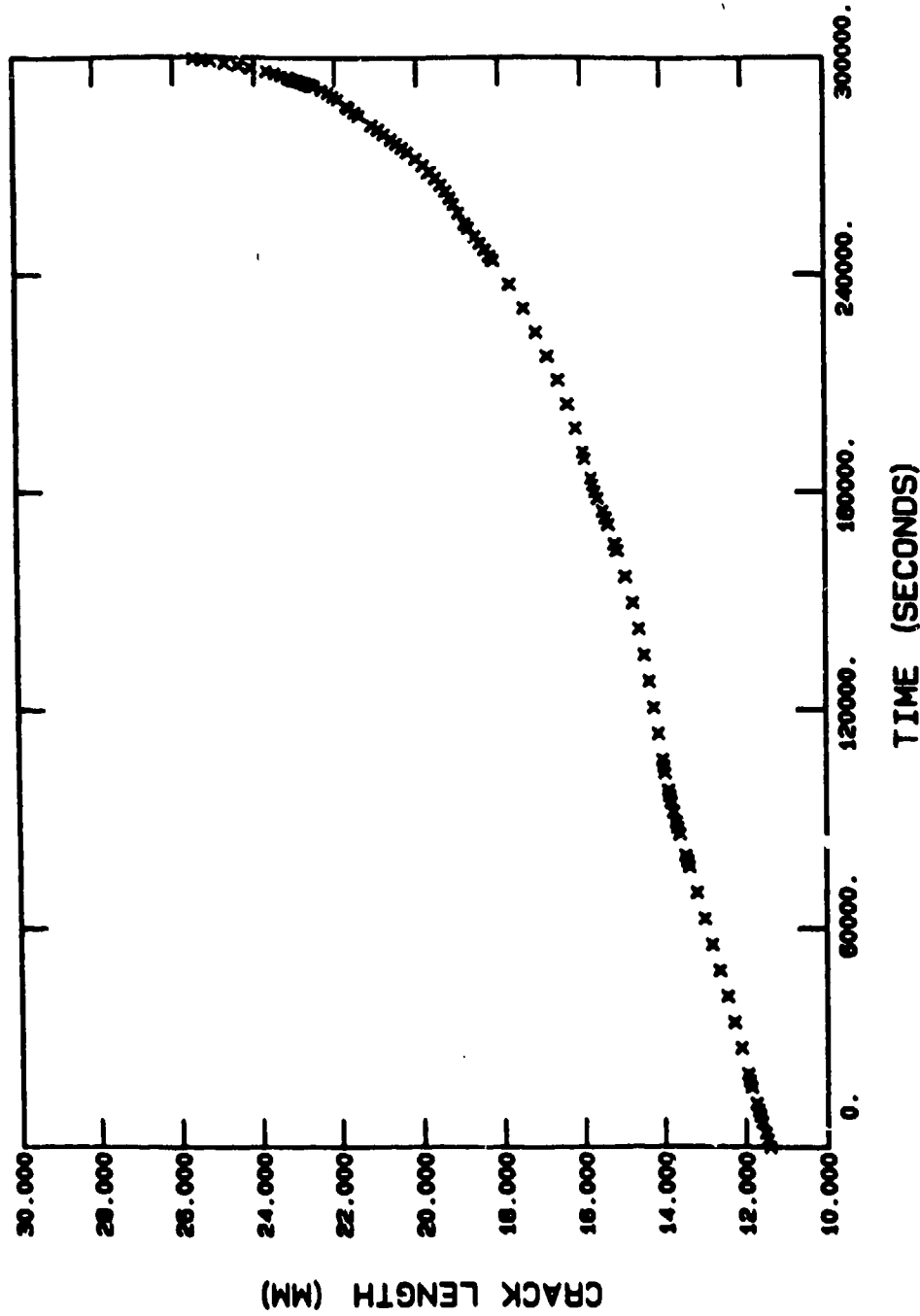


Figure 49. Crack Growth Versus Time for Specimen 88-114

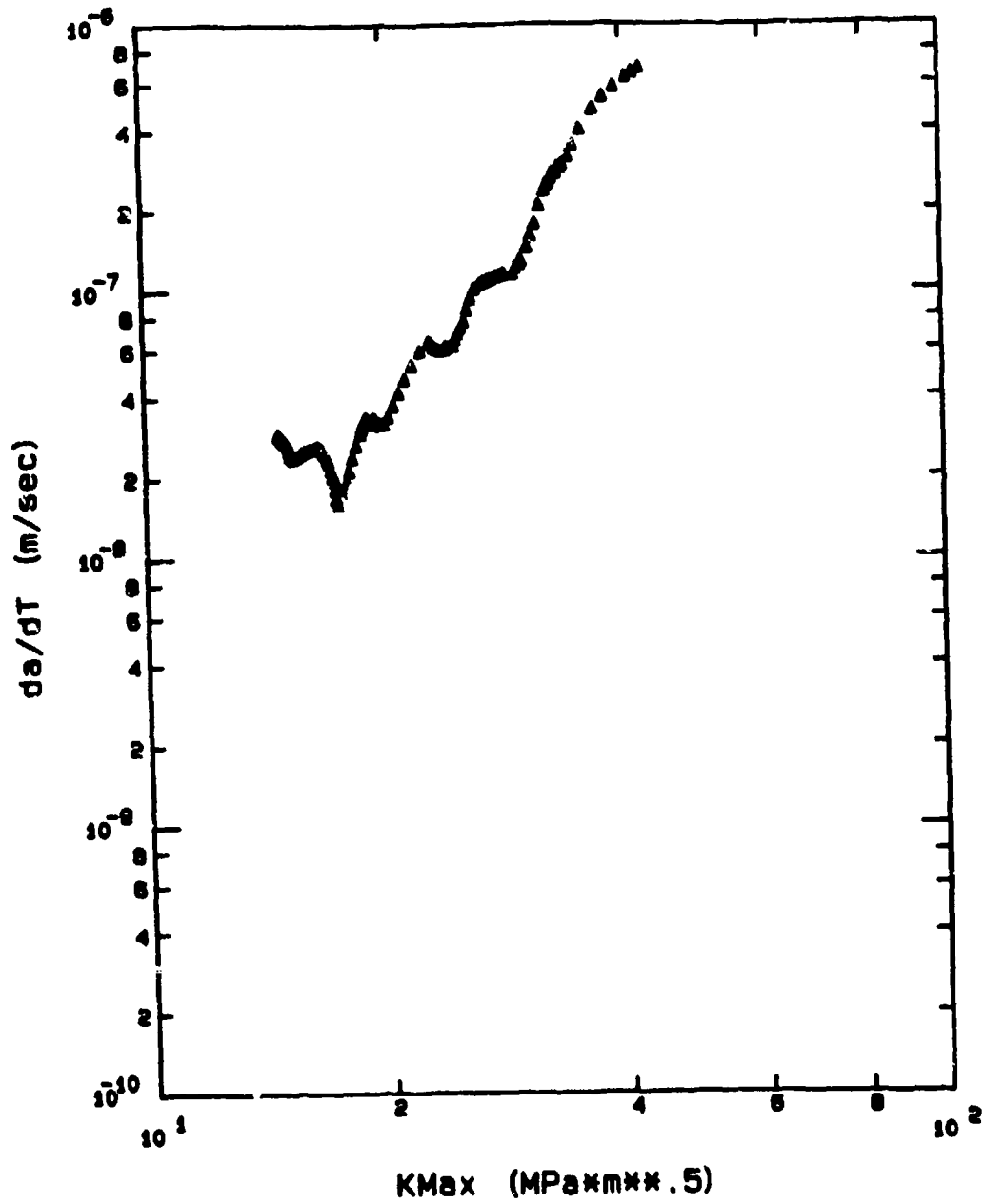


Figure 50. Crack Growth Rate Versus Maximum Stress Intensity for Specimen 88-114



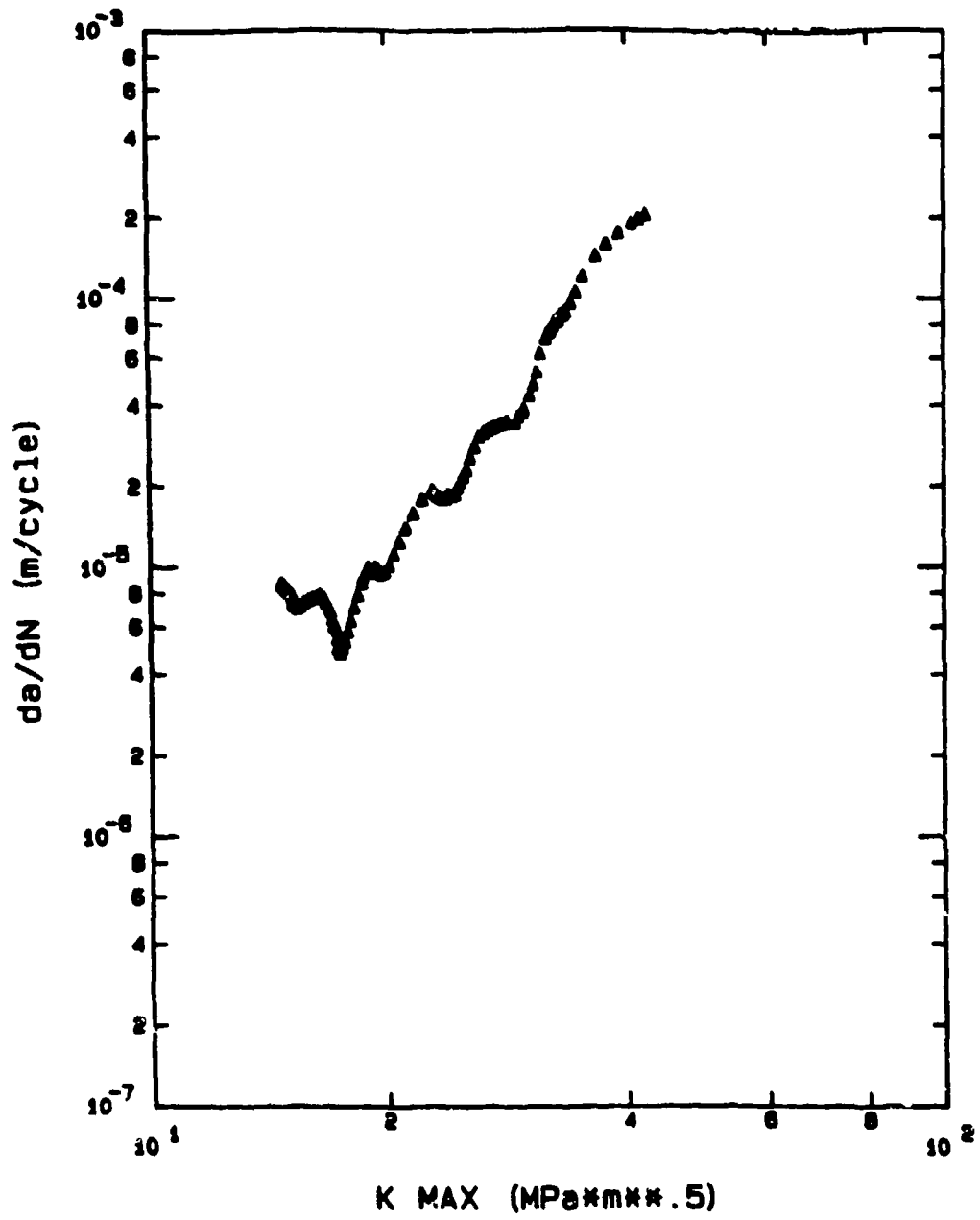


Figure 51. Crack Growth per Cycle Versus Maximum Stress Intensity for Specimen 88-114

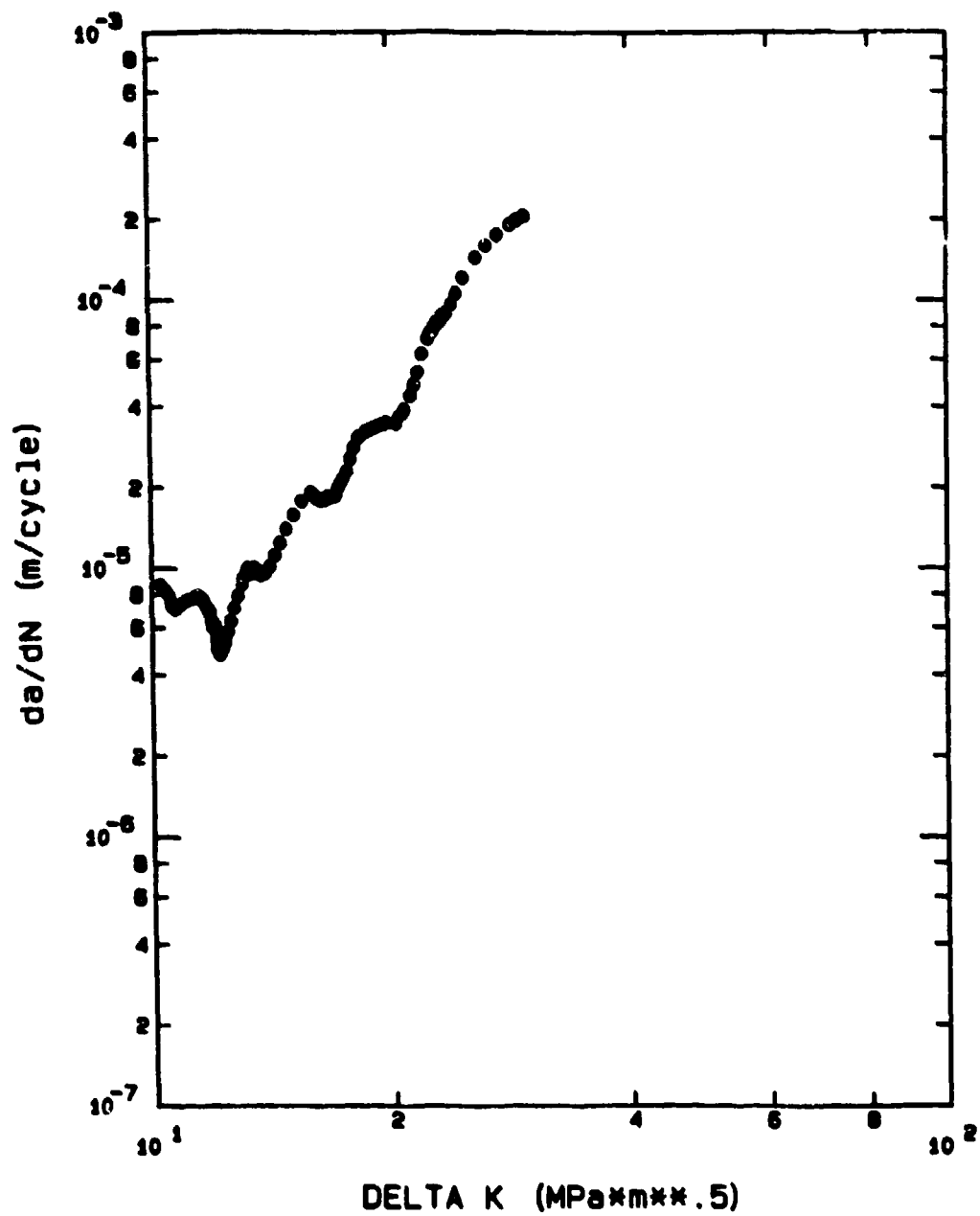


Figure 52. Crack Growth per Cycle Versus Delta Stress Intensity for Specimen 88-114

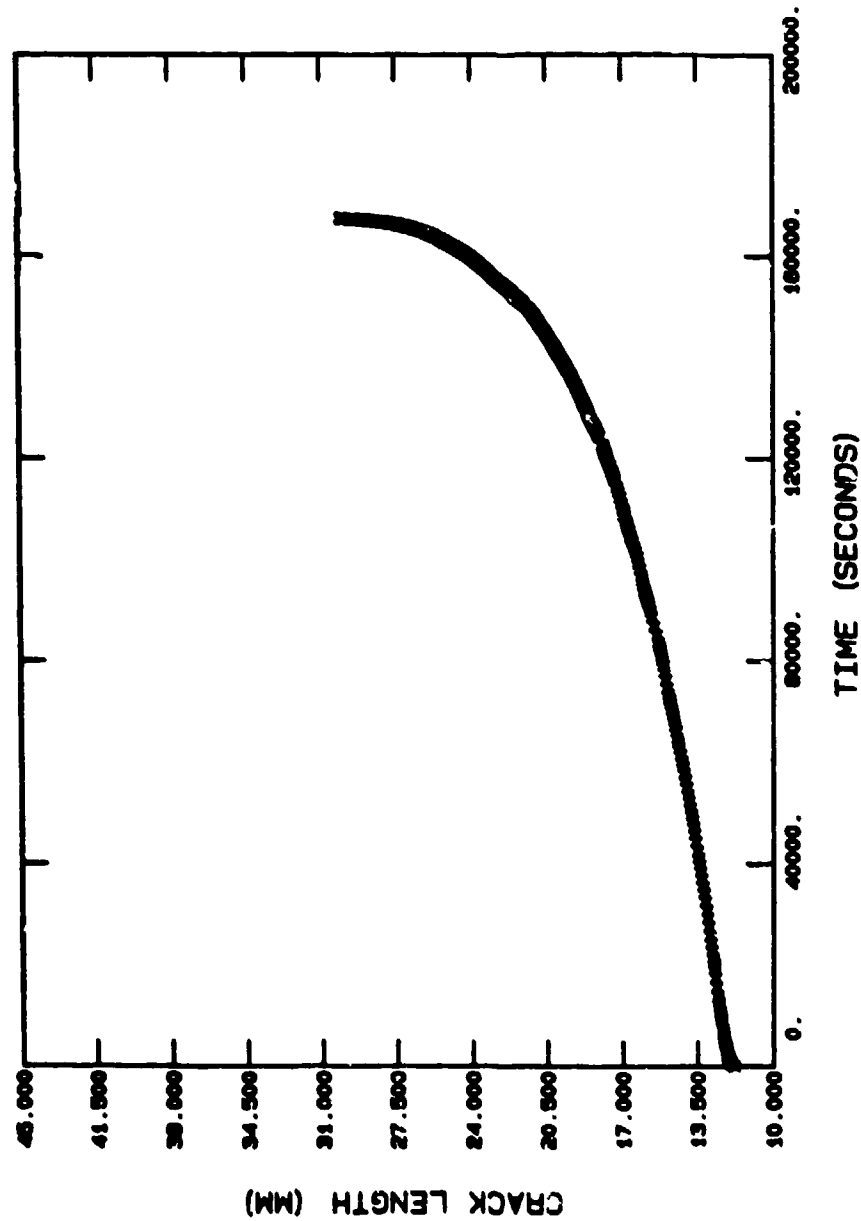


Figure 53. Crack Growth Versus Time for Specimen 88-115

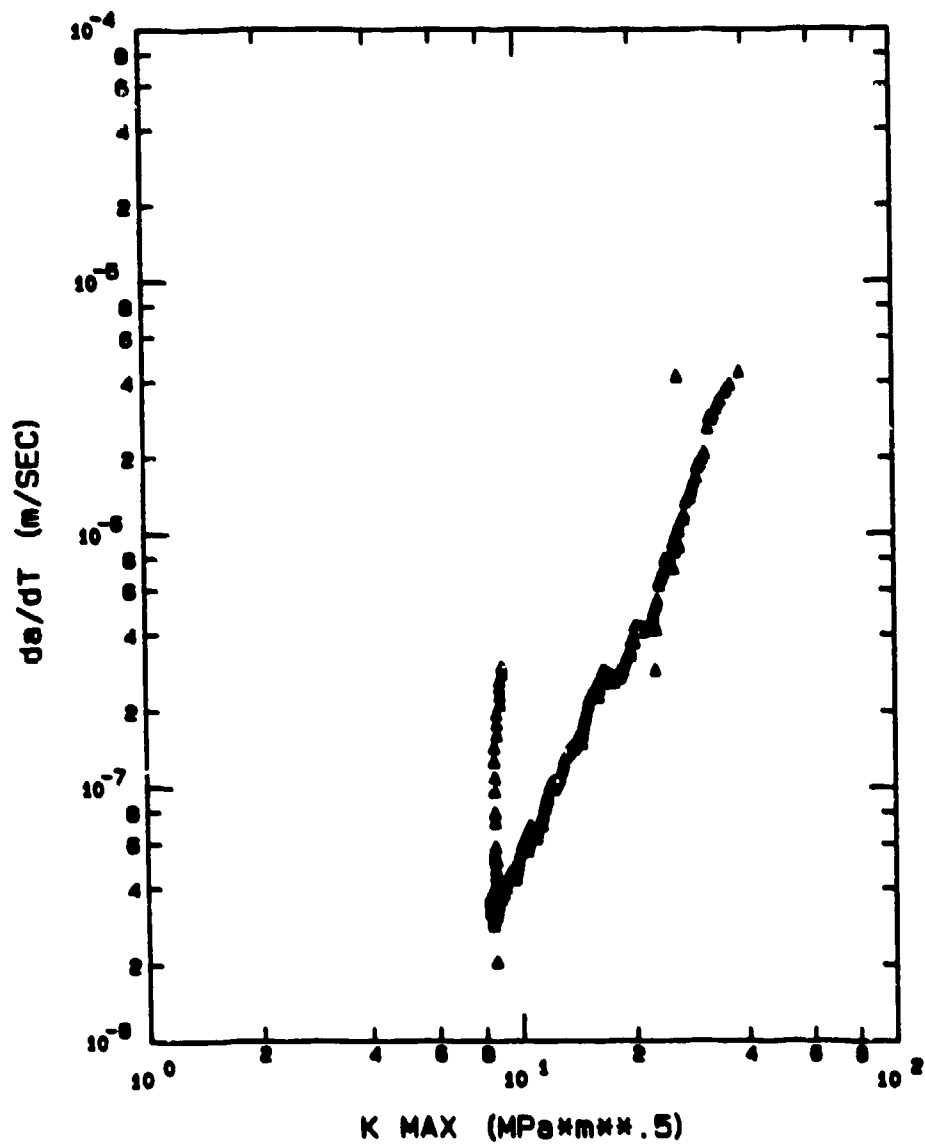


Figure 54. Crack Growth Rate Versus Maximum Stress Intensity for Specimen 88-115

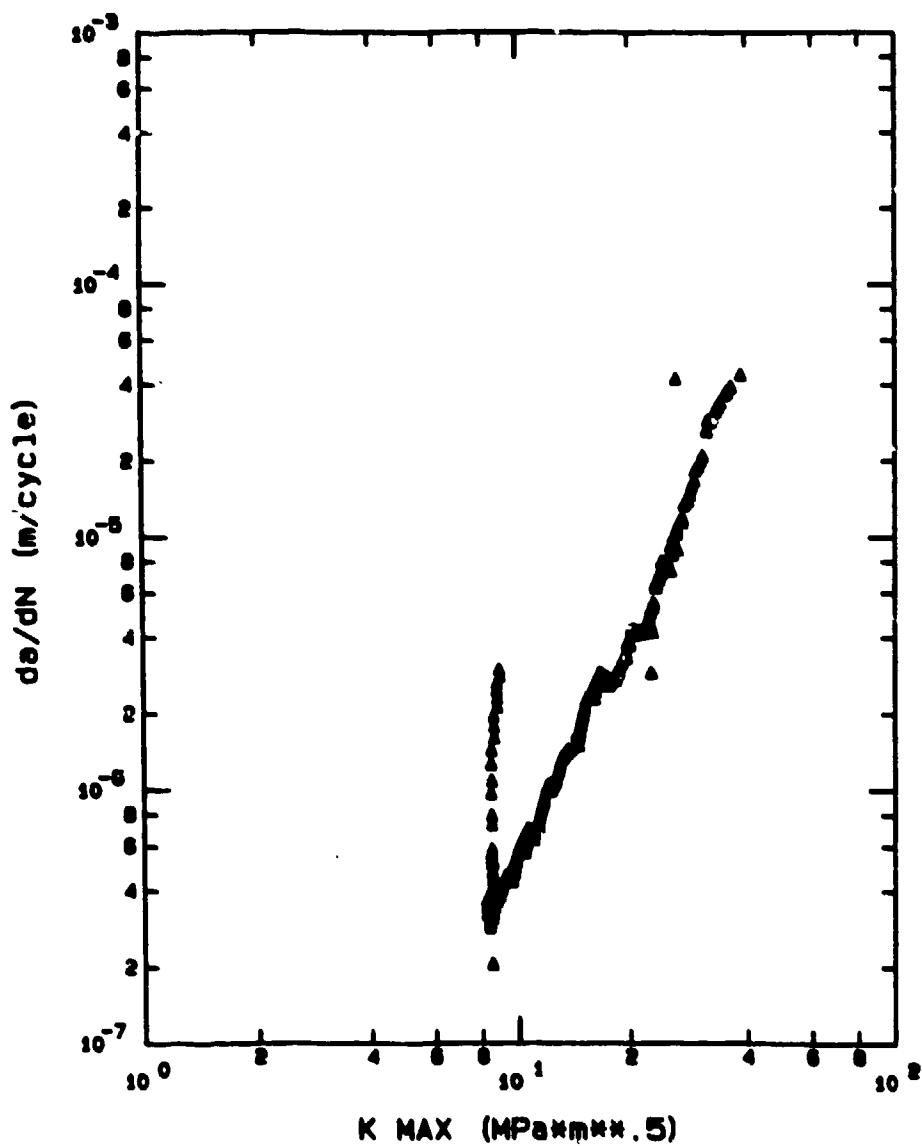


Figure 55. Crack Growth per Cycle Versus Maximum Stress Intensity for Specimen 88-115

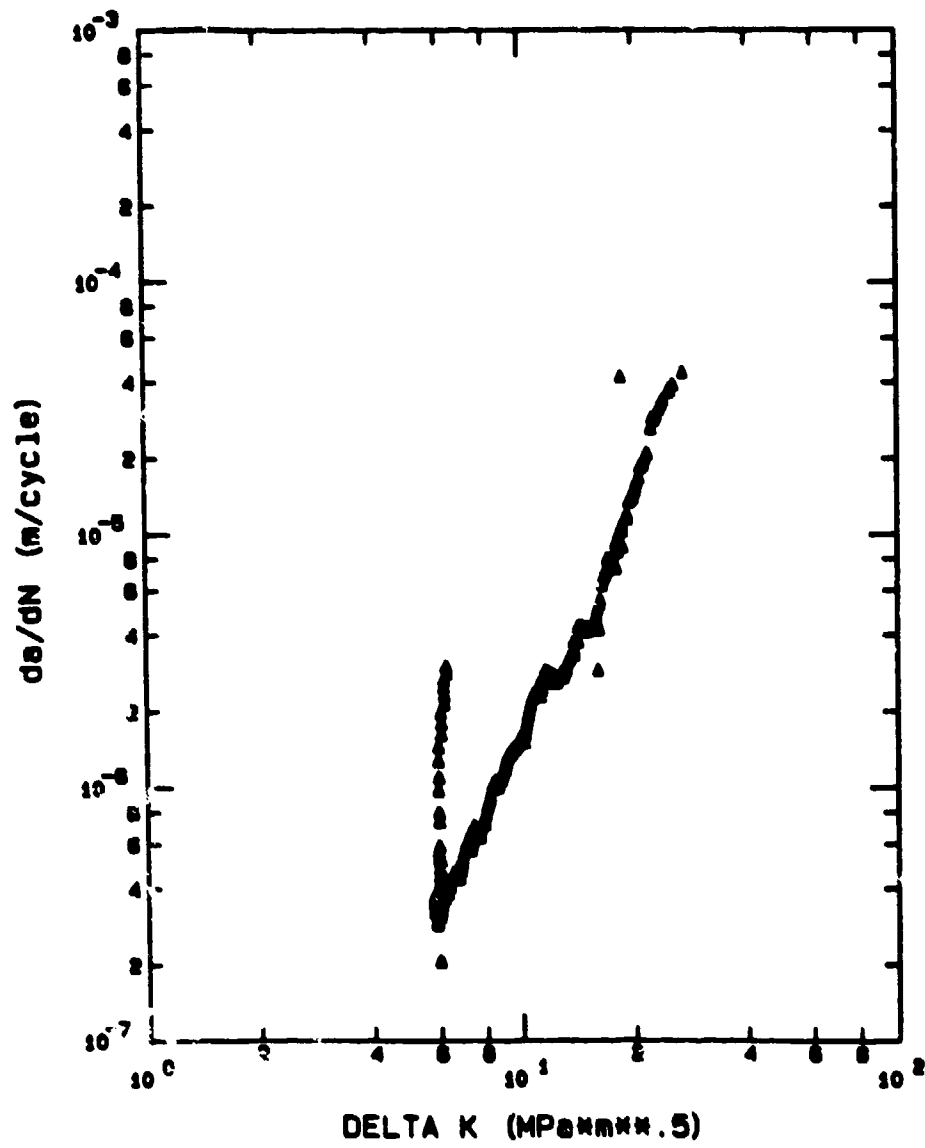


Figure 56. Crack Growth per Cycle Versus Delta Stress Intensity for Specimen 08-115

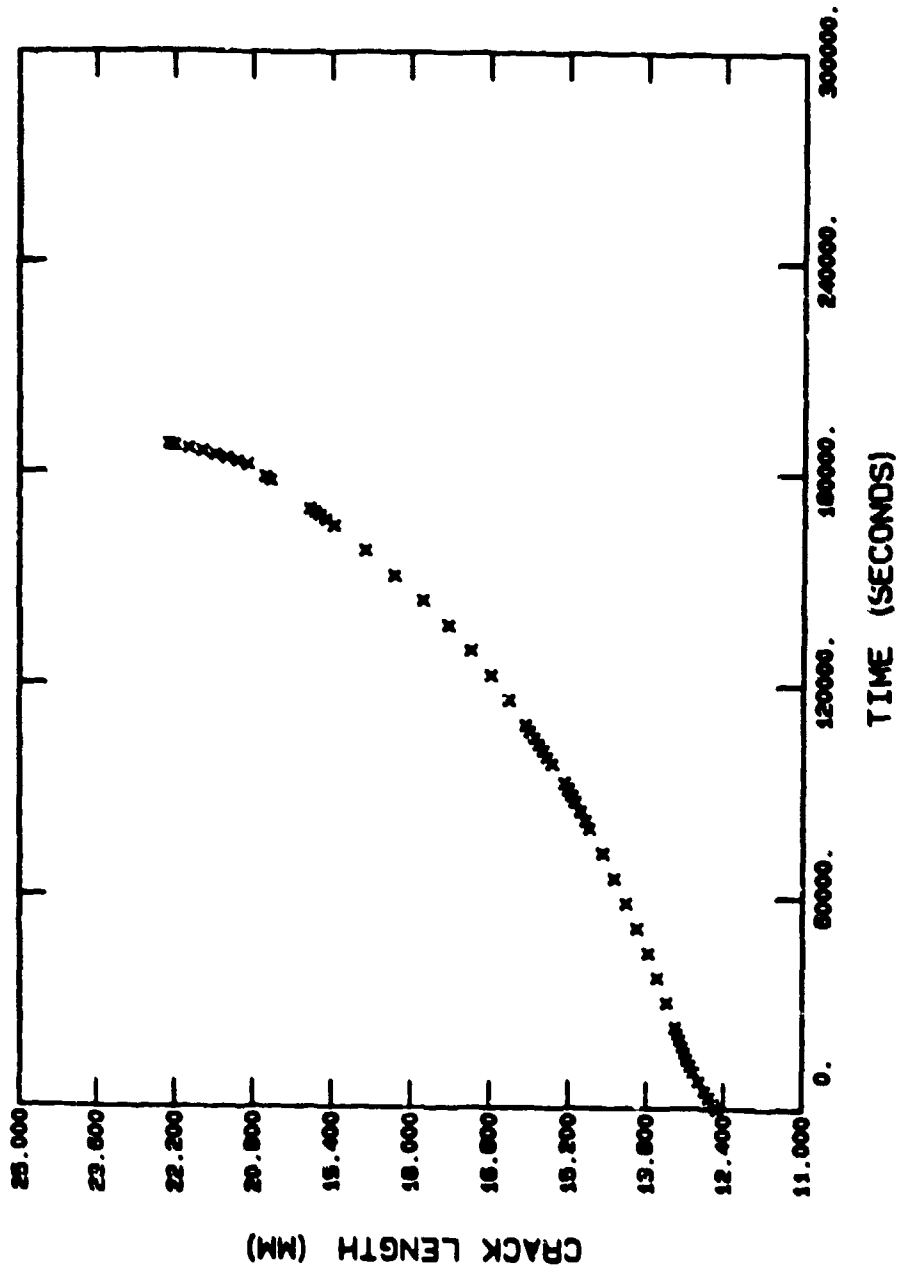


Figure 57. Crack Growth Versus Time for Specimen 88-116

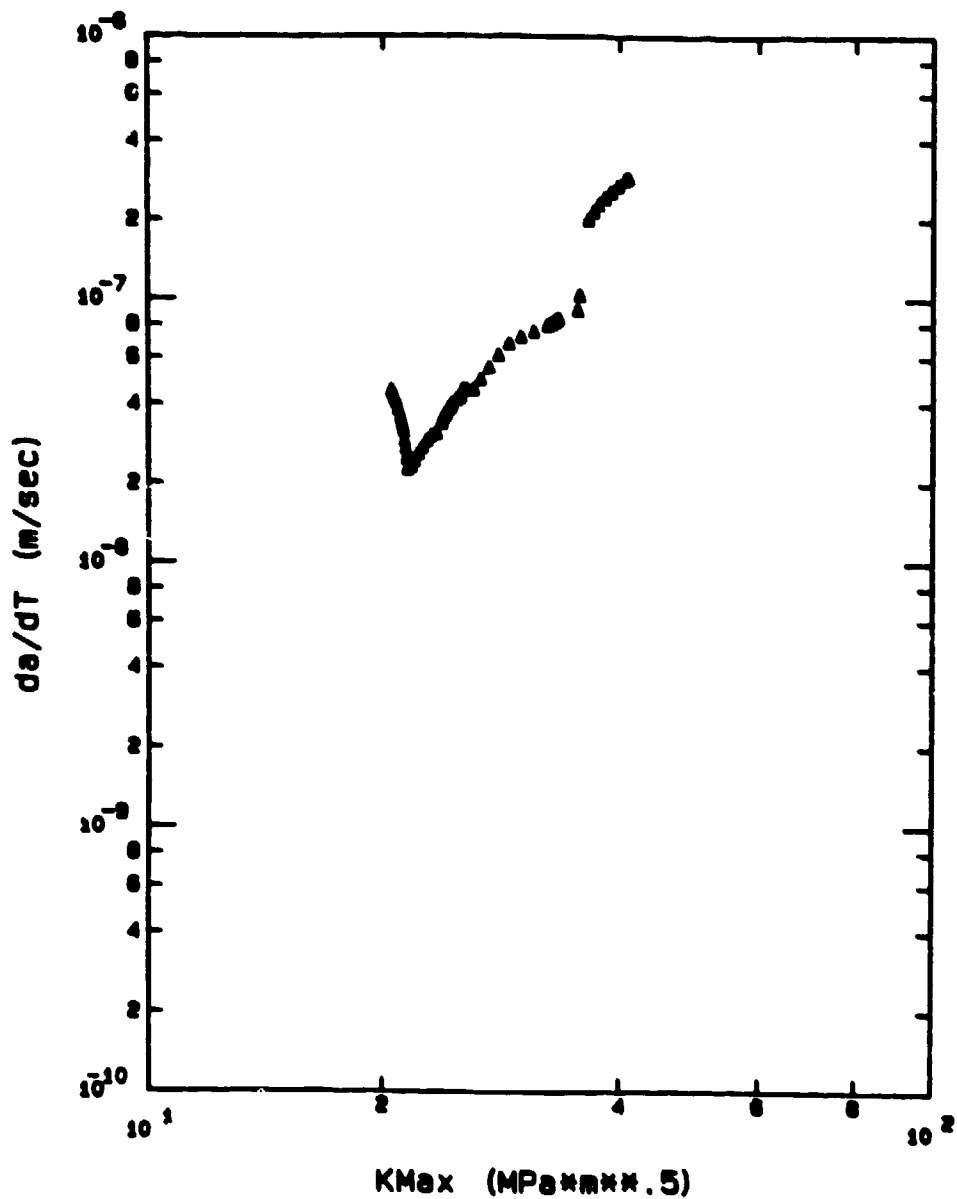


Figure 58. Crack Growth Rate Versus Maximum Stress Intensity for Specimen 88-116



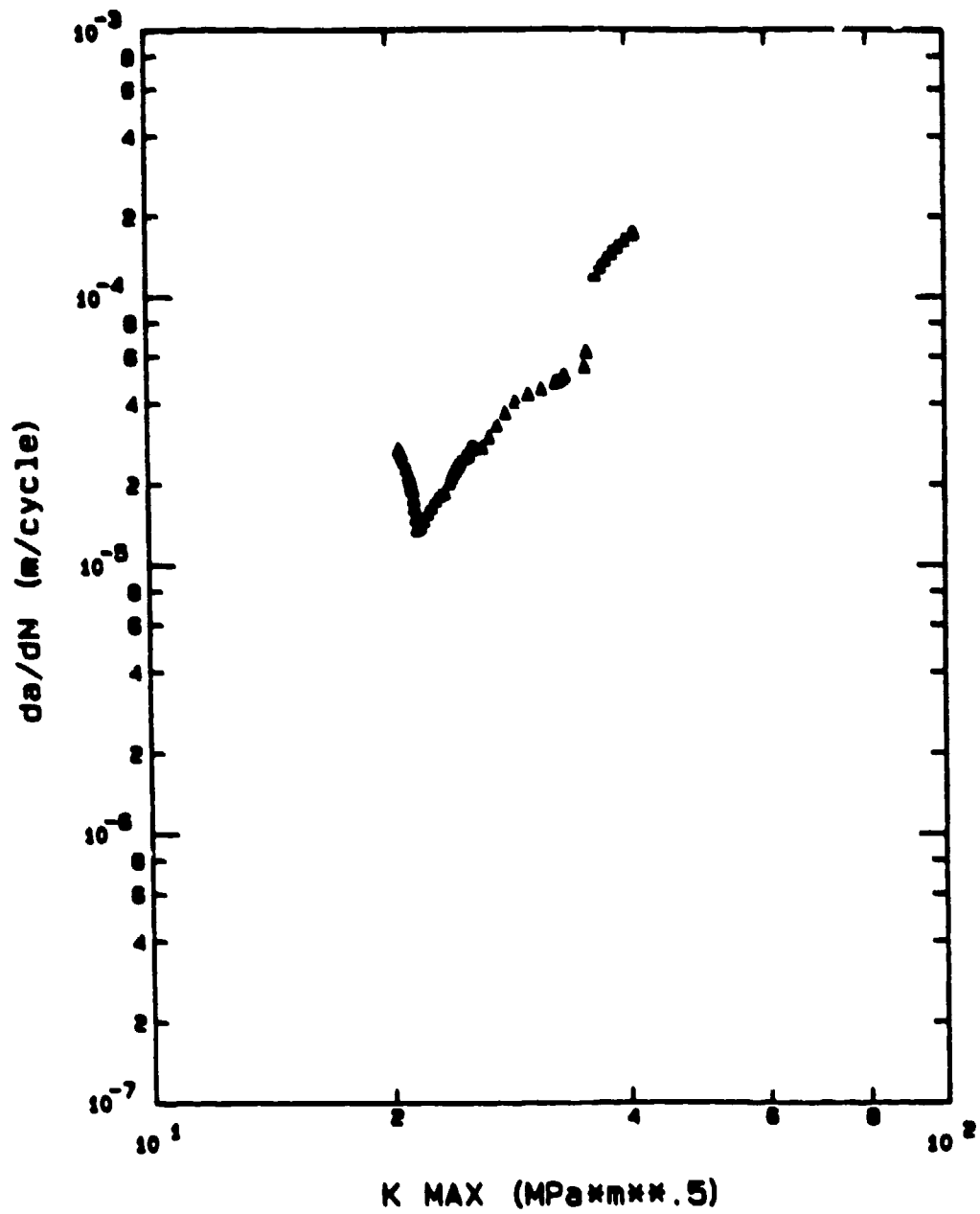


Figure 59. Crack Growth per Cycle Versus Maximum Stress Intensity for Specimen 08-116

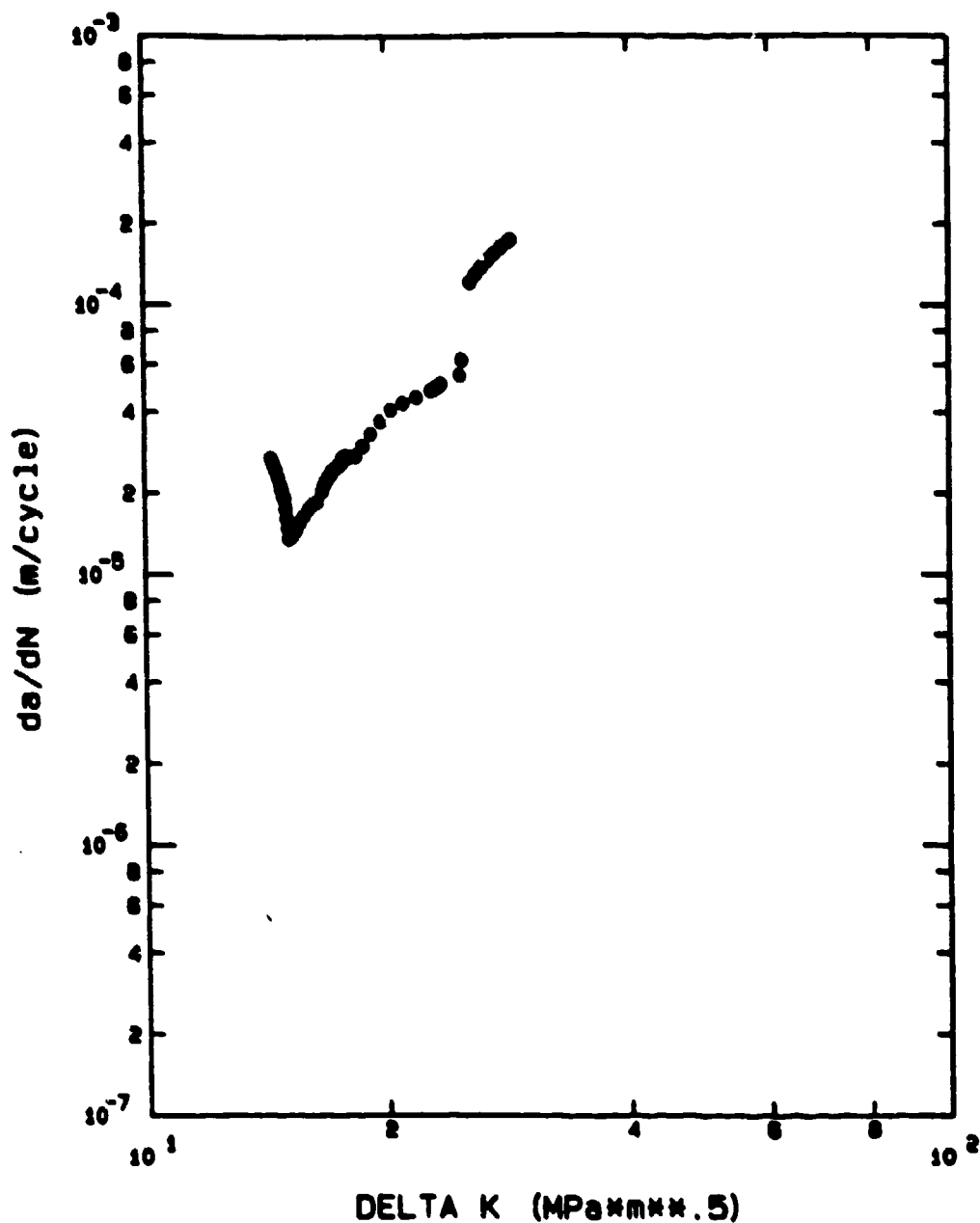


Figure 60. Crack Growth per Cycle Versus Delta Stress Intensity for Specimen 88-116

**Appendix D**

**Crack Growth Program**

```

10 REM
20 REM MSE Model Crack Growth Program for Ti3Al at 750 C
30 REM Sustained Load with Periodic .1Hz Fatigue Cycles
40 REM
50 DEFDBL K
60 REM
70 REM MSE Model Constants, first column for Fatigue
80 REM second column for sustained load
90 REM
100 KI=20.5:KIC=45.5
110 KT=6.2:KTC=19.984
120 KC=82:KCC=167
130 B=-12.94:BC=-14.18
140 P=-2.1:PC=-3.34
150 Q=1.21:QC=1.29
160 D=-5.88:DC=-4.65
170 INPUT "output filename";O$
180 REM
190 REM measured dimensions in inches for compact tension specimen
200 REM
210 INPUT "specimen width";W
220 INPUT "specimen thickness";BS
230 INPUT "notch length";AN
240 REM
250 REM test conditions
260 REM
270 INPUT "sustained MAX load";PS
280 INPUT "load ratio";R
290 INPUT "precrack or starting crack length from notch";A0
300 REM
310 REM Initial crack length in inches
320 REM
330 A=A0+AN
340 REM
350 REM Convert to mm for ASTM standard output
360 REM
370 AMM=A*25.4
380 OPEN "o",#1,O$
390 INPUT "hold time (minutes)";HT
400 REM
410 REM flag error if hold time less than cycle time
420 REM hold time measured from middle of cycles
430 REM
440 IF HT<1/6 THEN PRINT "hold time too short ( >.166667):goto 190
450 REM
460 REM allows for convergence test of data
470 REM
480 INPUT "desired time step (seconds)";DELTA
490 INPUT "maximum number of iterations ";N
500 REM
510 REM sets time and number of cycles to start at 0
520 REM

```

```

530 NCYCL=0
540 T=0
550 REM
560 REM sets flag to print data for every 30 minutes of test duration
570 REM
580 DP=1800/DELTA
590 PFLAG=DP
600 PRINT#1,"t(sec)","cycle","K MPa*m.5","deltaK","dadt m/s","a mm"
610 FOR I=1 TO N
620 REM
630 REM calculate stress intensity factor in MPa*m.5
640 REM
650 K=.886+4.64*A/W-13.32*(A/W)^2+14.72*(A/W)^3-5.6*(A/W)^4
660 K=K*PS*1.0988435#/(1000*BS*W.5)*(2+A/W)/((1-A/W)1.5)
670 REM
680 REM upper limit flag to stop calculations
690 REM
700 IF K>60 THEN GOTO 1030
710 DELTAK=K*(1-R)
720 REM
730 REM calculate fatigue growth rate contribution
740 REM
750 K1=(K/KI)
760 K2=LOG(K/KT)
770 K3=LOG(KC/K)
780 DADTF=EXP(B)*K1P*K2Q*K3D
790 REM
800 REM calculate sustained load growth contribution
810 REM
820 IF K<KTC THEN DADTC=0:GOTO 870
830 K1=(K/KIC)
840 K2=LOG(K/KTC)
850 K3=LOG(KCC/K)
860 DADTC=EXP(BC)*K1PC*K2QC*K3DC
861 REM
862 REM CALCULATE BILINEAR CORRECTION FOR HOLD TIME < 10 MINUTES
863 REM
864 OFSET=1
865 IF HT>10 THEN GOTO 870
866 IF HT>.522 THEN OFSET=-.225*HT+3.25:GOTO 870
867 OFSET=6*HT
870 DADT=OFSET*DADTF/(6*HT)+DADTC
880 T=T+DELTA
890 REM
900 REM calculate number of cycles
910 REM
920 NCYCL=INT(T/(60*HT))
930 IF PFLAG<DP THEN PFLAG=PFLAG+1:GOTO 1000
940 PRK=K
950 PRINT#1,T,NCYCL,PRK,DELTAK,DADT,AMM
960 PFLAG=0
970 REM

```

```
980 REM calculate new crack length
990 REM
1000 AMH=AMH+DADT*DELTA*1000
1010 A=AMH/25.4
1020 NEXT I
1030 CLOSE
1040 END
```

## Bibliography

1. ASTM. 1979 Annual Book of ASTM Standards. American Society for Testing and Materials, Philadelphia, PA, 1979.
2. ASTM. Annual Book of ASTM Standards. Part 10; Metals-Mechanical, Fracture, and Corrosion Testing; Erosion and Wear; Effect of Temperature, 1981.
3. Broek, David. Elementary Engineering Fracture Mechanics. Fourth Edition, Netherlands: Martinus Nijhoff Publishers, 1986.
4. Diboine A. and Pineau, A. "Creep Crack Initiation and Growth in Inconel 718 Alloy at 650° C" Fatigue and Fracture of Engineering Materials and Structures, Volume 10, Great Britain, 1987.
5. Donath, Robert C. "Crack Growth Behavior of Alloy IN 100 Under Sustained Load at 732° C." AFWAL-TR-80-4131, Wright-Patterson AFB, OH, April 1981.
6. Ellison, E. and Harper, M. "Creep Behaviour of Components Containing Cracks-A Critical Review." Journal of Strain Analysis, Volume 13, Great Britain, 1978.
7. Harms, Captain Kevin E. Overload Effects on Sustained Load Crack Growth at Elevated Temperature. MS Thesis, AFIT/GAE/AA/84D-8. School of Engineering, Air Force Institute of Technology (AU), Wright-Patterson AFB OH, December 1984.
8. Harris, J. A. and others. "Concept Definition: Retirement for Cause of F-100 Rotor Components", AFWAL-TR-80-4118. Wright-Patterson AFB, OH 1980.
9. Heil, Major Michael L. Crack Growth in Alloy 718 Under Thermal-Mechanical Cycling. PhD dissertation. School of Engineering, Air Force Institute of Technology (AU), Wright-Patterson AFB, OH, November, 1986.
10. Jain, S.K., and others. Fatigue and Fracture of Titanium Aluminides. Third interim technical report, 1 April 1986-30 September 1986. Allison Gas Turbine Division of General Motors.
11. Maxwell, D. C. and others. "Evaluation of COD Compliance Determined Crack Growth Rates." AFWAL-TR-84-4062, Interim Report for November 1981-January 1983, University of Dayton Research Institute, Dayton OH, 1984.

12. Miller, Captain Douglas L. Sustained Load Crack Growth in Inconel 718 Under Non-Isothermal Conditions. MS Thesis, AFIT/GAE/AA/83D-15. School of Engineering, Air Force Institute of Technology (AU), Wright-Patterson AFB, OH, December 1983.
13. Nicholas, T. and others. "A Model for Creep/Fatigue Interactions in Alloy 718." Fracture Mechanics: Sixteenth Symposium, ASTM STP 868, American Society for Testing and Materials, Philadelphia, PA, 1985.
14. Pernot, Lieutenant John J. Thermal Mechanical Fatigue Testing of a Titanium-Aluminide Alloy. MS Thesis, AFIT/GAE/AA/87D-18. School of Engineering, Air Force Institute of Technology (AU), Wright-Patterson AFB OH, December 1987.
15. Sadananda, K. and Shahinian, P. "Application of Fracture Mechanics Techniques to High Temperature Crack Growth." Fracture Mechanics, 1978.
16. ----- . "Creep Crack Growth in Alloy 718.", Metallurgical Transactions, Volume 8A, March 1977.
17. ----- . "Creep-Fatigue-Environment Interactions", Proceedings of the TMS-AIME Mechanical Metallurgy Committee, Milwaukee WI, September 18-19, 1979.
18. ----- . Review of the Fracture Mechanics Approach to Creep Crack Growth in Structural Alloys. Engineering Fracture Mechanics, Vol 15, Great Britain, 1981.
19. Saxena A. and Bassani J. "Time-Dependent Fatigue Crack Growth Behavior at Elevated Temperature." Proceedings of the Metallurgy Society of the AIME, February 27-29, 1984.
20. Saxena A. and Han J. Evaluation of Crack Tip Parameters for Characterizing Crack Growth Behavior in Creeping Materials. Georgia Institute of Technology, 1984.
21. Utah, D. A. "Crack Growth Modeling in an Advanced Powder Metallurgy Alloy, General Electric Company, AFWAL-TR-80-4098, Wright-Patterson AFB, OH, 1980.
22. Weerasooriya, T. and Nicholas, T. Hold-Time Effects in Elevated Temperature Fatigue Crack Propagation: Interim Report, January 1983-January 1984. AFWAL-TR-84-4184. Materials Laboratory, Air Force Wright Aeronautical Laboratories (AFSC), Wright-Patterson AFB, OH, March 1985.



## Vita

Ernest Aaron Staubs was born on 8 November 1960 in Lowell, Massachusetts. He graduated from high school in Memphis, Tennessee in 1978 and attended Christian Brothers College, where he received the degree of Bachelor of Science in Mechanical Engineering in May 1982. Upon graduation, he entered the USAF Officers Training School where he received his commission in October 1982. He was then assigned as the Mechanical Integration Project Officer for the Peacekeeper ICBM Instrumentation and Flight Safety System at the Ballistic Missile Office (BMO), Norton AFB, California. In July 1986, he served as the Branch Chief for Peacekeeper ICBM Assembly and Test, also at BMO, until entering the School of Engineering, Air Force Institute of Technology, in May 1987.

Permanent Address: 4263 Mackham Cove  
Memphis, Tennessee 38118

UNCLASSIFIED  
 SECURITY CLASSIFICATION OF THIS PAGE

REPORT DOCUMENTATION PAGE

Form Approved  
 OMB No. 0704-0188

1a. REPORT SECURITY CLASSIFICATION <b>UNCLASSIFIED</b>		1d. RESTRICTIVE MARKINGS	
2a. SECURITY CLASSIFICATION AUTHORITY		3. DISTRIBUTION/AVAILABILITY OF REPORT <b>Approved for public release; distribution unlimited</b>	
2b. DECLASSIFICATION/DOWNGRADING SCHEDULE		5. MONITORING ORGANIZATION REPORT NUMBER(S)	
4. PERFORMING ORGANIZATION REPORT NUMBER(S) <b>AFIT/GAE/AA/88D-36</b>		7a. NAME OF MONITORING ORGANIZATION	
6a. NAME OF PERFORMING ORGANIZATION <b>School of Engineering</b>	6b. OFFICE SYMBOL (if applicable) <b>AFIT/ENY</b>	7b. ADDRESS (City, State, and ZIP Code)	
6c. ADDRESS (City, State, and ZIP Code) <b>Air Force Institute of Technology Wright-Patterson AFB OH 45433-6583</b>		9. PROCUREMENT INSTRUMENT IDENTIFICATION NUMBER	
8a. NAME OF FUNDING/SPONSORING ORGANIZATION <b>U.S. Wright Aeronautical Labs</b>	8b. OFFICE SYMBOL (if applicable) <b>MLLN</b>	10. SOURCE OF FUNDING NUMBERS	
8c. ADDRESS (City, State, and ZIP Code) <b>Wright-Patterson AFB OH 45433</b>		PROGRAM ELEMENT NO.	PROJECT NO.
		TASK NO.	WORK UNIT ACCESSION NO.
11. TITLE (Include Security Classification) <b>INVESTIGATION OF CRACK GROWTH IN TITANIUM ALUMINIDE AT ELEVATED TEMPERATURES</b>			
12. PERSONAL AUTHOR(S) <b>Ernest A. Staubs, Capt, USAF</b>			
13a. TYPE OF REPORT <b>MS</b>	13b. TIME COVERED FROM _____ TO _____	14. DATE OF REPORT (Year, Month, Day) <b>1988 December</b>	15. PAGE COUNT <b>129</b>
16. SUPPLEMENTARY NOTATION			
17. COSATI CODES		18. SUBJECT TERMS (Continue on reverse if necessary and identify by block number)	
FIELD <b>11</b>	GROUP <b>6</b>	SUB-GROUP <b>01</b>	
		<b>Creep, Fatigue, Crack Propagation, Titanium Aluminide, Damage Modeling, Thesis. (JES)</b>	
19. ABSTRACT (Continue on reverse if necessary and identify by block number)  <b>Thesis Advisor: Shankar Mall, Professor Department of Aeronautics and Astronautics</b>			
20. DISTRIBUTION/AVAILABILITY OF ABSTRACT <input checked="" type="checkbox"/> UNCLASSIFIED/UNLIMITED <input type="checkbox"/> SAME AS RPT. <input type="checkbox"/> DTIC USERS		21. ABSTRACT SECURITY CLASSIFICATION <b>UNCLASSIFIED</b>	
22a. NAME OF RESPONSIBLE INDIVIDUAL <b>Shankar Mall, Professor</b>		22b. TELEPHONE (Include Area Code) <b>(513) 255-3517</b>	22c. OFFICE SYMBOL <b>ENY</b>

Approved for Release by  
 Authority Not Determined  
 12 Jan 1989

UNCLASSIFIED

This study investigates crack growth at elevated temperatures in a titanium-aluminide alloy (Ti<sub>3</sub>Al). The objectives are to determine the creep crack growth characteristics and the applicability of linear cumulative damage modeling to the Ti<sub>3</sub>Al alloy. All tests were conducted on compact tension specimens of Ti<sub>3</sub>Al under isothermal conditions. Sustained load tests were used to characterize creep crack growth behavior. A fatigue test and several hold-time tests were used to test the applicability of linear cumulative damage modeling. The linear elastic stress intensity factor,  $K$ , was used as a correlating parameter for all the tests. A model was generated using baseline data from the sustained load and fatigue tests and compared with the hold-time tests.

The test results showed that sustained load crack growth is insensitive to temperature. Crack growth rates for all tested temperatures were only a factor of five apart between the slowest and fastest growth rates. The threshold stress intensity level,  $K_{th}$ , was estimated to be 20 MPa $\sqrt{m}$ ; the stress intensity at failure,  $K_{IC}$ , was calculated to be about 46 MPa $\sqrt{m}$ .

The results from the fatigue and hold-time tests showed crack growth rates increased with decreasing hold time. The crack growth per cycle for the hold-time tests was faster than a simple summation of the fatigue and creep crack growth contributions. It was consistently two to three times faster than the fatigue baseline.

A linear cumulative damage model was developed using data from the sustained load and fatigue tests. Crack growth rates calculated using the model were accurate or conservative for the ten minute hold time test, but were 2 to 3 times less than the growth rates for the other hold time tests based on summation of the sustained load and fatigue growth rates only. A mixed-mode correction factor added to the model produced more accurate results.

*Keywords* →

UNCLASSIFIED